TRANSIENT EFFECTS IN

GEOTHERMAL CONVECTIVE SYSTEMS

**A thesis submitted in partial fulfilment of
the requirements of the degree of Doctor of Philosophy
at the University of Auckland**

Roland N. Horne

**School of Engineering
Department of Theoretical and Applied Mechanics**

March 1975

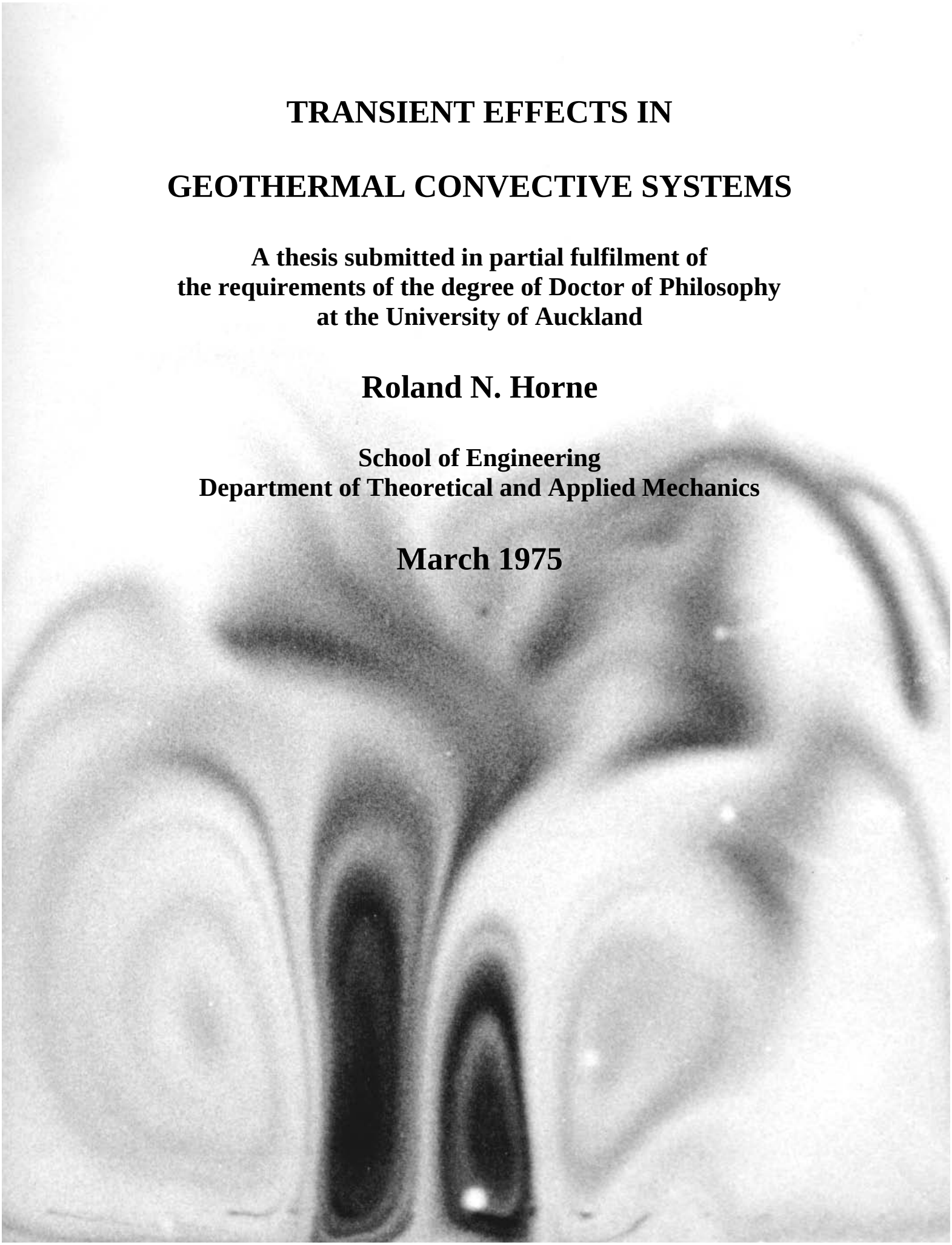

(blank)

ABSTRACT

This work is a detailed analysis of the transient behaviour of geothermal convective systems. The flow in these systems is found to be fluctuating or regular oscillatory in a simplified two-dimensional model and these unsteady effects persist when the model is refined to include the concepts of temperature dependent viscosity and fluid withdrawal and recharge. The analysis is extended into three dimensions to verify this behaviour. The supplementary exploration of added salinity gradients indicates transient effects of a different kind in this case. The examination of the porous insulator problem confirms the results of previous authors and verifies the viability of the numerical methods that are used throughout the investigation.

ACKNOWLEDGEMENTS

During the last three years the research that has lead to the presentation of this thesis has been assisted by many people. Most credit is due to my supervisor Dr M.J. O'Sullivan who originally inspired the work and has given much advice since.

The Hele-Shaw apparatus used for the experimental work was borrowed from the Department of Civil Engineering and I am grateful for the assistance of technicians Mr C. Raymond and Mr D. Browne, who helped set it up. I am also indebted to Dr John Meikle and the Auckland Industrial Development Division of the D.S.I.R. for the use of their AGA Thermovision camera. The many photographs taken of these experiments were processed by the Photographic departments of the University of Auckland and the A.I.D.D.

Referencing of earlier publications has been facilitated by the library staff of the School of Engineering, particularly Mrs Alison Reid who helped with several translations from French.

A large portion of this work has depended on the extensive use of computer facilities and the aid of the University of Auckland Computer Centre is appreciated. Most of the calculations were performed on the Burroughs B6700 although early development of the programs was done on the IBM 1130 in 1972.

Parts of the work have appeared previously in Horne and O'Sullivan (1974 a and b) and I am indebted to Ms Kitty Young for the preparation of these two papers.

I would also like to thank Professor C.M. Segedin of the Department of Theoretical and Applied Mechanics, Associate Professor M.P. Hochstein of the Department of Geology, University of Auckland, and Dr Ian Donaldson and Dr Robin Wooding of the D.S.I.R., Wellington for the various helpful discussions I have had with each of them.

The text has been typed by Ms Mamie Long who was fortunately persuaded out of her retirement from such tasks.

CONTENTS

NOTATION

All variables and operators used are defined when they first appear in the text, however the commonly used ones are summarised here.

Dimensional Variables

$b1, b2, b$ - Coefficients of variation of viscosity v with temperature T.

g - The gravitational acceleration

k - The permeability of the medium

m - The porosity of the medium

P - The dynamic pressure

S - The mean flux velocity

t - Time

$\underset{\sim}{x}$ - Spatial dimensions

C - Concentration of dissolved mineral salts

C_o, C_1 - Minimum and maximum values of C

$\underset{\sim}{F}$ - Buoyancy force

K_{ij} - Thermal dispersion tensor

T - Temperature

T_o, T_1 - Maximum and minimum values of T

a - Thermal expansion coefficient

α_1, α_2 - Linear and quadratic thermal expansion coefficient

a' - Solutal expansion coefficient

$\beta_1, \beta_2, \beta_3$ - Viscosity variation coefficients

κ - Thermal diffusivity

κ' - Solutal diffusivity

χ - Ratio of volumetric heat capacities

μ - Dynamic viscosity of fluid

ν - Kinematic viscosity of fluid

ν_o - Low temperature value of ν

ρ - Density of fluid

ρ_o - Low temperature value of ρ

Non-Dimensional Variables

f - Fraction of lower boundary heated

q - Strength of fluid sink

$\underset{\sim}{u}$ - Velocity due to flow into sink

$\underset{\sim}{u}'$ - Velocity not due to flow into sink

C - Concentration

Nu	- Nusselt number
P	- Pressure
R	- Rayleigh number
S	- Solutal Rayleigh number
$\underset{\sim}{U}$	- Fluid velocity
X	- Spatial dimensions
Y	- Buoyancy ratio
AX, ΔY	- Spatial increments
Δτ	- Time increment
ν'	- Viscosity
ρ'	- Density
θ	- Temperature
ψ	- Stream function
$\underset{\sim}{\theta}$	- Vector potential
T	- Time

Operators

δ	- Jacobian
∇^2	- Laplacian

Chapter 1 - INTRODUCTION

1.1 THE PRECEPT

Geothermal Regions

This work is an attempt to determine the various ways fluid may flow through the permeable material of a geothermal system under the influence of thermally or solutally produced buoyancy effects. If an enclosed porous region is saturated with a fluid that has a temperature dependent density, then by introducing a high temperature anomaly at the base *of* the system it is possible, under certain conditions, to create movement of the fluid as it becomes buoyant and rises through the material. This is the process of natural convection in a porous medium and is the driving mechanism in many geophysical situations where heat is convected to the earth's surface from an energy source deep below ground. In transporting heat from an inaccessible base formation these hydrothermal systems provide a valuable source of energy which in small ventures may be exploited for home heating or factory processes, or in larger projects for the generation of electrical power. Hydrothermal fields have been developed for power production in Larderello, Italy, in the Geysers, U.S.A., in Kamchatka **U.S.S.R.**, and in Wairakei and Kawerau, New Zealand, and it is expected that this energy resource will become increasingly important in future with development of fields in Iceland, Japan, Hungary, Mexico, El Salvadore, Kenya, Ethiopia, the Phillipines, Indonesia, Chile, Guadeloupe, Taiwan, Turkey and Communist China. Therefore the modelling of convective flow through porous media is important from a practical viewpoint since it is required to enable engineers to predict the behaviour of a geothermal system under exploitation. This type of flow is also of general interest to theoreticians since it is one of the simplest examples of hydrodynamic instability, and furnishes parallels with more complex fluid problems, for example the natural convection of a Newtonian fluid in an open region. Furthermore there are additional practical applications, not related to geothermal flows, to the cooling of nuclear reactor cores and the efficiency of porous insulators, for instance fibreglass house insulation or refrigerator walls. It is not surprising then that this problem has, in its various forms, received attention for some time and this study surveys and extends the current state of research in the field and reviews the interrelations between the many solutions previously obtained.

Unsteady Solutions

This work supersedes many earlier studies in that it pays strict attention to the variation of conditions in geothermal regions as time passes. The investigation examines the evolution of a geothermal system, with a particular view to ascertaining the implications of artificial development and exploitation. Furthermore it demonstrates that under certain conditions convective flow in porous

media could remain transient indefinitely due to inherent fluid instabilities, The conditions under which these unsteady flows can occur have been modelled by earlier studies but these were often apparently contradictory and the processes involved were not fully explained. It still remained for the present study to verify the existence of fluctuating convective instabilities in porous media and to determine whether such effects may have an unexpected and major influence on a geothermal system, for example by causing a change from a hot water to a steam dominated formation.

1.2 THE WAIRAKEI GEOTHERMAL REGION

The Physical System

The New Zealand geothermal regions lie in a long trough extending roughly NE-SW across the North Island, approximately five kilometres wide and deep, filled with volcanic debris and contained at the sides betwaen relatively impermeable walls of non-fragmented ignimbrite as in figure 1.2.1.

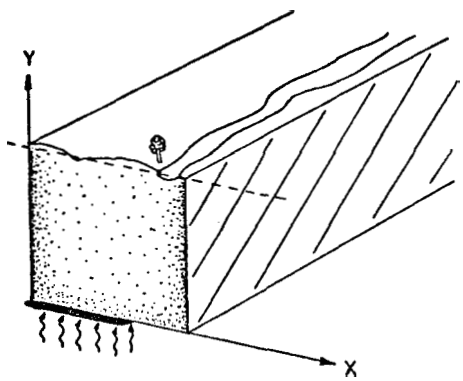

FIGURE 1.2.1 - Sketch of problem configuration - New Zealand geothermal system.

It is not known whether the base of the formation is impermeable or not, but heat is introduced in some way through this boundary and is transported upwards by convection of the water that fills the interstices of the porous rock, or by conduction through the material itself. The origin is unclear but it has been suggested by Mercer (1973) that this heat is derived from the global tectonics associated with the trench system. On reaching the surface of the earth this heat produces hydrothermal phenomena such as steaming ground, fumaroles and hot springs.

The fluid which saturates porous geothermal beds may be water, steam, brine or a mixture of each. The Wairakei system is generally known as a hot water system (Kruger 1973) since the water in it holds only a small amount (< 12000 ppm) of dissolved mineral salts and the steam phase is restricted to the surface region down to approximately 400 m below ground. Above this region there are periodic surface phenomena such as geysers and hot lakes which occur due to interactions between the steam and water phases, but the overall convective pattern of the system is mainly influenced by the larger scale motion which originates at greater depth between 2 and 5 km at which the fluid is wholly liquid. Below the shallow two phase region are the artificial flows produced by withdrawal of fluid through boreholes and it is expected that these effect the overall flow more significantly.

Model Systems

When creating an experimental or numerical model of a physical system it is necessary to be able to accurately represent all the essential features of the actual prototype. Unfortunately this is not usually possible in geothermal applications since the region of interest extends so far below ground that its exact nature is not directly determinable. The Wairakei geothermal field is the most significantly developed hot water system in the world and as such has been the subject of various theories which differ in their explanation of the structure of the system. Some studies restrict the region of interest to the shallow surface system and use averaged parameters to represent the lower convecting flows - Mercer (1973) is an example of such a "reservoir" model. This kind of approach may be used to represent, in plan detail only, the response of the upper geothermal reservoir under a given set of lower reservoir conditions. The behaviour of the lower system, which may also be effected, is not modelled at all (Mercer 1974). A better representation of the system requires the modelling of the convection throughout the region, right down to the source of the geothermal energy. Donaldson (1962) initially proposed a two layer model system consisting of a homogeneous porous layer overlying a homogeneous impermeable layer heated from below. Later (1968 and 1970) he refined this model to a permeable channel representation which was then more specifically relevant to the upper reservoir. Such a representation presupposes the existence of a bed of material that is anisotropically permeable, with greater permeability in the horizontal direction. Such beds are evident in the geological studies of Healy and Hochstein (1973); these are at shallow levels and are fed with preheated water from a deeper system. A layer representation has also been used for a larger scale model by McNabb (1965) who envisaged the deep system as having its base above a lava lake or similar magmatic heat source. Elder (1966a) has presented a comprehensive review of several possible configurations for both the reservoir and deep systems. The current investigation is concerned with the modelling of the deep system.

The Current Model

Bearing in mind the configuration of figure 1.2.1, the model region is chosen initially to represent an infinitely long trench of rectangular cross-section, completely filled with a homogeneous and isotropic porous medum which is wholly saturated with water. The heat source at the base of the region could be of arbitrary shape, as has been considered by Taunton and Lightfoot (1970) but because of the lack of information about the heat source this is an unnecessary generality and the source is more usually taken to be flat. The output of geothermal heat is

either by withdrawal of hot fluid through wells or by loss at the surface to the surrounding atmosphere. As has generally been the case these upper and lower boundaries are taken to be horizontal, constituting a type of system labelled by Elder (1966a) as a "wet-convector". Inclined systems have been studied by Bories, Combarnous and Jaffrenou (1972), Kaneko, Mohtadi and Aziz (1974) and Bories and Combarnous (1973) but are not considered here.

Since it is unknown whether or not fluid flows in through the base of the formation, both possibilities are modelled. If a magmatic intrusion or lava lake is viewed as being covered by a supercritical gas sheath that constitutes a phreatic surface, then liquid transfer across the boundary is prohibited and the lower boundary may be assumed to be impermeable. The production of magmatic water or the large scale introduction of meteoric water through major horizontal fissures as is proposed by Donaldson (1974) constitutes the alternative configuration in which the base is permeable. Following Wooding (1957), the enclosing vertical boundaries are assumed to be impervious and also relatively non-conducting (Elder 1967a).

1.3 PAST WORK

Convection in a Porous Medium

The classic configuration which has been the most commonly modelled is the box or infinite slab of porous material heated uniformly from below. The initial onset of convection in such a region was the subject of early analytical studies by Horton and Rogers (1945) and by Lapwood (1948) and later experimental and numerical studies by Wooding (1957), Donaldson (1962) McNabb (1965), Katto and Masuoka (1967), Elder (1966a, 1967a & b), Bories and Thirriot (19691, Combarnous (1970), Palm, Weber and Kvernvold (1972), Holst and Aziz (1972a) and Yen (1974) who all derived steady solutions to the problem. However Combarnous and Le Fur (1969) discovered in their experiments that there is a second mode of convection at higher values of the defining dimensionless parameter - the Rayleigh number (see section 2.1) - and this second mode was later reported by Caltagirone, Cloupeau and Combarnous (19711, and Combarnous and Bia (1971), to be a fluctuating pattern of two dimensional rolls.

This second mode has yet to be observed in numerical solutions, for one of three reasons. Firstly, the earlier numerical studies (for example Donaldson (1962), Elder (1966a, 1967a)) presupposed a steady solution and did not include the transient terms in their equations of motion. In view of the fluctuating solutions which were discovered later, and of Elder's own admission (Elder 1967a) that unsteady convective instabilities cannot be examined under the assumption of quasi-steadiness, these analyses may seem inappropriate. However this is not so as due to limitations of the numerical methods used the only flows studied were under the benevolent conditions of a low Rayleigh number for which steady flows do occur. When the flows are more vigorous the numerical procedures considered up to the present time become unstable due to the false production of kinetic energy and this is the second reason why the range of numerical solutions has been so restricted, Thus the transient representations of Elder (1967b and and Holst and Aziz(1972b) which use

similarnumerical methods could not have produced solutions in the unsteady mode, Thirdly, despite the limitations of the techniques, the algorithms and computational machinery still would not have been fast enough to develop the solutions for a duration sufficient for the nature of the unsteady effects to become clearly apparent.

Various linear and non-linear stability analyses have been performed by Westbrook (1969), Beck (1972), Busse and Joseph (1972) and Gupta and Joseph (1973) but once again these authors either ignored transient effects or considered a range of conditions in which they could not occur. The more recent analysis by Straus (1974) attempted to explain the transition observed by Combarnous and Le Fur (1969) as **a** transition from two-dimensional to three-dimensional flows, however it seems apparent that Straus (1974) did not consider the results of Caltagirone et al (1969) since he too specifically precludes oscillatory effects. Similarly **the** experimental conditions of Yen (1974) duplicate those of Caltagirone et al (1969) but no reference is made to this earlier investigation and no mention of the form of the solution is reported.

Therefore to avoid the limited applicability of these earlier solutions, this study uses more sophisticated numerical procedures that are based on the transient equations of motion and which are stable enough and fast enough to allow lengthy solutions under a range of conditions that may be expected to occur in geothermal regions (including those under which unsteady flows are evident).

Convection of a Newtonian Fluid

Since a unified appraisal of the set of closely interrelated problems considered in this work has not previously appeared it is expedient to draw parallels with convection in a fluid layer (the Benard problem) which has been more widely reported. Corresponding steady solutions have been obtained by **Fromm** (1965), Veronis (1966), Plows (1968) and Brown (1973) and the special considerations of non-uniform heating, temperature dependent viscosity and horizontal temperature gradient have all been investigated in the Bènard problem by Weber (1973), by Torrance and Turcotte (1971) and by Wirtz, Briggs and Chen (1972) and Gill and Kirkham (1970) respectively. Of these three situations only the last has previously been fully considered in the porous medium problem.

The stability of this and closely related problems has been considered for layers by Chandrasekhar (1961), Gill and Davey (1969), Willis and Deardorff (1967 & 1970), Krishnamurti (1970 a&b), Busse and Whitehead (1971 & 1974) and Homsy **(1973 &** 1974), for channels by Birikh, Gershuni, Zhukhovitski and Rudakov (1972), for arbitrary containers by Joseph (1971) and generally by Gebhart (1973). These investigators are all notable in that collectively they observed that the mode of convection may change completely with variation of the defining parameters, that one or more ***of*** the higher modes may be unsteady or oscillatory, and that under certain circumstances the oscillation may take the form of paired disturbances rising in the convective plane.

Numerical studies of the Benard problem have been somewhat more successful than their porous medium counterparts. A forerunner of instabilities that were discovered later was perceived in the numerical study of Elder (1966b) in the form of "secondary flows" which he speculated might have been due to disturbances

inherent in the numerical method exciting other modes of the system. This was confirmed some time later by the comprehensive numerical investigation by Moore and Weiss (1973) who used more advanced numerical techniques and obtained an oscillatory solution in a square two-dimensional region heated from below. The generation of disturbances that they observed is very similar to that obtained in this work and their explanation of the mechanism emphasises the same processes, Similar explanations of analogous oscillatory behaviour in simple loop models have been proposed, first by Keller (1966) then more fully by Welander (1967) who later (1971) extended the concept to include similar effects in a stratified fluid layer.

The numerical analysis of the convection equations has more commonly been considered for the Benard rather than the porous medium problem, although these studies provide the basis of the numerical methods that are used here. The representation of the advection terms in the heat transport equations (see section 4.2) has been studied variously by Crowley (1967), Wilkes and Churchill (1966), Torrance (1968), and Fromm (1969 a & b) and these analyses are directly applicable to the problem at hand since the same terms appear (and are equally difficult to represent).

Although results for the Bbnard problem are not directly applicable to convective flow in a porous medium it is interesting to note the similarities and differences as they arise, since suggested mechanisms for processes in either situation can often indicate lines of approach to be followed in the other.

1.4 THE SCOPE OF THIS WORK

A mathematical formulation of the modelling of flow in geothermal regions is proposed in chapter 2, including transient flows, non-uniform heat input at the base of a system, temperature dependent viscosity and a variety of fluid withdrawal conditions. A single, exact model which encompasses all the relevant features of a geothermal region is impractical due to the difficulty in determining the details of real system. Therefore a range of models is proposed to include more than one possible configuration.

It is demonstrated experimentally in chapter 3 that the flow in the two-dimensional model region described in section 2.2 may undergo irregular fluctuations or regular oscillations under certain conditions. Although the first of these effects has been observed previously in the experiments of Caltagirone et el. (1969) there is a later and seemingly contradictory experimental study by Yen (1974) who reported steady solutions. To resolve this uncertainty a different approach is taken and a numerical representation used. To investigate the unsteady effects it is necessary to use the transient form of the equations (derived in section 2.1) and examine the development of the flow over a long period in time, which most earlier studies have neglected to do. For this purpose a set of numerical techniques is derived in chapter 4 that is sufficiently rapid to allow lengthy solutions. These techniques rely on the energy conservation properties of the Arakawa differencing schemes (Arakawa 1966) to avoid the numerical instabilities that restricted earlier studies into investigating cnly relatively slow flows.

In chapter 5 the numerical verification of the previous experimental results is produced - the apparent contradiction in the earlier works is due to the existence of alternative steady and unsteady solutions under the same boundary conditions (but different initial conditions). The regular oscillatory solutions of chapter 3 are also confirmed and explained,

The regeneration of water in a geothermal system by seepage of groundwater has a prominent influence on the flow and this concept is included in the numerical models in section 5.4 (for the first time in a transient analysis). The inclusion of these recharge conditions is necessary for the representation of artificial withdrawal and reinjection in an exploited geothermal system, and simulations of developed systems are performed in section 5.4.

Past models of geothermal regions usually considered the porous rock formation to be saturated with pure water of constant viscosity. To examine the advisability of making this assumption the effects of temperature dependent viscosity is investigated in section 5.5, and the possibility of dissolved mineral salts is allowed in the separate analysis of chapter 7.

The flow equations may be solved in either two or three dimensions. The two-dimensional approach permits beneficial economies in the usage of computational resources but it is considered essential to extend the analysis to three dimensions for at least part of the work (see chapter 6) to confirm the significance of the solutions generated in two dimensions.

The effects that these several conditions have on the overall flow in a geothermal region are various and complex and is preferable to consider them separately. The direct and precise modelling of the Wairakei geothermal region lies slightly beyond this work, but the contiguous consideration of all the individual effects represented here could simulate the system quite fully. By presenting a range of solutions it is possible to obtain a more general understanding of the fundamental mechanisms, before attempting to construct a single, tenaciously accurate model in which separate effects may interact and mask observation of the basic processes governing the behaviour of the system.

Having derived a solution technique with a specific application to geothermal modelling it is interesting to apply it to a different situation also. In chapter 8 the methods are modified slightly to allow representation of the porous insulator problem mentioned in section 1.1. The results of this simpler investigation are readily comparable with previous work on this problem, thus permitting further evaluation of the viability, of the techniques. Furthermore the flow mechanisms are related to those in the geothermal case and furnish some interesting parallels (see chapter 9).

Chapter 2 - MATHEMATICAL FORMULATION

2.1 THE EQUATIONS OF MOTION

The equations governing the convective flow of fluid through a permeable material have various forms depending on which of the range of simplifying assumptions are invoked and which dependent variables are used. Several different representations are presented here. Basically the system of equations represent four physical relations - conservation of mass, momentum and energy and the empirical equations of state. The working fluid is assumed to be incompressible and Newtonian, representing the flow of pure water or at worst a dilute aqueous solution of mineral salts (see chapter 7).

Conservation of Mass

The form of the continuity equation relevant to flow through porous media is that given by Aravin and Numerov (1965), namely

$$\frac{\partial \rho}{\partial t} + \frac{\partial (\rho q_i)}{\partial x_i} = 0 \quad , \tag{2.1.1}$$

where q_i, as defined by Elder (1966a) and Wooding (1957), is the mean *flux* velocity of the fluid through the medium which fills space x_i at time t. The mean flux velocity should not be confused with the mean velocity of the fluid through the interstices of the porous medium. The flux velocity is smaller by a factor m, the porosity of the material.

Conservation of Momentum

The usual form of the Navier-Stokes equation is modified by the incorporation of the experimental Darcy's Law (Yih 1969, p.379), replacing the viscous terms with terms that account for the flow resistance of the porous material:

$$\rho \frac{Dq_i}{Dt} = \rho F_i - \frac{\partial p}{\partial x_i} - \frac{\mu}{k} q_i \quad . \tag{2.1.2}$$

Here F_i is the buoyancy force, p is the dynamic pressure in the fluid, μ is the dynamic viscosity of the fluid and k is the permeability of the medium.

The Wairakei geothermal formation has significantly anisotropic permeabilities with the horizontal permeability larger than the vertical permeability by a factor of approximately **10.** However thrbughout most of the region these two properties are uniform **so** it is possible to use the same value for both and adjust the horizontal and vertical length scales accordingly. Beck (1972) has observed that the form (2.1.2) of the momentum equation is not always satisfactory due to the disparity between the order of the space derivatives in the equation and the usual number of boundary conditions, however for natural convective problems where inertia effects may be ignored this difficulty does not arise.

Conservation **of** Energy

Since the flow is slow and therefore predominantly determined by differences between boundary and fluid temperatures and not by energy dissipation effects, the appropriate form of the energy equation as given by Rubin (1974) is

$$\frac{\partial T}{\partial t} + \lambda q_i \frac{\partial T}{\partial x_i} = \frac{\partial}{\partial x_i}\left(K_{ij} \frac{\partial T}{\partial x_j}\right) , \qquad (2.1.3)$$

where λ is the ratio of the volumetric heat capacity of the fluid to that of the saturated formation, and K_{ij} is the thermal dispersion tensor. The thermal dispersion tensor incorporates two properties of the system - firstly the molecular diffusivity and secondly the intrinsic dispersivity of the porous medium which is effectively a measure of the uncertainty that a particular small parcel of fluid will keep to a theoretically averaged ***mean*** flow path as it moves in a tortuous manner through the interstices of the material. The behaviour of a particle **of** fluid moving through a porous material is similar to that of a particle in a turbulent flow and the dispersivity may be envisaged as analogous to an eddy diffusivity. Dybbs and Schweitzer (1973) have produced a more rigorous derivation of the set of conservation equations for flow in a porous medium **by** defining the flow in the interstices and then averaging throughout the material, thus avoiding the use of the empirical Darcy's Law (although this is a consequence in some cases). They arrive at a concept which they term the "convective diffusivity" but which is another representation of the intrinsic dispersivity. In a non-homogeneous porous medium the flow may be vigorous in certain areas and consequently dispersion effects surpass those of diffusion, **so** the thermal dispersion tensor must be represented in its complete form, including both longitudinal and lateral fluid dispersion. However for the very slow flows **of** natural convection in geothermal areas, dispersion effects are small and the thermal dispersion tensor reduces to the scalar molecular diffusivity κ of the saturated porous material (Rubin 1974). Elder (1966a) and Combarnous (1972) both propose that an estimate of this term **may** be obtained from

$$\kappa = (1-m)\kappa_{rock} + m.\kappa_{water} , \qquad (2.1.4)$$

where m is the porosity **of** the rock. In general the thermal diffusivity is neither constant nor isotropic in geothermal areas, but for simplicity it is taken to be **so.** At Wairakei the difference in horizontal and vertical permeabilities means that diffusion may also be less in the vertical direction however as was observed earlier this difficulty may be avoided by vertically "stretching" the

solutions obtained using an isotropic diffusivity. The variation of thermal diffusivity throughout the various geological formations which make up the system is difficult to determine and since the exact geophysical structure is unknown there is no other choice but to assume a constant value. Previous authors have taken κ to represent the thermal diffusivity of the medium alone, but Katto and Masuoka (1967) showed that the form (2.1.4) **is** required to obtain agreement between theoretical and experimental results. Combarnous (1972) has found experimentally that the heat transfer coefficients are characteristic of the particular fluid and medium, and it is hoped that the incorporation of both solid and liquid terms takes account of this difficulty. The effect of the thermal conductivity of the saturating fluid on the heat transfer in a porous medium has also been observed by Maksimov and Stradomskii (1971).

The Equations of State

The fluid properties which may vary with temperature are the viscosity and the density, and it is necessary to use empirical formulae to represent the relationships between these quantities. Different representations have been used in the past, most authors - Horton and Rogers (1945), Lapwood **(1948)**, Wooding (1957), McNabb (1965), Donaldson (1962), Elder (1967 a & b) etc. - used a linear relationship for density and assumed that the viscosity was constant. Elder (1966a) has considered temperature dependent viscosity but without recording what effect this would have on the flow. For a temperature differential of **250°C** the viscosity of water varies by a factor of approximately 10, so the assumption of constant viscosity is seemingly inappropriate in a geothermal context, and furthermore the variation of density in this range is more closely quadratic. Thus the fluid density is better described by

$$\rho = \rho_o(1 - \alpha_1(T - T_o) - \alpha_2(T - T_o)^2) \quad , \qquad (2.1.5)$$

and the viscosity by

$$\nu = \frac{\nu_o}{1+b_1(T-T_o)+b_2(T-T_o)^2+b_3(T-T_o)^3} \qquad (2.1.6)$$

where α_1 is the more commonly used linear coefficient of thermal expansion of the fluid.

The Boussinesq Approximation

It is usual in convection problems, as for example in Yih (1969 p.441), Torrance (1968), Wooding (1957) and Nield (1968), to invoke the Boussinesq approximation by assuming that the variation of fluid density need only be considered in buoyancy terms; in the inertia and continuity terms the density is taken to be constant. For steady state analyses (e.g. Donaldson 1962) the Boussinesq approximation is unnecessary as all the density terms may be combined into the fluid velocity terms to create "mass transfer" equations. In such **a** case the kinematic viscosity replaces the dynamic viscosity and the mass flux replaces the flux velocity, but otherwise the equations are essentially the same as they would

be if the Boussinesq approximation were used, Thus the net effect of the Boussinesq approximation on the complete transient equations is an unimportant change in the viscosity term (for water the dynamic and kinematic viscosities are almost the same at most temperatures) and a misrepresentation of the terms

$$\frac{\partial \rho}{\partial t} + q_j \frac{\partial \rho}{\partial x_j} ,$$

in the continuity equation.

If the change in temperature relative to the absolute temperature in any part of the fluid is small, the change in density is an order of magnitude less and can be neglected as far as continuity is concerned.

Since the thermal diffusivity is a function of thermal conductivity, density and heat capacity, then it is a further consequence **of** the Boussinesq approximation that this quantity is also constant.

Thus, invoking Boussinesq and substituting for the buoyancy terms, the equations become

$$\frac{\partial q_i}{\partial x_i} = 0 , \qquad (2.1.7)$$

$$\frac{Dq_i}{Dt} = -g_i \left(\frac{\rho-\rho_o}{\rho_o} \right) - \frac{1}{\rho_o} \frac{\partial p}{\partial x_i} - \frac{\nu}{k} q_i , \qquad (2.1.8)$$

and $$\frac{\partial T}{\partial t} + \lambda q_i \frac{\partial T}{\partial x_i} = \kappa \nabla^2 T , \qquad (2.1.9)$$

where the Laplacian $\nabla^2 \equiv \frac{\partial^2}{\partial x^2} + \frac{\partial^2}{\partial y^2} + \frac{\partial^2}{\partial z^2}$.

Order of Magnitude Analysis

At this stage the momentum equations may be simplified further after comparison of the relative magnitudes of the separate terms. If **U** is a representative velocity of the fluid passing through the interstices of the porous material, and d is a length representative of those interstices, then for the inertia, viscous, pressure and buoyancy terms respectively,

$$\frac{Dq_i}{Dt} = 0 \left(\frac{U^2}{d} \right) ,$$

$$\frac{\nu}{k} q_i = 0 \left(\frac{m\nu U}{d^2} \right) ,$$

$$\frac{1}{\rho_o} \frac{\partial p}{\partial x_i} = 0(g) ,$$

and $$g\left(\frac{\rho-\rho_o}{\rho_o}\right) = 0(g\Delta\rho) .$$

The ratio of inertial to viscous terms is then of order $\frac{mUd}{\nu}$, and for flows in which this parameter (the Reynolds number) is much less than unity, the inertia terms may be neglected. This condition is satisfied for the slow percolation of water through soil (Batchelor 1967 p.223) and also for natural convective flows. Elder (1966a) observes that with a maximum flux velocity of 10^{-4} cm/sec and a gap size of 1 mm, the Reynolds number is typically of the order 10^{-3}. It should also be remembered that a low Reynolds number was a prerequisite for the assumptions made earlier, that dispersion effects may be ignored and that Darcy's Law is valid.

As a consequence of Darcy's Law, the pressure and viscous terms are of similar order of magnitude, and the appearance of convective flows in this problem indicates that the buoyancy effects are capable of overcoming viscous dissipation and therefore both pressure and buoyancy terms must remain in the momentum equation. By this argument, equations (2.1.8) reduce to

$$g_i\left(\frac{\rho-\rho_o}{\rho_o}\right) + \frac{1}{\rho_o}\frac{\partial p}{\partial x_i} + \frac{\nu}{k} q_i = 0 \qquad (2.1.10)$$

Non-Dimensionalisation

The equations may now be expressed in non-dimensional form, following a similar analysis to that of Torrance (1968), by introducing the new variables

$$\tau = (\kappa/a^2)t \ ,$$

$$X_i = \frac{x_i}{a} \ ,$$

$$P = \left(\frac{a^2}{\rho_o \kappa^2}\right) p \ ,$$

$$U_i = \left(\frac{a}{\kappa}\right) q_i \ ,$$

$$\theta = \frac{T-T_o}{T_1-T_o} = \frac{T-T_o}{\Delta T} \ ,$$

$$\rho' = \frac{\rho}{\rho_o} \ ,$$

and $\nu' = \frac{\nu}{\nu_o}$,

after which the equations become

$$\frac{\partial U}{\partial X_i} = 0 \ , \qquad (2.1.11)$$

$$\frac{\partial P}{\partial X_i} + \frac{g_i a^3}{\kappa^2}(\rho'-1) + \frac{\nu a^2}{k\kappa}\nu' U_i = 0 \ , \qquad (2.1.12)$$

and $$\frac{\partial \theta}{\partial \tau} + \lambda U_j \frac{\partial \theta}{\partial x_j} = \nabla^2\theta \ , \qquad (2.1.13)$$

where now $\nabla^2 \equiv \frac{\partial^2}{\partial X^2} + \frac{\partial^2}{\partial Y^2} + \frac{\partial^2}{\partial Z^2}$.

Introducing the relations

$$\alpha = \frac{\alpha_2}{\alpha_1} \Delta T \quad ,$$

$$\text{and} \quad \beta(\theta) = 1+b_1(\theta.\Delta T)+b_2(\theta.\Delta T)^2+b_3(\theta.\Delta T)^3 \quad ,$$

$$\text{or} \quad \beta(\theta) = 1+\beta_1\theta+\beta_2\theta^2+\beta_3\theta^3 \quad ,$$

and expressing the density and viscosity variations in full,

$$\rho' = 1 - \alpha_1(\theta.\Delta T) - \alpha_2(\theta.\Delta T)^2 \quad , \qquad (2.1.14)$$

$$\text{and} \quad \nu' = \frac{1}{\beta(\theta)} \quad , \qquad (2.1.15)$$

then the momentum equations become,

$$\frac{\partial P}{\partial X_i} = \frac{g_i \alpha_1 a^2 \Delta T}{\kappa^2}(\theta+\alpha\theta^2) - \frac{\nu_o a^2}{k\kappa}\frac{U_i}{\beta(\theta)} \quad . \qquad (2.1.16)$$

Redefining $P^* = \frac{k\kappa}{a^2\nu_o} P$,

and rewriting **(2.1.16)**, dropping the stars immediately for convenience, then

$$\frac{\partial P}{\partial X_i} = \frac{R}{\lambda}(\theta+\alpha\theta^2) - \frac{U_i}{\beta(\theta)} \quad , \qquad (2.1.17)$$

where R is known as the Rayleigh number and is defined by

$$R = \frac{g_i a k(T_1-T_o)\alpha_1}{\kappa \nu_o}\lambda \quad . \qquad (2.1.18)$$

This definition differs to that of earlier authors (e.g. Elder 1966a) due to the inclusion of the term λ which is necessary for the correct representation of the heat content of the solid/liquid combination. Equations **(2.1.11)**, (2.1.17) and **(2.1.13)** are now the governing equations of the flow,

The Rayleigh Number

As R increases from below a critical value of R_c ($4\pi^2$ **for** the region considered by Lapwood 1948), the flow process changes from conduction to convection. This transition has already received some attention from Katto and Masuoka (1967) Westbrook (1969), Beck (1972) and Busse and Joseph (1972) and is not of particular interest in this investigation. However the second transition discovered by Combarnous and Le Fur (1969) in the range 240-280 has been shown by Caltagirone et al. (1971) to mark the first appearance of the fluctuating convective state.

This transition is below the range of values of R that is considered likely in geothermal regions (10^3-10^4). The uncertainty in this figure is due to the difficulty in determining the medium properties at depth. A range of values between **0** and **2000** is considered here as this includes both known regime transitions.

It should be noted that the Rayleigh defined by (2.1.18) is based upon the ***cold water*** viscosity, as has generally been the case in modelling of hydro-thermal systems. However the added complication of variable viscosity gives the Rayleigh number a new meaning; with a temperature differential of 250°C the effective local Rayleigh number close to the heater may be ten times the apparent "cold water" value. Therefore in solutions generated using a variable viscosity model the Rayleigh number considered must be much smaller to maintain the character of the flows (to maintain consistency with previous work all the values cited above are for the *constant* viscosity case).

2.2 BOUNDARY CONDITIONS

There are two types of boundary conditions to be employed here, thermal conditions (temperature) and fluid conditions (velocity and pressure). The fluid boundaries are also divided into two sub-types, enclosed boundaries and those through which fluid may pass freely (hereafter kncwn a recharge boundaries).

Temperature Conditions

Heat input at the base is achieved by using an isothermal condition

$$\theta\big|_{Y=0} = f(X,Z) \quad . \tag{2.2.1}$$

At ground level heat is lost by convective transfer to the atmosphere at a rate proportional to the difference between the ground and air temperatures,

$$-k_c \frac{\partial T}{\partial Y}\bigg|_{Y=1} = h(T-T_o) \quad , \tag{2.2.2}$$

where k_c is the conductivity of the fluid saturated material and h is the convective heat loss coefficient. Now for a saturated medium k_c is typically 3×10^{-3} cal/cm/sec/°C , for a horizontal ground surface h is of the order of 2×10^{2} cal/cm^2/sec/°C and in geothermal regions the average temperature gradient is of order 5×10^{-3} °C/cm. Therefore to maintain a balance between the two types of heat transfer in (2.2.2), the temperature difference between ground and air must be extremely small. It is found in calculations using the exact condition that for a closed surface the maximum temperature gradient $\frac{\partial T}{\partial Y}\big|_{Y=1}$ is such that $(T-T_o)$ is at most of order 10^{-5} °C while for recharge surfaces it may reach 10^{-4} °C. Therefore it is satisfactory to employ a simpler boundary condition $T=T_o$ or $\theta=0$, as if the atmosphere were an infinite heat sink.

The impermeable side walls confining the porous region are of relatively low thermal conductivity, particularly for flows in which convective heat transfer may be expected to dominate, as is the case for Rayleigh numbers above R_c .

Therefore these vertical walls act approximately like insulated boundaries and the temperature gradient normal to the boundary is taken to be zero. This zero gradient condition allows these boundaries to be considered lines of symmetry in which case the region may be imagined to be extended in either direction normal to the boundary by the addition of "mirror-images" of the flow within these boundaries.

Enclosed Boundaries

The simplest and most commonly considered model is that having closed boundaries. In this case the flow of fluid into or out of the problem region is prohibited by requiring that the velocity normal to all boundaries be zero. This configuration is not an accurate representation of Wairakei or of the many other real systems where groundwater flow does occur near to the surface and possibly also at the base of the formation. However below the surface the Waiora aquifer at Wairakei is overlain by the less permeable Huka Falls aquitard, so the closed boundary model does have some practical foundation. Its main use however is in providing a comprehensive array of solutions that may be compared to the many earlier experimental analyses for such a region (in particular the unsteady solutions of Caltagirone et al. 1971), and which provide an insight into the flow processes without unnecessary complications.

Recharge Boundaries

Fluid may enter or leave geothermal areas by either natural or artificial processes. At Wairakei there is significant natural discharge and recharge of surface water, at a rate of 440 kg/sec (Fisher 1964). The artificial removal of fluid through boreholes takes place at rate 4–5 times that of the natural discharge and provides the fundamental means of energy retrieval from the system. With such prominent flows as these it is desirable to avoid the restriction of a closed boundary model and allow fluid to flow freely into or out of the upper boundary of the model. This represents the natural conditions and provides a recharge source for the fluid sinks in the models of the exploited field that are considered later. Such a natural recharge condition has been modelled previously in the quasi-steady, low Rayleigh number analysis by Elder (1967a) and a more artificial condition by Donaldson (1962) who considered a specific surface outflow.

The recharge condition is incorporated by specifying that the pressure at the surface is uniform (i.e. atmospheric) and it is then a consequence of Darcy's Law (equation 2.1.2) that the velocity tangential to the horizontal surface is zero.

2.3 TWO-DIMENSIONAL REGIONS

Justification

As has been described in section 1.2, the Wairakei geothermal system is situated in a trench of porous rock that is much longer than it is wide or deep. Taking the length of the rectangular trench model to be infinite, and assuming that the flow is unvarying in this dimension, allows the governing equations to be redefined in only two dimensions, although this must be done with caution. Beck (1972) has used an energy method to show that at low Rayleigh numbers just above the critical value, the most favoured mode of flow in a box of porous material would be two-dimensional rolls. This has been confirmed for long regions by Holst and Aziz (1972b) at higher Rayleigh numbers, but it is not certain that this would always be so. For wider porous layers Bories, Combarnous and Jaffrenou. (1972) have found experimentally that as the Rayleigh number is increased the preferred mode is initially polyhedral cells, and only later as the Rayleigh number increases above 280 are purely two-dimensional effects (unsteady rolls) observed. These fluctuating two-dimensional rolls have been frequently reported in three-dimensional experimental regions by various French authors - Caltagirone et al. (1971), Combarnous and Bia (1971), Bories, Combarnous and Jaffrenou (1972) and Bories and Combarnous (1973), and as these unsteady solutions are of particular interest in this work it is legitimate, at least for the initial appraisal of the problem, to use a simplified two-dimensional form of the governing equations. Three-dimensional effects undoubtedly do occur in both the real situation and in theoretical models, as has been shown numerically by Holst and Aziz (1972b), experimentally by Bories and Thirriot (1969) and analytically by Straus (1974), therefore for completeness a three-dimensional exploration of the two-dimensional solutions is necessary. However, the two-dimensional flows are more simply and more economically simulated and therefore have been more extensively studied here than the three-dimensional flows.

The Governing Equations

The equations of motion written in two-dimensional form are

$$\frac{\partial U}{\partial X} + \frac{\partial V}{\partial Y} = 0 \quad , \tag{2.3.1}$$

$$\frac{\partial P}{\partial X} = -\frac{U}{\beta(\theta)} \quad , \tag{2.3.2}$$

$$\frac{\partial P}{\partial Y} = \frac{R}{\lambda}(\theta+\alpha\theta^2) - \frac{V}{\beta(\theta)} \quad , \tag{2.3.3}$$

$$\text{and} \quad \frac{\partial \theta}{\partial \tau} = \nabla^2\theta - \lambda\left(U\frac{\partial \theta}{\partial X} + V\frac{\partial \theta}{\partial Y}\right) \quad , \tag{2.3.4}$$

where now $\nabla^2 \equiv \frac{\partial^2}{\partial X^2} + \frac{\partial^2}{\partial Y^2}$.

The pressure may be eliminated from (2.3.2) and (2.3.3) by cross-differentiation and subtraction, reducing the equations to

$$\frac{R}{\lambda}(1+2\alpha\theta)\frac{\partial \theta}{\partial X} + \left(\frac{\partial U}{\partial Y} - \frac{\partial V}{\partial X}\right)\frac{1}{\beta(\theta)} + \left(V\frac{\partial \theta}{\partial X} - U\frac{\partial \theta}{\partial Y}\right)\frac{\beta'(\theta)}{[\beta(\theta)]^2} = 0 \quad . \tag{2.3.5}$$

Now, the continuity equation (2.3.1) may be satisfied identically in the usual way (Yih **1969 p.14)** by defining a stream function ψ **,** such that

$$U = \frac{R}{\lambda} \frac{\partial \psi}{\partial Y} \quad , \qquad \text{(2.3.6)}$$

$$\text{and} \quad V = -\frac{R}{\lambda} \frac{\partial \psi}{\partial X} \quad ,$$

after which **(2.3.5)** becomes

$$\nabla^2 \psi = -(1+2\alpha\theta) \frac{\partial \theta}{\partial X} \beta(\theta) + \left(\frac{\partial \psi}{\partial X} \frac{\partial \theta}{\partial X} + \frac{\partial \psi}{\partial Y} \frac{\partial \theta}{\partial Y}\right) \frac{\beta'(\theta)}{\beta(\theta)} \quad , \qquad \text{(2.3.7)}$$

and (2.3.4) becomes

$$\frac{\partial \theta}{\partial \tau} = \nabla^2 \theta - R\left(\frac{\partial \psi}{\partial Y} \frac{\partial \theta}{\partial X} - \frac{\partial \psi}{\partial X} \frac{\partial \theta}{\partial Y}\right) \quad . \qquad \text{(2.3.8)}$$

Stream Function Equation Reformulation

Although in this form **(2.3.7)** and **(2.3.8)** are a suitable pair of governing equations for the flow, it turns out that the products of first derivatives in **(2.3.7)** are in a form that is difficult to represent satisfactorily numerically (see section **4.2) so** it is beneficial to reformulate them replacing **(2.3.7)** by coupled equations in ψ and **P .**

The non-linear terms

$$\frac{\partial \psi}{\partial X} \frac{\partial \theta}{\partial X} + \frac{\partial \psi}{\partial Y} \frac{\partial \theta}{\partial Y}$$

in **(2.3.7)** originate from the term

$$\left(V \frac{\partial \theta}{\partial X} - U \frac{\partial \theta}{\partial Y}\right) \frac{1}{\beta(\theta)}$$

in **(2.3.5)** which may be rewritten in Jacobian form as

$$-(\theta+\alpha\theta^2) \frac{\partial \theta}{\partial X} + \frac{\lambda}{R} \left(\frac{\partial P}{\partial Y} \frac{\partial \theta}{\partial X} - \frac{\partial P}{\partial X} \frac{\partial \theta}{\partial Y} \right)$$

by substitution of **U** and V from **(2.3.2)** and **(2.3.3).** If **(2.3.2)** and **(2.3.3)** are differentiated and added then, by using **(2.3.1)** also, a single equation for the pressure is obtained,

$$\nabla^2 P = \frac{R}{\lambda} (1+2\alpha\theta) \frac{\partial \theta}{\partial Y} - \frac{R}{\lambda} \delta(\psi,\theta) \frac{\beta'(\theta)}{[\beta(\theta)]^2} \quad ,$$

$$\text{where} \quad \delta(\psi,\theta) \equiv \frac{\partial \psi}{\partial X} \frac{\partial \theta}{\partial Y} - \frac{\partial \psi}{\partial Y} \frac{\partial \theta}{\partial X} \quad .$$

If **P** is now scaled by a factor A/R then **(2.3.7)** finally becomes

$$\nabla^2 \psi = -\frac{\partial \theta}{\partial X} [(1+2\alpha\theta)\beta(\theta) + \theta(1+\alpha\theta)\beta'(\theta)] - \delta(P,\theta)\beta'(\theta) \quad . \qquad \text{(2.3.9)}$$

The pressure is defined by

$$\nabla^2 P = (1+2\alpha\theta)\frac{\partial\theta}{\partial Y} + \delta(\psi,\theta)\frac{\beta'(\theta)}{[\beta(\theta)]^2} \quad , \tag{2.3.10}$$

and the same heat transport equation (2.3.8) completes the governing set of three equations.

The Constant Viscosity Model

A special case of these equations is the simple linearly dependent density and constant viscosity model which has α_2 zero and b_1, b_2 and b_3 all zero. This means that $\alpha=0$, $\beta(\theta)=1$ and $\beta'(\theta)=0$, therefore equation (2.3.7) reduces to

$$\nabla^2\psi = -\frac{\partial\theta}{\partial X} \quad , \tag{2.3.11}$$

and there are just two governing equations again since the heat transport equation (2.3.8) *is* unchanged and the pressure equation (2.3.10) is now no longer needed since the reformulation of the stream function equation (2.3.7) is unnecessary. Alternatively the stream function may be eliminated in favour of a pressure formulation although this is harder to represent numerically. Whichever formulation is used, this simpler model produces results that are qualitatively similar to the more precise variable viscosity model (see section 5.5) which requires a more complicated numerical solution technique.

Thermal Boundary Conditions

The heat input distribution at the lower boundary is represented as a fraction f of the base held at an elevated temperature $\theta=1$ and the remainder at the lower temperature $\theta=0$. Thus the form of the thermal boundary conditions introduced in section 2.2 that is relevant to two-dimensional regions is

$$\theta\Big|_{Y=0} = \begin{cases} 1 & 0 \le X \le f \\ 0 & f < X < 1 \end{cases} \quad , \tag{2.3.12}$$

$$\text{and} \quad \theta\Big|_{Y=1} = 0 \quad , \tag{2.3.13}$$

on the horizontal boundaries and

$$\frac{\partial\theta}{\partial X}\Big|_{X=0,1} = 0 \quad , \tag{2.3.14}$$

on the insulated vertical boundaries.

Fluid Boundary Conditions

As a consequence of (2.3.6), the zero normal velocity condition on impermeable boundaries implies that the stream function is constant (arbitrarily zero),

$\psi = 0$ on all closed boundaries.

Furthermore the zero tangential velocity on recharge boundaries implies that the gradient normal to these boundaries is zero,

$\frac{\partial \psi}{\partial Y} = 0$ on (horizontal) open boundaries.

Pressure Boundary Conditions

When using the variable viscosity model a set of pressure boundary conditions is also required, for the solution of (2.3.10). These conditions are derived from the substitution of the fluid boundary conditions into (2.3.2) and (2.3.3) and are

$\frac{\partial P}{\partial X} = 0$ on vertical boundaries,

$\frac{\partial P}{\partial Y} = (\theta + \alpha\theta^2)$ on closed horizontal boundaries,

and $P = O$ on recharge horizontal boundaries.

Boundary conditions for a simple, enclosed, two-dimensional, constant viscosity model are illustrated in figure 2.3.1.

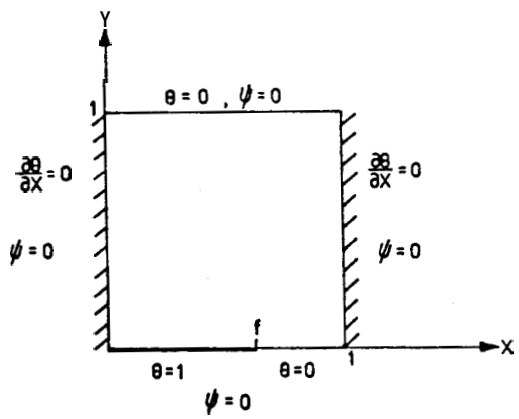

FIGURE 2.3.1 - Boundary conditions for an enclosed, two-dimensional, constant viscosity model.

Taking the divergence of **(2.4.2)** and substituting continuity **(2.4.1)**

$$\nabla^2 P = \frac{R}{X} \frac{\partial \theta}{\partial Y} ,$$

or scaling the pressure by $\frac{R}{\lambda}$,

$$\nabla^2 P = \frac{\partial \theta}{\partial Y} . \qquad (2.4.4)$$

The velocity vector may be eliminated between **(2.4.2)** and **(2.4.3)** such that

$$\frac{\partial \theta}{\partial \tau} = \nabla^2 \theta + R \frac{\partial P}{\partial \underset{\sim}{X}} \cdot \frac{\partial \theta}{\partial \underset{\sim}{X}} - R\theta \frac{\partial \theta}{\partial Y} . \qquad (2.4.5)$$

These last two equations are then the governing pair for the problem, in a form described here as the *pressure formutation.* For reasons which are explained later (section **4.2)** this form is not always satisfactory for numerical representations.

The Vector Potential Formulation

Due to the solenoidal form of $\underset{\sim}{U}$ in **(2.4.1)**, there is an alternative formulation described by Holst and Aziz (1972b), in which a vector potential $\underset{\sim}{\phi}$ may be introduced such that

$$\frac{X}{R} \underset{\sim}{U} = \nabla \times \underset{\sim}{\phi} \qquad (2.4.6)$$

Then, taking the curl of equation **(2.4.2)**,

$$\frac{\lambda}{R} (\nabla \times \underset{\sim}{U}) = \nabla \times (\underset{\sim}{j}\, \theta) \quad \text{since} \quad \nabla \times \nabla P = 0 ,$$

$$\text{or} \quad \frac{\lambda}{R} (\nabla \times \underset{\sim}{U}) = \left(-\frac{\partial \theta}{\partial z}, 0, \frac{\partial \theta}{\partial x}\right) .$$

Now, from its definition $\underset{\sim}{\phi}$ is arbitrary to the gradient of a scalar, hence it is possible to specify

$$\nabla . \underset{\sim}{\phi} = 0$$

in the identify $\nabla \times \nabla \times \underset{\sim}{\phi} = \nabla(\nabla . \underset{\sim}{\phi}) - \nabla^2 \underset{\sim}{\phi}$,

whence $$\nabla^2 \underset{\sim}{\phi} = \left(\frac{\partial \theta}{\partial z}, 0, -\frac{\partial \theta}{\partial x}\right). \qquad (2.4.7)$$

Boundary Conditions

As in the two-dimensional formulation the boundary conditions on the pressure are, for closed boundaries

$$\frac{\partial P}{\partial \underset{\sim}{n}} = 0 , \qquad (2.4.8)$$

where $\underset{\sim}{n}$ **is** an outward pointing normal, and for recharge boundaries

$$P = 0 , \qquad (2.4.9)$$

The Heated Fraction f

The value of the parameter f is significant in this investigation as the variation of the lower temperature distribution highlights the influences that boundary conditions have on this particular type of flow problem, These effects have not so far been reported by other authors. When f=1 the boundary is uniformly heated, which is the classic configuration considered for either the enclosed or the semi-infinite porous layer by Horton and Rogers (1945), Lapwood (1948), Wooding (1957), Donaldson (1962), McNabb (1965), Elder (1966a, 1967 a & b, 1968), Katto and Masuoka (1967), Westbrook (1959), Combarnous and Le Fur (1969), Combarnous (1970), Bories and Thirriot (1969), Combarnous and Bia (1971), Caltagirone et al. (1971), Palm, Weber and Kvernvold (1972), Beck (1972), Busse and Joseph (1972), Holst and Aziz (1972 a & b), Gupta and Joseph (1973), Combarnous and Bories (1974), Yen (1974) and Straus (1974). In this form the problem is symmetrical and lends itself well to several different methods of solution, and the authors referenced above have used a variety of experimental, numerical and analytical techniques. Although this uniformly heated problem has been extensively investigated, the range of solutions is not yet exhaustive. In particular the contradictory experimental results of Caltagirone et al. (1969) and Yen (1974) suggest further examination of the problem.

Despite the attention paid to it the uniform heat input boundary condition may be of limited practical significance since the nature of the physical heat source is unknown, but may not be so benevolently uniform. If the lower boundary is heated non-uniformly (i.e. $f < 1$) the symmetry of the uniform problem is lost and the range of solution techniques is restricted to numerical or experimental simulations.

2.4 THREE-DIMENSIONAL REGIONS

The Governing Equations - Pressure Formulation

The solution of the full three-dimensional equations numerically is a very time consuming procedure and it is therefore expedient to use the simplest possible form of the governing equations. Therefore the assumption of constant viscosity is made and the equations (2.1.11), (2.1.17) and (2.1.13), rewritten in vector form, become

$$\nabla . \underset{\sim}{U} = 0 \quad , \tag{2.4.1}$$

$$\underset{\sim}{U} = \frac{R}{\lambda} (\underset{\sim}{j}\, \theta) - \nabla P \quad , \tag{2.4.2}$$

where $\underset{\sim}{j}$ is the unit vector pointing vertically upwards,

and $$\frac{\partial \theta}{\partial \tau} = \nabla^2 \theta - \lambda \underset{\sim}{U} . \frac{\partial \theta}{\partial \underset{\sim}{X}} \quad . \tag{2.4.3}$$

In the enclosed region the boundary conditions on the flow field are, as before, that the velocity normal to the boundary is zero. For instance on the planes X=0,1 the velocity component U is zero, which from equation (2.4.6) implies that potential components ϕ_2 and ϕ_3 are linear functions of Z and Y respectively. Following around the remaining boundary planes and avoiding inconsistencies on the edges it turns out that ϕ_2 and ϕ_3 must both be constant (arbitrarily zero) on X=0,1 . Due to the solenoidal property of $\underset{\sim}{\phi}$ it is then a consequence that the normal gradient of ϕ_1 must also be zero. Thus for a cubic region the boundary conditions on $\underset{\sim}{\phi}$ are,

$$\begin{aligned} \frac{\partial \phi_1}{\partial X} &= \phi_2 = \phi_3 = 0 \qquad X = 0,1, \\ \frac{\partial \phi_2}{\partial Y} &= \phi_1 = \phi_3 = 0 \qquad Y = 0,1, \\ \frac{\partial \phi_3}{\partial Z} &= \phi_1 = \phi_2 = 0 \qquad Z = 0,1, \end{aligned} \tag{2.4.10}$$

for closed boundaries, while on a horizontal recharge boundary

$$\frac{\partial \phi_1}{\partial Y} = \frac{\partial \phi_3}{\partial Y} = 0 \quad .$$

As a consequence of equation (2.4.7) and the boundary conditions (2.4.10) the component ϕ_2 of the vector potential is zero everywhere within the region. Thus the final form of the vector potential equations may now be written

$$\nabla^2 \phi_1 = \frac{\partial \theta}{\partial Z} \quad , \tag{2.4.11}$$

$$\nabla^2 \phi_3 = - \frac{\partial \theta}{\partial X} \quad , \tag{2.4.12}$$

$$\text{and} \quad \frac{\partial \theta}{\partial \tau} = \nabla^2 \theta - R\left(\frac{\partial \phi_3}{\partial Y} \frac{\partial \theta}{\partial X} - \frac{\partial \phi_3}{\partial X} \frac{\partial \theta}{\partial Y} + \frac{\partial \phi_1}{\partial Z} \frac{\partial \theta}{\partial Y} - \frac{\partial \phi_1}{\partial Y} \frac{\partial \theta}{\partial Z}\right) \quad . \tag{2.4.13}$$

2.5 FLUID SINKS AND SOURCES

Sinks on Vertical Boundaries

Should a fluid sink (or source) be present in a two-dimensional region, further conditions are necessary to include it in the model. The simplest case is a sink of strength q on one of the vertical boundaries, say at a point $(0, Y_o)$, then the boundary condition is

$$\psi|_{X=0} = - q \qquad Y_o < Y \leq 1 \quad , \tag{2.5.1}$$

resulting in a normal velocity of

$$U_{sink} = \frac{\Delta\psi}{\Delta Y} = -\frac{q}{\Delta Y} \quad , \qquad (2.5.2)$$

and a volume discharge of

$$\int_{\Delta Y} |U_{sink}| dY = q \quad . \qquad (2.5.3)$$

Clearly if ψ is still zero at the top of the vertical boundary on which there is no sink, then the condition (2.5.1) is only valid if ψ is variable along the top horizontal boundary. Therefore it is always necessary to include a recharge boundary at the surface if a sink is present, in order to allow the satisfaction of overall conservation of mass.

Sinks or Sources Within the Boundaries

If the sink lies strictly inside the region, say at a point (X_o, Y_o), then an alternative formulation is required. Using the constant viscosity model equations as a base, but without introducing the stream function, then the governing equations become:

$$\frac{\partial U}{\partial X} + \frac{\partial V}{\partial Y} = g(X,Y) \qquad (2.5.4)$$

where g(X,Y) represents flow to the sink,

$$\frac{\partial P}{\partial X} = -U \quad , \qquad (2.5.5)$$

$$\frac{\partial P}{\partial Y} = \frac{R}{\lambda}\theta - V \quad , \qquad (2.5.6)$$

and $$\frac{\partial \theta}{\partial \tau} = \nabla^2\theta - a\left[U\frac{\partial \theta}{\partial X} + V\frac{\partial \theta}{\partial Y}\right] \quad . \qquad (2.5.7)$$

The boundary conditions are still that U is zero on the vertical boundaries, V is zero on the lower horizontal boundary and P is zero on the upper (recharge) horizontal boundary.

In order to accommodate the singular nature of the flow the velocity field is separated into parts, one which defines the flow of fluid into a point sink in an infinite space and another which both represents the convective flow and satisfies the finite physical boundary conditions. These two fields are superposed such that

$$U = u + u' \quad ,$$
$$\text{and} \quad V = v + v' \quad ,$$

where u and v are the sink velocities and obey the relationship

$$\frac{\partial u}{\partial x} + \frac{\partial v}{\partial y} = g(X, Y) \quad .$$

The velocities u' and v' must then satisfy

$$\frac{\partial u'}{\partial x} + \frac{\partial v'}{\partial y} = 0$$

and be consistent with the modified boundary conditions that are a superposition of the real conditions and the false boundary flux due to u and v .

The stream function may then be defined as before, except that now

$$u' = \frac{R}{A} \frac{\partial \psi}{\partial Y} ,$$

and $$v' = - \frac{R}{A} \frac{\partial \psi}{\partial X} ,$$

and the flow equation becomes

$$\nabla^2 \psi = - \frac{\partial \theta}{\partial X} + \frac{\lambda}{R} \left(\frac{\partial v}{\partial X} - \frac{\partial u}{\partial Y} \right) . \qquad (2.5.8)$$

The heat transport equation (2.5.7) is then

$$\frac{\partial \theta}{\partial \tau} = \nabla^2 \theta - R.\delta(\psi,\theta) - \lambda \left[\frac{\partial (u\theta)}{\partial X} + \frac{\partial (v\theta)}{\partial Y} - \theta.g(X,Y) \right] . \qquad (2.5.9)$$

The stream function boundary conditions are, on the three closed boundaries

$$\psi = g(X,Y) , \qquad (2.5.10)$$

and on the top recharge boundary

$$\frac{\partial \psi}{\partial Y} = - u . \qquad (2.5.11)$$

For a point sink of strength q at location (X_o, Y_o) the sink flow is defined by

$$u = - \frac{q}{2\pi} \frac{\cos\theta_o}{r_o} \quad ; \quad v = - \frac{q}{2\pi} \frac{\sin\theta_o}{r_o} , \qquad (2.5.12)$$

$$\text{where } \tan\theta = \frac{Y-Y_o}{X-X_o} , \quad r_o^2 = (X-X_o)^2 + (Y-Y_o)^2 , \qquad (2.5.13)$$

$$\text{and } g(X,Y) = - \frac{q}{2\pi} \left(\frac{2}{r_o^2} - 2 \right) . \qquad (2.5.14)$$

At the sink point (X_o, Y_o) , u and v are undefined and g(X,Y) has a singularity, so it is necessary to take special precautions when representing this point. This may be done by specifying

$$\frac{\partial (u\theta)}{\partial X} + \frac{\partial (v\theta)}{\partial Y} - \theta.g(X,Y) = 0 ,$$

and $$\frac{\partial v}{\partial X} - \frac{\partial u}{\partial Y} = 0$$

at the singularity. These two relationships are consequences of the zero net production of thermal energy and zero net increase in vorticity at the sink. Alternatively this difficulty may be evaded, where finite difference methods are used, by placing the sink at a location that lies strictly between nodes of the grid.

Chapter 3 - EXPERIMENTAL SOLUTION IN TWO-DIMENSIONAL REGIONS

The Experimental Analogy

The two-dimensional flow of fluid through a porous medium is directly analogous to the flow in a Hele-Shaw cell (Wooding **1960).** It is shown by Yih (1969 **p.382)** that the mean flow in a Hele-Shaw cell with plate separation **b** provides a simple analogy to the mean seepage flow through a material with permeability k **= b /12.** Given then. that a fluid moves similarly through the two systems, **it** remains to establish that they are also thermally comparable. This is not strictly so as heat is inevitably lost to the surroundings through the glass plates of the Hele-Shaw cell, introducing temperature gradients in the third spatial direction, and also the heat transfer between solid and liquid phases is different in the porous medium. However, the volumetric ratio of solid to liquid is similar, and by scanning the Bele-Shaw cell with an infra-red "Thermovision" camera **it** was found that the mean temperature through the thicknesses of the glass and the water is comparable with the mean temperature at a similar point in a fluid saturated porous medium as reported by Caltagirone et al. **(1971).** Thus although the plate insulation is not complete and the analogy therefore only an approximate one, the apparatus is useful for indicating salient features of the flow.

Experimental Details

The cell is heated along its base by a copper heating jacket through which hot water is passed at a constant rate for the duration of the experiment. Two input configurations are considered, a fully-heated and a half-heated lower boundary, **or** f = 1.0 and f = 0.5 respectively.

Ti-e upper boundary is a free surface and is therefore a streamline of the flow. Since this surface does not noticeably alter shape from its initial rest condition during the experiments, the upper boundary is analogous *to* the closed horizontal surface in the models proposed in section 2.2. Heat is lost to the air space at the top of the cell and the surface remains approximately isothermal for the duration of the experiments. Motion of the water in the cell is detected by the injection of dye through small holes in one of the plates, generating streaklines which are unfortunately rather diffuse due to the gradual nature of the flow. The temperature throughout the region is visualised with the infra-red camera, giving a direct representation of isotherms as in figure 3.1.

The Results

Two flows are reported, at Rayleigh numbers of approximately **1000** and **1600** for each **of** the two configurations. The uniformly-heated flows develop from an intricate "proto-sub1ayer" similar to that described by Elder **(1968)** as is seen in figure 3.2, and later exhibit the fluctuating behaviour observed by Caltagirone et **a1.(1971),** generating smaller pairs of cells between dominating circulations, as in figure 3.2 and more clearly in figure 3.3.

The flow changes character completely if only half the boundary **is** heated. The pattern soon becomes largely unicellular and instead of irregular fluctuations the behaviour is oscillatory, periodically generating "tongues" of fluid in the ascending and descending regions of the flow. In figure 3.4 **(A** to **F)** these tongues may best be seen by observing the prominent triangular streakline in the lower left of **(A).** In **(B)** the triangle is depressed at the top as the descending tongue begins to develop and impressed at the bottom as an ascending thermal forms over the heater. The triangle is further distorted in **(C)** as the descending disturbance moves across and down, while the thermal, now quite prominent, moves leftwards across the heater. In **(D)** and (E) the upper tongue continues its downward flight while the lower one reaches the left wall and begins to elongate up it. Finally in **(F)** the ascending disturbance has shot rapidly up the left boundary and the descending one has been completely dissipated. At this time the flow is at a similar stage to figure (A). The period **of** this oscillation is approximately *900* seconds in the experiment, which corresponds to a non-dimensional time of **0.003.** The passage of two ascending disturbances is seen in the streakline and isotherm plots of figure **3.5** at a Rayleigh number of **1000** only in this case the descending fluctuations are not apparent.

These results confirm the earlier experimental work of Caltagirone et a1. **(1971)** and appear to refute the assertion of Yen (1974) that the flows are steady. The reason for the contradiction is still not clear, particularly since these experiments are neither exhaustive nor rigorous. Furthermore there is an additional point which requires explanation, namely the reason why the solution is more regular in the half-heated case. In the following chapters an alternative approach is used to confirm the existence ***of*** these effects by representing the flows numerically.

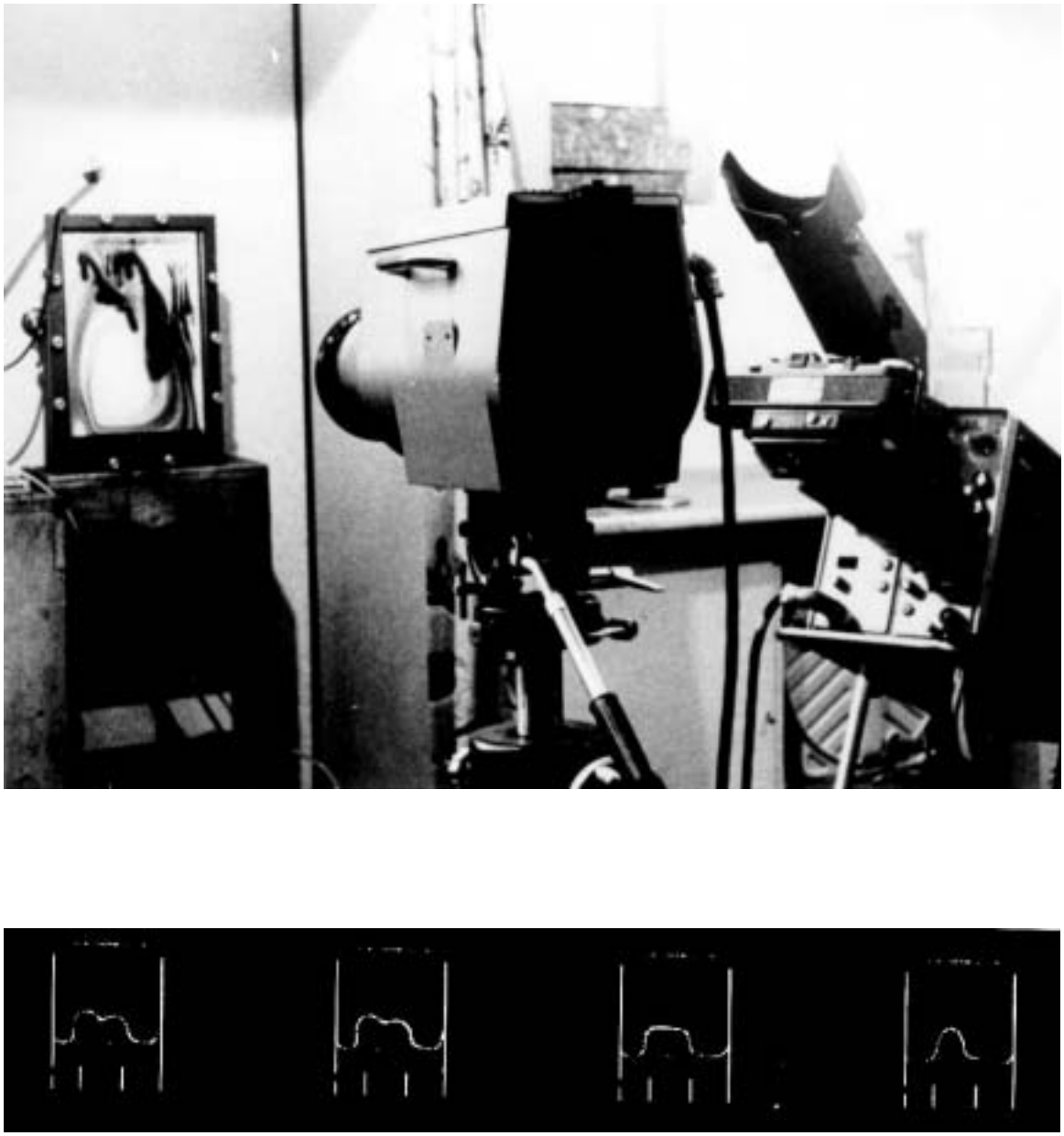

Figure 3.1: The Hele Shaw Cell and the AGA Thermovision Camera and Monitor, and a Typical Set of Thermographs. (This sequence of isotherms follows that of figure 3.3).

Figure 3.2: Experimental Solution for Rayleigh Number of 1600 - Fully Heated Boundary. Sequence recorded at 5 minute intervals.

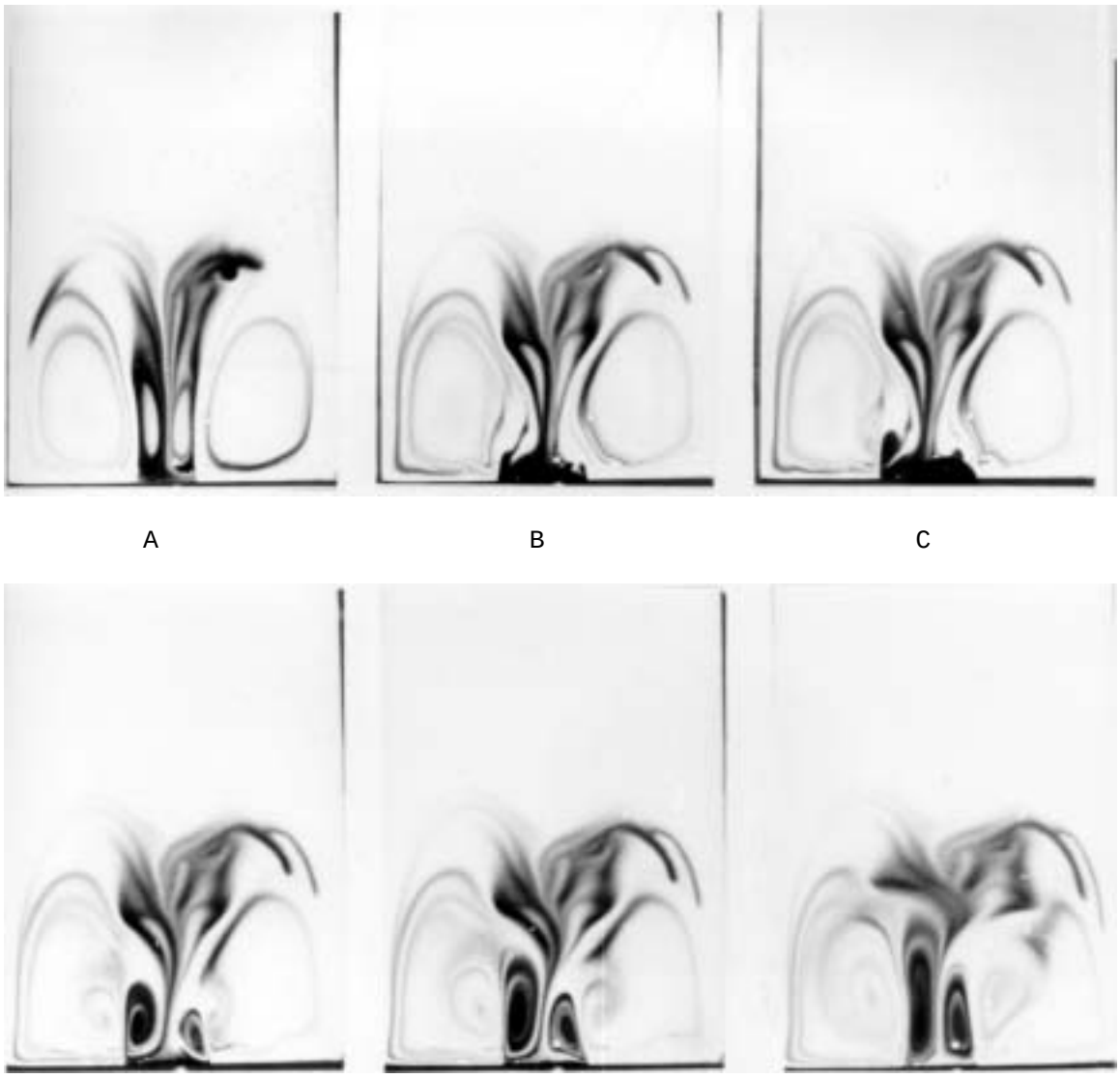

Figure 3.3: Experimental Solution (Streaklines) for Rayleigh Number of 1000 - Fully Heated Boundary.

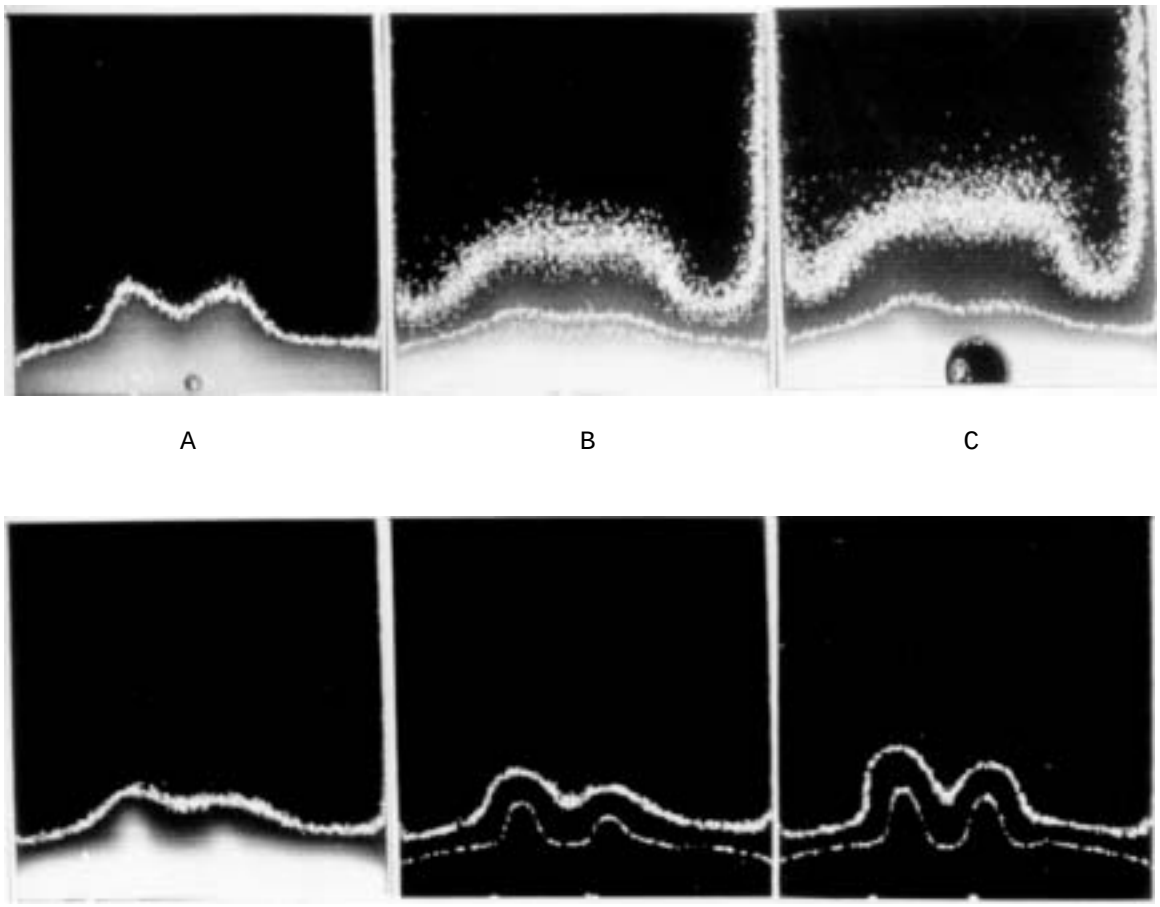

Figure 3.3 contd.: Experimental Solution (Isotherms) for Rayleigh Number of 1000 - Fully Heated Boundary. See figure 3.1 for the continuation of this sequence).

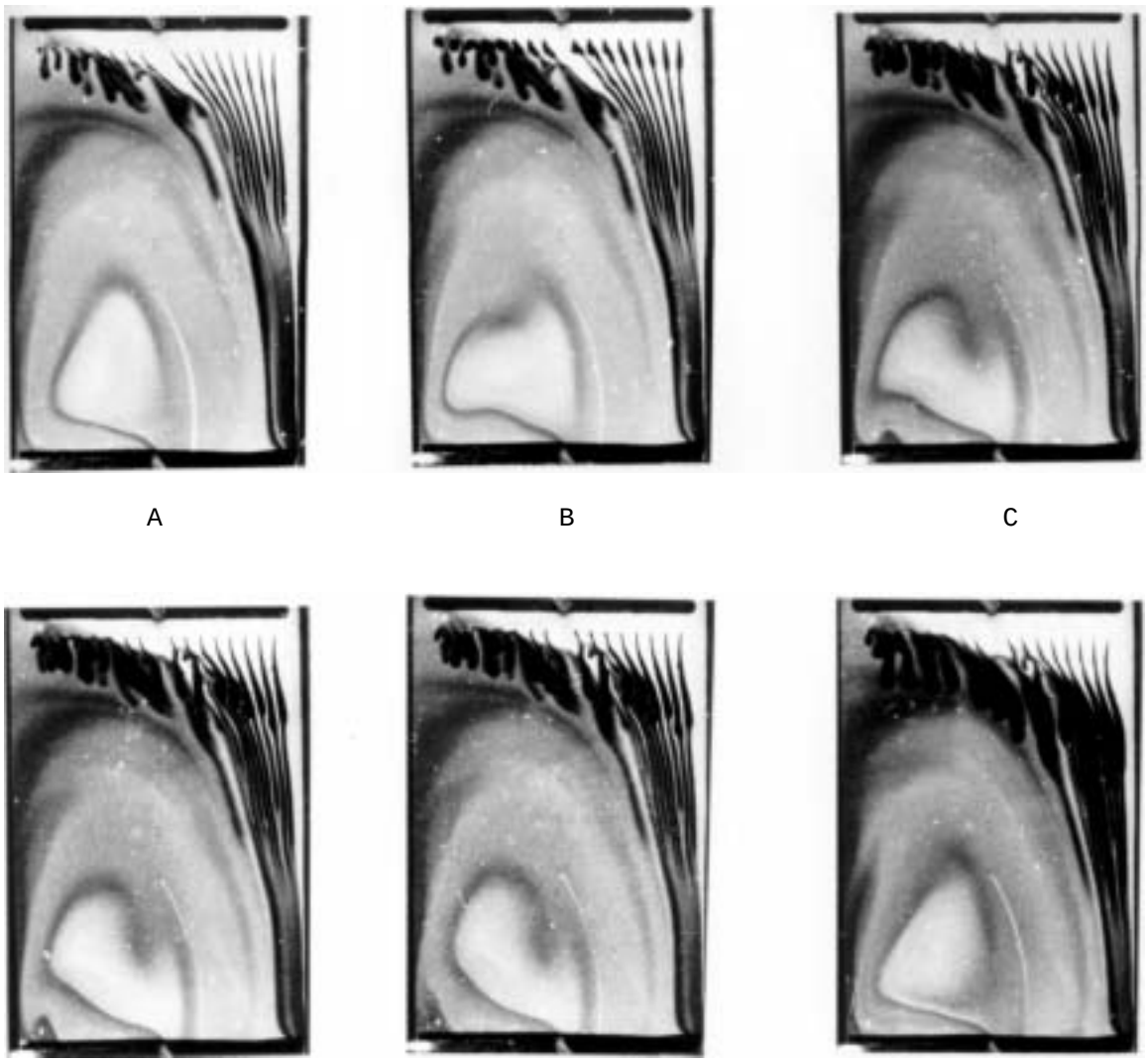

Figure 3.4: Experimental Solution for Rayleigh Number of 1600 - Half Heated Boundary.

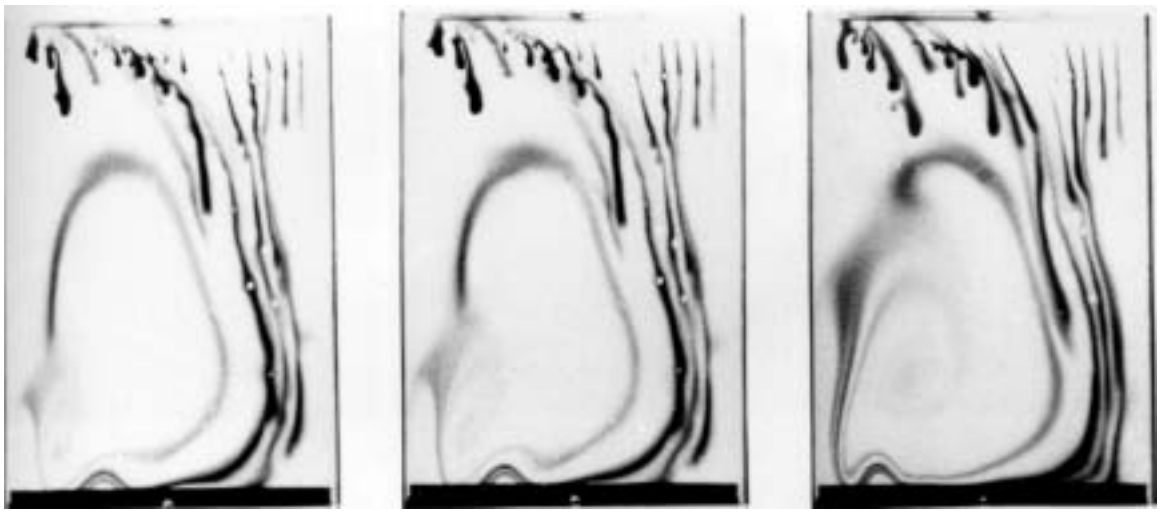

A B C

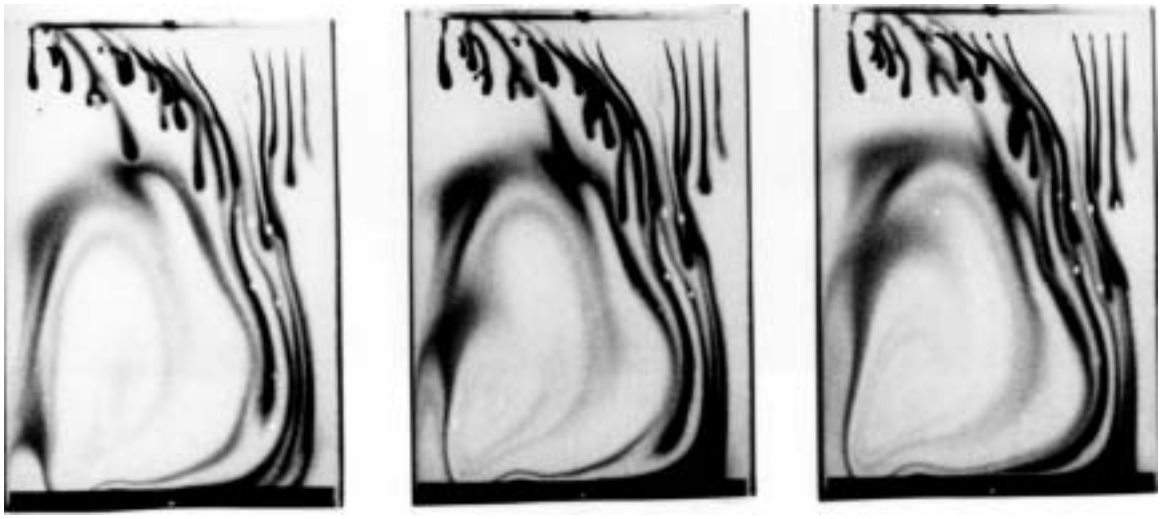

D E F

Figure 3.5: Experimental Solution (Streaklines) for Rayleigh Number of 1000 - Half Heated Boundary.

A B C

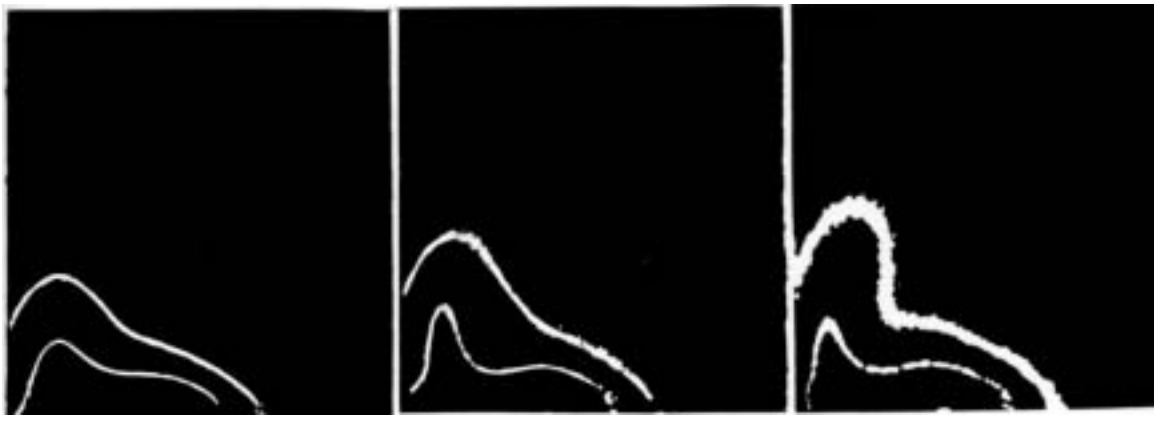

D E F

Figure 3.5 contd.: Experimental Solution (Isotherms) for Rayleigh Number of 1000 - Half Heated Boundary.

Chapter 4 - NUMERICAL METHODS

4.1 PREVIOUS NUMERICAL SOLUTIONS

Caltagirone et al. (1969) discovered the fluctuating flow in convection in a porous medium experimentally, however all earlier and even later numerical studies either found steady solutions or did not continue simulations long enough to determine the true nature of the flow. As was observed in section 1.3, this was largely due to limitations of the numerical techniques employed. The transient analysis by Elder (1967b) is of particular interest since the flow region and the equations of motion are very similar to those proposed here for an enclosed, constant viscosity model. However the numerical techniques used by Elder (1967b) and also those of Holst and Aziz (1972b) (which are described in Aziz and Hellums 1967), namely a successive over-relaxation method for the solution of Poisson's equation and centred differencing for the first derivatives in the heat flow equation, are necessarily an iterative and comparatively slow procedure. Therefore until the application of the more advanced numerical techniques in the present work, numerical exploration into the type of flow examined by Caltagirone et al. (1971) has not been possible. It is interesting to note here that in the Newtonian fluid layer problem the numerical results of Moore and Weiss (1973) superseded those of Fromm (1965) and Veronis (1966) in the description of an oscillatory regime, largely because of the extensive and efficient numerical experiments performed. Moore and Weiss (1973) quote computing times of 5 hours on an IBM 360/44 to perform 4000 time steps of their numerical procedure, but the equations here are simpler and similar runs (on a Burroughs B6700) would take only 50 minutes.

4.2 FINITE DIFFERENCE METHODS

The numerical solution of convection equations is of interest to numerical analysts as well as to fluid dynamicists because of the difficulty in representing them satisfactorily in difference form. Kreiss and Oliger (1973) have examined a wide variety of techniques that are applicable to long time numerical integration, including the finite difference schemes which are considered here.

The Advection Terms

Torrance (1968) gives a summary of several finite difference methods, both explicit and implicit, with special consideration given to the parabolic heat transport equation (in this case equation **2.1.13).** The main difficulty in solving this equation numerically arises from the representation of the non-linear terms. In two dimensions these terms appear in Jacobian form

$$J = \frac{\partial\psi}{\partial Y}\frac{\partial\theta}{\partial X} - \frac{\partial\psi}{\partial X}\frac{\partial\theta}{\partial Y} \quad , \tag{4.2.1}$$

and are generally known as the ***advection*** terms. Arakawa (1966) has explained that **a** simple finite difference approximation using central differences causes numerical instability due to the occurrence of aliasing errors. High order variations in the fields being calculated cannot be resolved between the grid points of *a* finite difference mesh and consequently some lower order variations are represented as having an unrealistically high kinetic energy that physically would have been dissipated by higher order effects. This kinetic energy can be "accumulated" by the numerical procedure and gives rise to the aliasing instability. ***An*** example of such an unstable approximation would be the central difference

$$\left(\frac{\partial\psi}{\partial Y}\frac{\partial\theta}{\partial X}\right)^{n}_{i,j} \simeq \frac{\psi^{n}_{i,j+1}-\psi^{n}_{i,j-1}}{2.\Delta Y} \cdot \frac{\theta^{n}_{i+1,j}-\theta^{n}_{i-1,j}}{2.\Delta X} \quad , \tag{4.2.2}$$

where $\psi^{n}_{i,j} = \psi(i\Delta X, j\Delta Y, n\Delta\tau)$,

$\theta^{n}_{i,j} = \theta(i\Delta X, j\Delta Y, n\Delta\tau)$,

and ΔX, ΔY and $\Delta\tau$ are the spatial and time increments respectively.

In this form the approximation of the advection term does not conserve the kinetic energy of the system, and the numerical solution may produce unrealistically vigorous flows. The false energy which appears in the advection term is partially dissipated by the diffusion term in **(2.1.13)** and thus the effect on the solution is governed by the relative magnitudes of these two terms. Since the advection is multiplied by the Rayleigh number, at larger values of R the diffusion terms are relatively weak. In fact the central differenced solutions are numerically unstable for Rayleigh numbers above 200 and even below that figure have dubious accuracy.

The Arakawa Schemes

To avoid aliasing errors Arakawa (1966) developed nine- and thirteen-point representations of the Jacobian J which conserve the kinetic energy and mean square temperature and which have a truncation error of similar order to the square and fourth power of the spatial increment ΔX (and are accordingly known as the second- and fourth-order Arakawa schemes - see appendix A). Unfortunately the complexity of the representation on both the nine- and thirteen-point templates makes an implicit implementation infeasible and it is therefore necessary to use an explicit method.

The expedience of using Arakawa methods has recently been questioned by Orszag and Iraeli (1974), largely on the grounds of accuracy and efficiency. In particular they suggest that the complexity of the Arakawa scheme means that it is less efficient than a technique using centred differences but with a false dissipation term added, however clearly there is a danger here than in attempting to dissipate the aliasing instability the physical instability will also be misrepresented. Therefore the Arakawa technique is preferable in this case, especially if it is made computationally efficient and the fourth-order scheme is used.

Non-Jacobian Non-Linear Terms

The Arakawa scheme has been derived for products of first derivatives in Jacobian form, and is not generally extendable to non-Jacobian products, for example the terms

$$\frac{\partial P}{\partial \underset{\sim}{X}} \cdot \frac{\partial \theta}{\partial \underset{\sim}{X}} \qquad (4.2.3)$$

which appear in the three-dimensional pressure formulation (equation 2.4.5) or the terms

$$\frac{\partial \psi}{\partial X}\frac{\partial \theta}{\partial X} + \frac{\partial \psi}{\partial Y}\frac{\partial \theta}{\partial Y} \qquad (4.2.4)$$

which appear in the two-dimensional variable viscosity model (equation 2.3.7). The first of these may be avoided by using the alternative vector potential approach (see section 2.4) and the variable viscosity equations may also be reformulated to bring the derivatives into Jacobian form (as was done in section 2.3). However this formulation is more time consuming since the number of governing equations must be increased from two to three.

Alternative Spatial Difference Schemes

Historically the first of these is the "upwind" differencing scheme similar to that of Runchal, Spalding and Wolfshtein (1969) which makes a one-sided difference approximation to the first derivatives in (4.2.1) or (4.2.4), using either forward or backward differencing depending on the direction of fluid flow at the point under consideration. This scheme, with its smaller five-point template, is readily implemented using an A.D.I. (alternating direction implicit) method (Mitchell, 1969, p.60) but has neither the conservation properties nor the precision of either of the Arakawa schemes, being only first-order accurate.

Another method of implementing the upwind differencing scheme is the strongly implicit procedure (S.I.P.) presented by Curry (1974) who uses it with central differences. This method is similar to A.D.I. in that it is an approximate method of solving the complete matrix equation. However, as its name suggests, S.I.P. is more strongly implicit as it solves the fully updated pentadiagonal matrix. It does this by factorising the matrix approximately into tridiagonal

upper and lower triangular matrices and iterating until the product of the factors approaches the true matrix. Although the upwind scheme is less accurate than the second order central differencing methods it is actually less susceptible to numerical instabilities. Therefore it can be used closer to the range of Rayleigh numbers at which the flow is unsteady, however the value of doing this is questionable.

A far more suitable approximation has been suggested by Kreiss and reported in Orszag and Israeli **(1974)**. This Kreiss differencing is fourth order accurate and obtains first derivatives

$$\theta'_i = \left(\frac{\partial \theta}{\partial X} \right)_i$$

by the solution of the tridiagonal system

$$\frac{1}{6} (\theta'_{i-1} + 4\theta'_i + \theta'_{i+1}) = D_o \theta_i$$

where $D_o \theta'_i$ is the central difference approximation to the derivative. This method is "highly recommended" by Orszag and Israeli **(1974)** but unfortunately its stability has yet to be examined and furthermore it is somewhat slower *to* compute than a fourth-order Arakawa implementation. It is useful however in that it can represent non-Jacobian terms such as **(4.2.4)** where the Arakawa schemes cannot.

A summary of the different space differencing methods considered is presented in table **I**, comparing the computation times for calculations of a constant viscosity model using a stream function formulation on a **33 x 33** mesh. The solutions of a simple closed problem at a Rayleigh number of **250** using upwind differencing, the second- and the fourth-order Arakawa methods are compared in figure 4.2.1 to the solution which uses the spectral representation described in section **4.3**.

TABLE I Spatial Differencing Techniques

Differencing	Order of Accuracy	Time/calc.(secs)	Advantages	Disadvantages
Central	Second	1.3	Simple, Implicit	Unstable
Upwind	First	**1.5**	Implicit	Unstable
Arakawa	Second	**1.3**	Stable	Explicit
Arakawa	Fourth	**1.4**	Stable	Explicit
Kreiss	Fourth	**2.2**	Simple	Stability Unknown

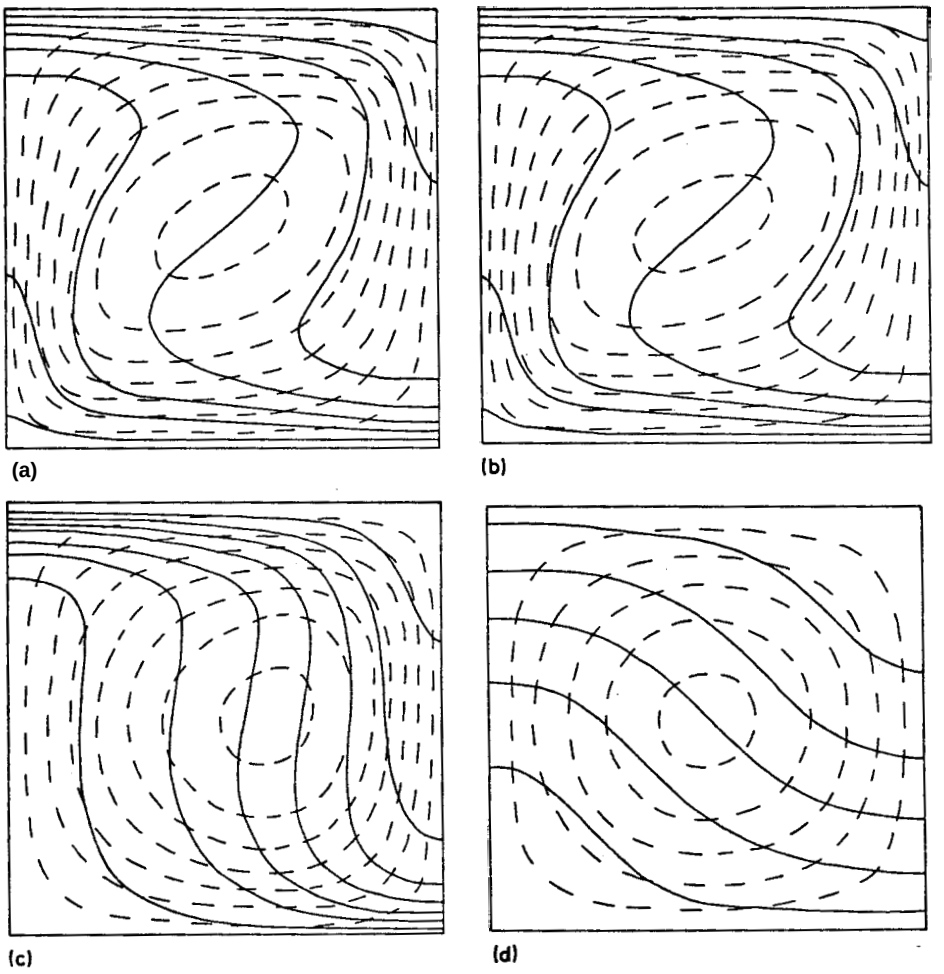

FIGURE 4.2.1 - Comparison of spatial differencing techniques. Solution generated under the same conditions using; (a) Second-order Arakawa differencing, (b) Fourth-order Arakawa differencing, (c) Upwind differencing, (d) Spectral Representation (at earlier time). Isotherms (——) and Streamlines (- - -).

The solutions generated using the spectral representation and upwind differencing methods have been illustrated in figure 4.2.1 before they reached a steady state and are therefore at an earlier time than the other two solutions. This is because the upwind scheme is unstable at this Rayleigh number - at this early stage the scheme has not even preserved the symmetry of the solution and at later times the results become wildly unrealistic. The spectral scheme is so time consuming to use that only a relatively short stage of the flow development can ever be simulated.

The pressure formulation of the equations for the constant viscosity system in the same simple test case has non-Jacobian non-linear terms and is therefore best solved by the Kreiss scheme. Figure 4.2.2 compares the solutions generated using second-order central differencing and fourth-order Kreiss differencing. The solution by the more accurate method is identical to the Arakawa solutions in figure **4.2.1** which'is a notable confirmation **of** the techniques, but the central differencing method is unsatisfactory since it gives totally unrealistic solutions even at the early stage at which the diagram is drawn and quickly becomes unstable at later times.

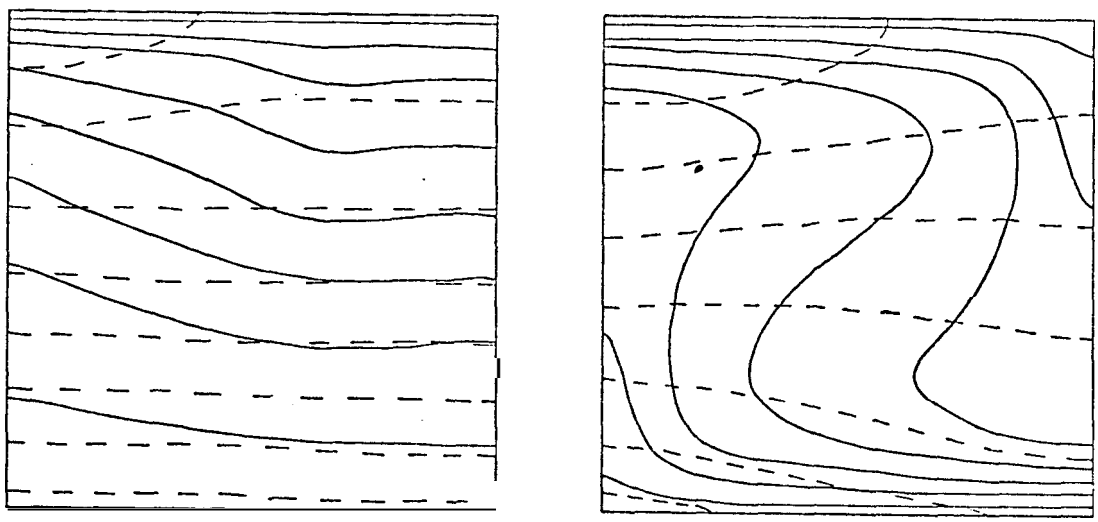

Figure **4.2.2.** - Comparison of spatial differencing techniques for non-Jacobian non-linear terms. Left : Second-order central differencing. Right : Fourth-order Kreiss differencing. Isotherms (——) and pressure isobars (-----)

Time Differencing

After selection of a difference scheme to represent the spatial derivatives, it **is** also necessary **to** approximate the time derivative in the heat transport equation. The simplest time differencing scheme is the first-order accurate forward difference

$$\left(\frac{\partial \theta}{\partial \tau} \right)^{n}_{i,j} \simeq \frac{\theta^{n+1}_{i,j} - \theta^{n}_{i,j}}{\Delta \tau} , \qquad (4.2.5)$$

which has the advantage that it requires only two time levels for its calculation, saving both computer time and memory. The second-order leap-frog method might seem

to be more acceptable, however it has been observed by Orszag and Israeli (1974) to be numerically unstable when used with Arakawa differencing, This instability is due to the solution at odd and even time steps becoming uncoupled, destroying the conservation properties of the Arakawa scheme as it develops in time. An alternative second-order scheme that does not suffer this instability is the Adams-Bashforth method (Lilly 1966) using three time levels,

$$\left(\frac{\partial\theta}{\partial\tau}\right)^{n}_{i,j} \simeq \frac{2}{3}\left(\frac{\theta^{n+1}_{i,j} - \theta^{n}_{i,j}}{\Delta\tau}\right) + \frac{1}{3}\left(\frac{\partial\theta}{\partial\tau}\right)^{n-1}_{i,j}, \qquad (4.2.6)$$

which normally requires about twice as many time steps over a given period to achieve the same accuracy as the leap-frog method (Orszag 1971b).

The fourth-order Runge-Kutta representation described by Carnahan, Luther and Wilkes (1969, p.363) is also applicable, but requires approximately twice as much memory space and is four times as time consuming as the forward difference (4.2.5), since it requires four time levels for each calculation. A more efficient fourth-order scheme is the Hamming predictor-corrector method, also given by Carnahan et al. (1969, p.390), which is faster but requires as much memory and more intricate programming than the Runge-Kutta method.

The time step $\Delta\tau$ must be very small to retain the semi-conservation properties of the space differencing schemes. Therefore for a fixed finite time interval there is little difference between the various time differencing schemes. In fact, comparison of solutions for identical configurations using first-, second- and fourth-order time differencing reveals that the choice of method is immaterial over the number of time steps that are required to simulate the appearance of an oscillatory or fluctuating solution (this is the "worst case" and may take a maximum of 1000-1200 time steps). The maximum size of the time step in any particular solution depends largely on the Rayleigh number, varying from 10^{-3} at R=200 to 10^{-5} at R=1250. In chapter 8 the solutions are known to be steady so a variable time step procedure, analogous to a relaxation process, is used, but this is not suitable for the cases considered so far in which the flows are likely to be unsteady.

The Thermal Diffusion Term

The last remaining term in the heat transport equation is the thermal diffusion term $\nabla^2\theta$. This term is less significant than the others in terms of the overall stability, having only a stabilising influence on the problem. However, if the accuracy of the solutions is to be consistent, then this term should also receive due attention. The standard five-point representation of the Laplacian

$$(\nabla^2\theta)^{n}_{i,j} \simeq \frac{\theta^{n}_{i+1,j} - 2\theta^{n}_{i,j} + \theta^{n}_{i-1,j}}{(\Delta X)^2} + \frac{\theta^{n}_{i,j+1} - 2\theta^{n}_{i,j} + \theta^{n}_{i,j-1}}{(\Delta Y)^2} \qquad (4.2.7)$$

is second-order accurate and has been used almost universally, but where a fourth-order scheme is used for the advection term, it is also possible to obtain similar accuracy in the diffusion term. This may be done at little extra cost in computer time since a large template of points has already been accessed by the program to evaluate the Arakawa terms. Orszag and Israeli (1974) propose the use of the

difference formula

$$(\nabla^2\theta)^n_{i,j} \simeq \frac{1}{(\Delta X)} \left[\frac{2}{3}(\theta^n_{i+1,j} + \theta^n_{i-1,j} + \theta^n_{i,j+1} + \theta^n_{i,j-1}) - \frac{10}{3}\theta^n_{i,j} + \frac{1}{6}(\theta^n_{i+1,j+1} + \theta^n_{i+1,j-1} + \theta^n_{i-1,j+1} + \theta^n_{i-1,j-1})\right] , \qquad (4.2.8)$$

which has fourth-order accuracy, although is only suitable for square meshes **(AX = ΔY)** when in this form.

The Stream Function Equation

Because of the simple shape of the region and the compact form of the stream function boundary conditions, the solution of the elliptic equation (2.3.7) or (2.3.11) is relatively simple to achieve, by applying the Buneman odd-even reduction method described by Busbee, Golub and Nielson **(1970)** which is a direct, non-iterative scheme for the solution of Poisson's equation on a finite mesh of points. This algorithm is considerably faster than classical successive over-relaxation techniques and therefore facilitates the repetitive solution of the stream function which is necessary for simulations of lengthy time developments.

The finite difference representation of the Laplacian uses the five point scheme similar to (4.2.7). The temperature gradient on the right hand side of **(2.3.11)** is then evaluated using central differences which are of similar second-order accuracy. It might appear that the fourth-order accurate form of the Laplacian (4.2.8) could be used with a corresponding application of the Kreiss fourth-order scheme to the temperature gradient term. This can in fact be done after modification of the Buneman algorithm (which is set out in full in appendix B) however the modified form is only one quarter as fast and the benevolent simplicity and rapidity of the numerical solution is destroyed. The type of solution required here would be rendered infeasible unless limitless computational resources were available.

The Pressure Equation

The pressure equation (2.3.10) is also a form of Poisson's equation and may be handled by an adaption of the Buneman algorithm used previously. The modified algorithm takes somewhat longer to compute since the solution matrix is larger due to the *Neumann* boundary conditions (normal derivative specified) on the pressure. Furthermore the solution of Poisson's equation with normal derivatives specified on all boundaries is not unique and it is necessary to adapt the algorithm to explicitly specify at least one pressure in the region (see appendix **D).** This is analogous to providing a gauge pressure,

The Governing Equations in Finite Difference Form

To summarise, the complete finite difference form of the equations used in this work for the simple constant viscosity, two-dimensional model is

$$(\nabla^2\psi)^n_{i,j} = -\left(\frac{\partial\theta}{\partial x}\right)^n_{i,j} , \qquad (4.2.9)$$

and

$$\frac{\theta^{n+1}_{i,j} - \theta^n_{i,j}}{\Delta\tau} = (\nabla^2\theta)^n_{i,j} - R.J^n_{i,j} , \qquad (4.2.10)$$

where $J^n_{i,j}$ is evaluated using the fourth-order Arakawa scheme, $(\nabla^2\theta)^n_{i,j}$ is evaluated using the fourth-order Laplacian (4.2.8), and equation (4.2.9) is second-order accurate and uses central differences throughout.

Boundary Conditions

The substitution of boundary conditions is one facet of numerical computations that often requires care, however for the simple problems with no fluid sinks or sources there is no particular problem. The Buneman algorithm for the solution of the stream function can be modified to accept either the closed, Dirichlet (ψ specified) or the recharge, Neumann boundary conditions and represents these with the same accuracy as the solution in the interior. The explicit solution of the heat transport also allows direct substitution of the isothermal conditions (2.3.12) and (2.3.13) and the insulated conditions (2.3.14) are achieved by invoking symmetry considerations and including "mirror-image" temperatures from beyond the boundary. The large number of points in both the Arakawa templates results in a boundary representation that is at least as accurate as the solution at interior points.

It should be noted here that it is the inclusion of these image temperatures that allows the use of the Arakawa schemes close to the vertical boundaries. However, one row in from either horizontal boundary the thirteen-point template attempts to reference points which lie outside the problem boundaries, and therefore the approximation is not permissible on these two rows (unlike the vertical boundaries there are no image temperatures beyond the horizontal boundaries). Therefore it is necessary wherever fourth-order Arakawa differencing is applied to revert to the second-order, nine-point template on the second and penultimate horizontal rows of the mesh.

Grid Mesh

The choice of mesh size requires some caution as it has been observed by Moore and Weiss (1973) that too coarse a grid may suppress unsteady behaviour - should it be present. The Buneman algorithm operates most efficiently when there are $2^k + 1$ sub-matrices in the solution equation (where k is any positive integer), which means that only certain sizes of mesh are permissible. If the odd-even reduction is performed by combination of row solution sub-matrices then there must be $2^k + 1$ rows in the original mesh (for practical problems this implies 17, 33 or 65 rows).

The reduction could equally well be performed by combining column sub-matrices, at least for the simple two-dimensional stream function solutions, in which case the number of *columns* must be $2^k + 1$. The column solution has the advantage that it enables convenient inclusion of Neumann recharge boundary conditions on the top horizontal boundary without significantly reducing the solution time, although for computer programs written in FORTRAN the arrays are usually handled more efficiently by the row solution method. It is also advantageous to use a square mesh ($\Delta X = \Delta Y$) in the finite difference schemes as this optimises the computation time of the Buneman algorithm.

With these requirements in mind, it remains to choose a mesh size by selecting a value of **k**. Generally a more vigorous solution requires a finer mesh, so for values of the Rayleigh number below 500 a 17 **x 17** mesh is constructed **(for** a square, enclosed region) while above this value a **33** *x* **33** grid is used. **A** still finer 65 *x* 65 mesh would be necessary for flows more energetic than those modelled in this work, but in these cases the solution process becomes lengthy. The recharge and porous insulator configurations require special considerations in the choice of a mesh size for their solution, and these are described later as they arise.

Sinks and Sources

The addition of a sink on a vertical boundary requires no special numerical treatment as there is only a minor change in the boundary conditions, which retain their Dirichlet type. However when the sink is located in the interior, the alternative analysis using equations **(2.5.8)** and **(2.5.9)** must be applied, which requires the evaluation of the terms u, v, g, $\frac{\partial v}{\partial X}$ and $\frac{\partial u}{\partial Y}$. This presents no great problem as these are all analytically defined functions and have easily calculable values at any point except the sink location point (X_o, Y_o). At this point the considerations of zero net vorticity and thermal energy production allows the two combinations of these terms to be equated to zero (see section **2.5**). Once again the values of the boundary conditions are altered but their type **is** retained and the same solution algorithms may be used.

4.3 VARIATIONAL TECHNIQUES

The Galerkin Method

A numerical method of solution for incompressible flow problems which has recently gained favour is the semi-analytical spectral representation presented by Orszag (1971 a, b, c) and Orszag and Israeli (1974) which is based on the Galerkin technique described variously by Schechter ***(1965)***, Kantorovich and Krylov (1964) and Mikhlin and Smolitsky **(1967)**. The spatial dependence of the temperature and flow fields are expanded into a truncated series of orthogonal functions, for example

$$\underset{\sim}{u}(\underset{\sim}{x}, t) \approx \sum_{n=1}^{N} c_n(t).\ a_n(\underset{\sim}{x}) \quad , \qquad (4.3.1)$$

for some finite cutoff value **N ,** where the orthogonal base functions $a_n(\underset{\sim}{x})$ must be consistent with the boundary conditions but are otherwise arbitrary. The Galerkin equations for the coefficients $c_n(t)$ are derived as in Schechter (1965) by minimising the error caused by substituting the approximation **(4.3.1)** into the equations which describe the field $\underset{\sim}{u}(\underset{\sim}{x},t)$. In this way a system of partial differential equations may be reduced to a coupled, ordinary differential set which is conceptually easier to solve numerically. The well known finite Fourier transform method is **a** special case **of** the Galerkin method in which the base functions are sines, cosines or complex exponentials. **In** this investigation the uniformly heated problem has periodic boundary conditions which makes it amenable to solution by Fourier analysis (see appendix **E),** which is the method used to generate the solution illustrated previously in figure 4.2.1. This form of the method is also used by Straus (1974) for the analytical study of the stability of this problem.

Speed of Calculation

One major disadvantage of the truncated Fourier series expansion is its complexity and the correspondingly interminable calculations required to compute the coefficients. For example the direct calculation of sine and cosine Fourier coefficients in the solution illustrated in figure **4.2.1** is at least an order of magnitude slower than a similarly accurate solution using the fourth-order Arakawa differencing scheme. However the method does have the attractive advantages that it is accurate, has conservation properties similar to the Arakawa schemes and takes proper account **of** the boundary conditions. Orszag (1971a) has invented a very worthwhile optimisation of the method that uses further complex exponential transforms ***to*** speed up calculation of the coefficients to a level that is at least comparable with finite difference schemes if the fast Fourier transform algorithm described by Cooley, Lewis and Welch (1967) is available.

This faster method is capable **of** adaption to the conditions used here, but unfortunately only in the simple case of uniform isothermal boundaries. Even then the complex Fourier transform is not itself directly applicable and requires anomalous definitions of the early terms in the series to avoid inconsistencies of symmetry (Orszag 1971b). Orszag (1971c) has demonstrated that a Chebyshev polynomial expansion can handle the boundary conditions satisfactorily without defining a special transform, but in this case fast Fourier transform techniques are no longer directly applicable. **To** derive a similar spectral method for the problem at hand is not infeasible **as** is evident from the parallel adaptation by Young (1974) but since the technique would still only be applicable to uniform boundary conditions, such an analysis is not attempted. The simple and direct calculation method is considerably easier to apply and although unsuitable for protracted solutions it provides a useful basis for comparison with the finite difference methods which are more generally valid.

Finite Element Methods

Another numerical method which is also derived from variational principles is the finite element approach which has been applied to fluid flow problems by Cullen (1974). This technique is a **more** functional method for the examination of real

Slow Heating

However, if the lower boundary is heated slowly to a final temperature $\theta=1$, a largely unicellular motion is obtained which is unsteady at all Rayleigh numbers larger than approximately **280** - a figure which is in agreement with the range **240 - 280** predicted by Caltagirone et al. **(1971)**, and identical to the value observed by Combarnous and Le Fur **(1969)**. This unsteady unicellular motion also develops if as well as rapid initial heating an initial unicellular perturbation is introduced to the flow. These fluctuating solutions exhibit a behaviour very similar to that observed in the Hele-Shaw results (chapter 3) which is comparable to the fluctuating convective state summarised by Bories and Combarnous **(1973)**. The fluctuating solution at **R=500** is illustrated in figure **5.1.2**, and the solutions for this section are summarised in table 11.

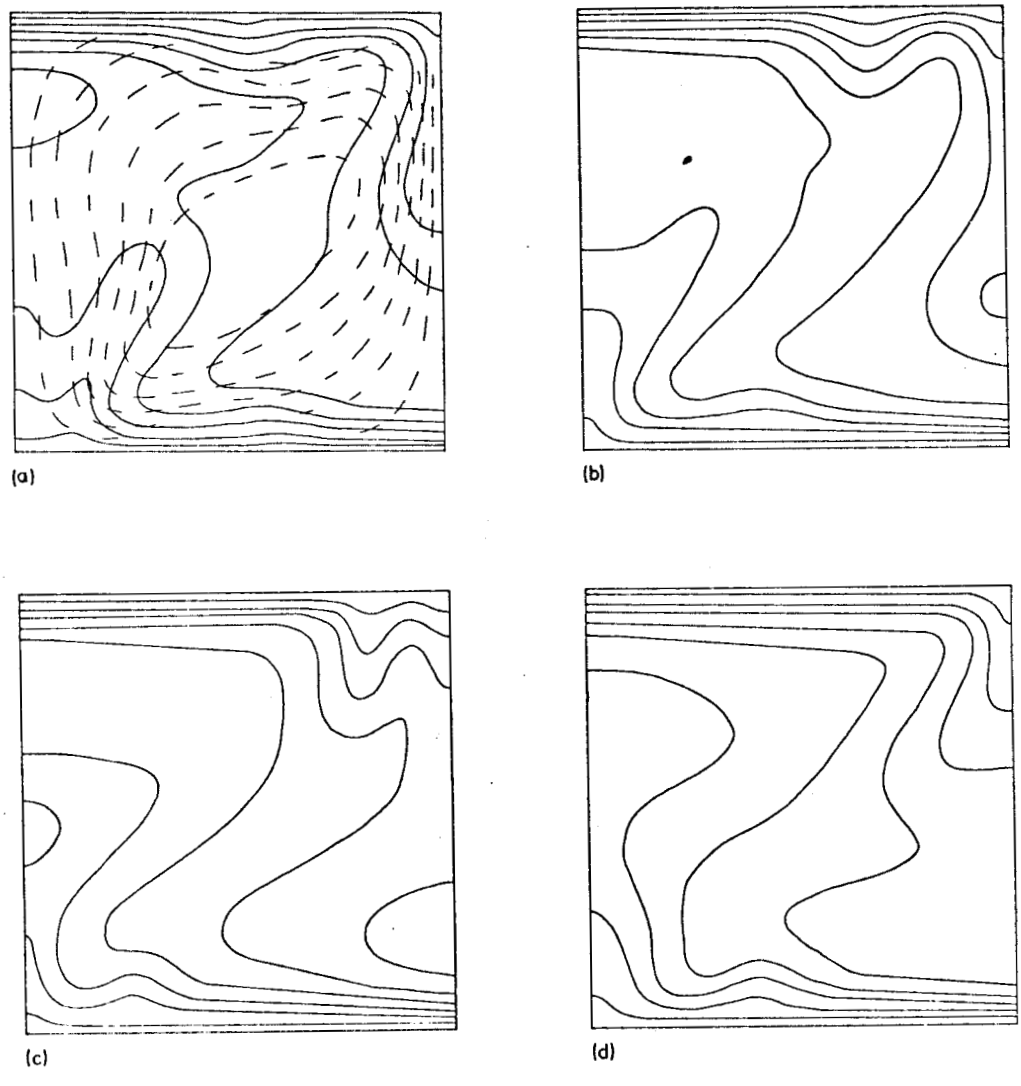

FIGURE 5.1.2 - Uniformly heated fluctuatlng solution at R = 500. An equally spaced sequence of Isotherms (full lines). Broken lines in (a) are streamlines.

Chapter 5 - RESULTS FOR THE TWO-DIMENSIONAL PROBLEMS

5.1 THE UNIFORMLY HEATED MODEL - f = 1

A set of solutions to the uniformly heated, constant viscosity problem was generated to obtain a representation of the experimental solutions reported by Combarnous and Le Fur (1969) and by Caltagirone et al. (1971). It was found that the results of these authors can only be reproduced when certain initial conditions are applied.

Rapid Heating

Beginning the solution with the initial condition that the flow is everywhere stationary and the lower boundary raised suddenly to the high temperature 8=1 , it is found that, in contradiction both to the experimental results of chapter 3 and to those of Caltagirone et al. (1971), the flows become multicellular and steady (or only mildly transient) at Rayleigh numbers between 300 and 500. Such a solution is seen in figure 5.1.1.

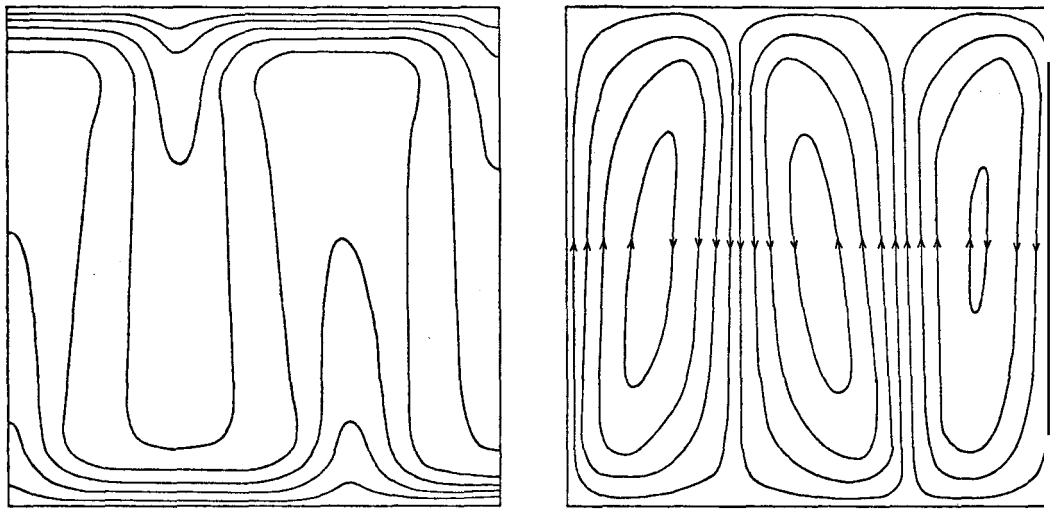

FIGURE 5.1.1 - Uniformly heated steady solution at R = 500. Left: Isotherms Right: Streamlines

systems with arbitrary shapes, but for the regular test systems considered here the finite difference solutions are simpler and faster. The finite element method requires the solution of matrices that are of similar size to those solved by the Buneman algorithm, but they are less sparse and must be solved by inefficient elimination techniques. Therefore the finite element method is not as useful for time dependent solutions and is unlikely to be workable in three dimensions.

Table II - Results for Uniformly Heated Problem

R	Mesh Size	Steady Solution		Fluctuating Solution		
		No. of Cells	Nu.†	Interval*	Nu_{mean}	Nu_{max}
50	17x17	1	1.01	-	-	-
250	17x17	1	4.51	-	-	-
375	17x17	2	6.17	0.0132	5.31	5.81
500	33x33	3	7.79	0.0068	6.30	7.11
750	33x33	-	-	0,0045	8.58	10.04
1000	33x33	-	-	0.0022	11.81	12.90
1250	33x33	-	-	0.0017	14.20	15.69

† Nu the Nusselt number is a parameter relating the convective heat transfer to the conductive heat transfer - see appendix C.

* The interval given is the closest period between any two successive relative maxima in temperature at a particular point in the field.

Heat Transfer

When the solution to a problem such as this tends towards a steady state (as it does in the multicelled solutions) it does so in such a way that the energy transferred by the system is maximised (see Platzman 1965). At a Rayleigh number of 500 the Nusselt number (which is directly related to the amount of heat convected across the system - see appendix C) for the steady tricellular mode is 7.79, whereas for the fluctuating state it varies in time with a mean value of 6.30 and a maximum of 7.11 (considered over a period in which four relative maxima appear). This indicates that the steady solution provides greater energy transfer at this Rayleigh number and is therefore the preferred mode of flow. However it appears that an energy maximum occurs during the formation of a steady pattern, and this may prevent such a solution from developing.

Solutions for steady convection in a porous layer with no restraining side walls have been obtained by Combarnous (1970) and O'Sullivan (1973) who discovered that Rayleigh numbers of approximately 280, 400 and 700 result in cell widths of 0.5, 0.33 and 0.25 respectively for the preferred flow. It is not surprising then that three cells are preferred in the solution at R=500 examined above.

The Solution Alternatives

For rapid initial heating a multicelled "proto-sublayer" forms in a manner similar to that described by Elder (1968) and the number of cells adjusts to form the preferred stable mode. However once a small initial unicellular motion has been introduced, either artifically or by commencing heating at an effective Rayleigh number at which the unicellular mode is preferred, the solution remains largely uni-

cellular and adopts the fluctuating convective state. In the experimental solutions of Caltagirone et al. **(1971)** and of chapter 3, slight physical disturbances or non-instantaneous experimental heating would explain the similar unsteady behaviour. In the Hele-Shaw experiments of chapter 3, the heating was sufficiently rapid to allow a "proto sublayer" to form initially but slow enough to result in an unsteady flow at later times.

The Steady Solutions

It seems probable that the steady multicellular alternative has less practical significance since it requires such artificial conditions for its original generation. Although stable and more "favourable" at later times, this solution is susceptible to two-dimensional, unicellular perturbation until quite late in its development. According to the analysis of Straus **(1974)** a steady two-dimensional solution is eventually destined to become unstable to three-dimensional perturbations at higher Rayleigh numbers. The steadiness of the flow in the solutions generated here becomes uncertain as the Rayleigh number is increased above **400.** In the solutions at Rayleigh numbers around **500** small fluctuations are present in a tri-cellular mode.

If a steady mode of convection occurs at Rayleigh numbers above this figure then the preferred number of cells would be four or more, which is beyond the resolution of a ***33x33*** mesh. In any event the results of Straus **(1974)** indicate that the preferred mode of flow at Rayleigh numbers above 400 (at which the flow is two-dimensional and tricellular) is three-dimensional. Further study requires the representation of three-dimensional flow and is considered later in chapter **6.**

The Unsteady Solutions

A possible explanation for the unsteady behaviour is that the fluctuations which appear in the unicellular solutions are an attempt by the system to resort to the more favourable steady multicellular pattern which **is** repressed by the dominant circulation. However there is a finite energy requirement to transform the solution from one alternative state to the other **-** once formed, the fluctuating convective state is stable to temperature perturbations. **An** attempt to assist the solution between states was made by the introduction of thermal energy in the form of a **10%** random variation **(or** "noise") however this proved unsuccessful. This indicates that both solutions are physically significant although the reason for the existence of two solutions is still not clear.

In the following section the results indicate that altering the heating element reinforces or reduces the "unfavourability" of the single-celled mode, and thus solutions **to** the non-uniformly heated problem clarify the processes observed here.

The Fluctuation Period

The fluctuation period is defined as the closest interval between any two successive relative temperature maxima at a reference point in the field. The log-log plot in figure 5.1.3 indicates that the fluctuation period is proportional to $R^{-3/2}$

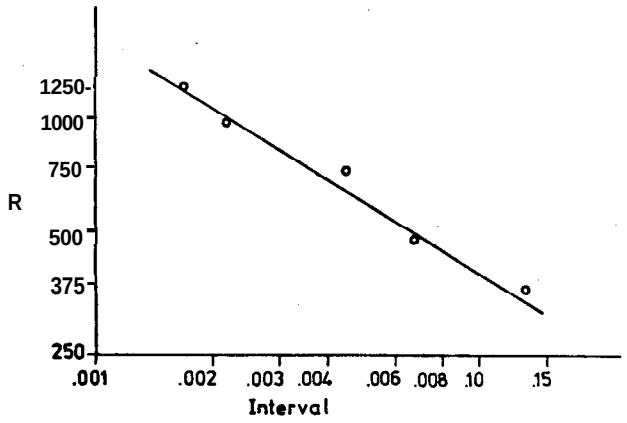

FIGURE 5.1.3 - Plot of fluctuation interval vs Rayleigh number R for uniformly heated solutions. Log-log scale.

The Nusselt Number Variation

The mean Nusselt number for the fluctuating solutions and the steady state Nusselt number for the steady solutions are plotted in figure 5.1.4. The values lie close to the lower bound of the envelope results of Elder (1967a), Combarnous and Le Fur (1969), Buretta and Berman (1974) and Gupta and Joseph (1973) that are summarised in a single plot by Gupta and Joseph (1973 p.513) which is reproduced in outline here.

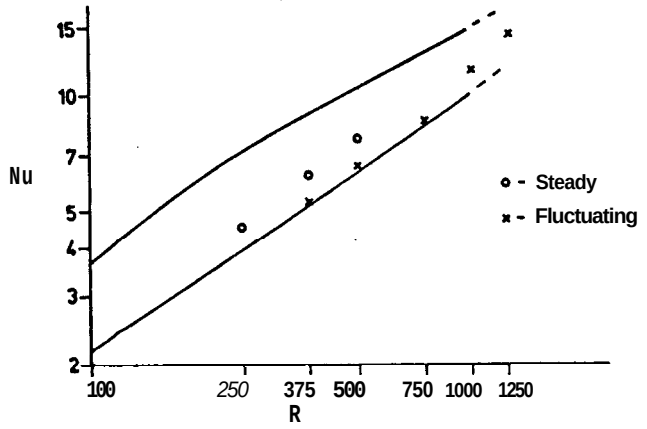

FIGURE 5.1.4 - Plot of Nusselt number Nu vs Raylelgh number R for uniformly heated solutions. Full lines are the delimiters of the range of values obtained by earlier authors (see text). Log-log scale.

5.2 THE NON-UNIFORMLY HEATED MODEL - f < 1

The Range of Results

For simulations of flow in a region heated non-uniformly from below and with constant viscosity, a range of Rayleigh numbers between 250 and 1250 was employed and a diversity of input conditions was achieved by using values of f=0.25, 0.5 and 0.75. The results of these simulations are summarised in table III and include completely regular oscillatory flows. Such flows have not been previously obtained numerically. The period τ_p of these oscillations is defined as the interval between successive temperature maxima at a point in the rising plume of the flow.

Table III - Results for Non-Uniformly Heated Problem

			Steady Solutions		Oscillatory Solutions		
f	R	Mesh Size	No. of Cells	NU	τ_p	Nu_{mean}	Nu_{max}
0.75	250	17x17	3	3.36			
	500	17x17	3	6.02			
	750	17x17	3	7.45			
	1000	33x33	3	8.41			
	1250	33x33	3	9.15			
0.50	250	17x17	1	3.45			
	375	17x17	1	4.20			
	500	17x17			0.0093	4.41	4.42
	500	33x33			0.0091	4.42	4.43
	625	33x33			0.0064	5.18	5.26
	750	33x33			0.0053	6.33	6.51
	1000	33x33			0.0031	8.05	8.29
	1250	33x33			0.0024	9.53	9.87
0.25	250	17x17	1	3.29			
	375	17x17	1	4.09			
	500	17x17			0.0194	4.63	4.72
	750	17x17			0.0089	4.95	5.01
	1000	33x33			0.0063	5.59	5.77
	1250	33x33			0.0051	7.62	7.97

The Oscillatory Solutions

The oscillatory solutions to the half-heated problem are comparable with the Hele-Shaw results of chapter 3, however certain features that are not immediately obvious in the experiments are now apparent. It seems that the rising disturbances are generated at approximately twice the frequency of the descending ones so that two ascending thermals pass in every complete cycle, the first largely dissipating before

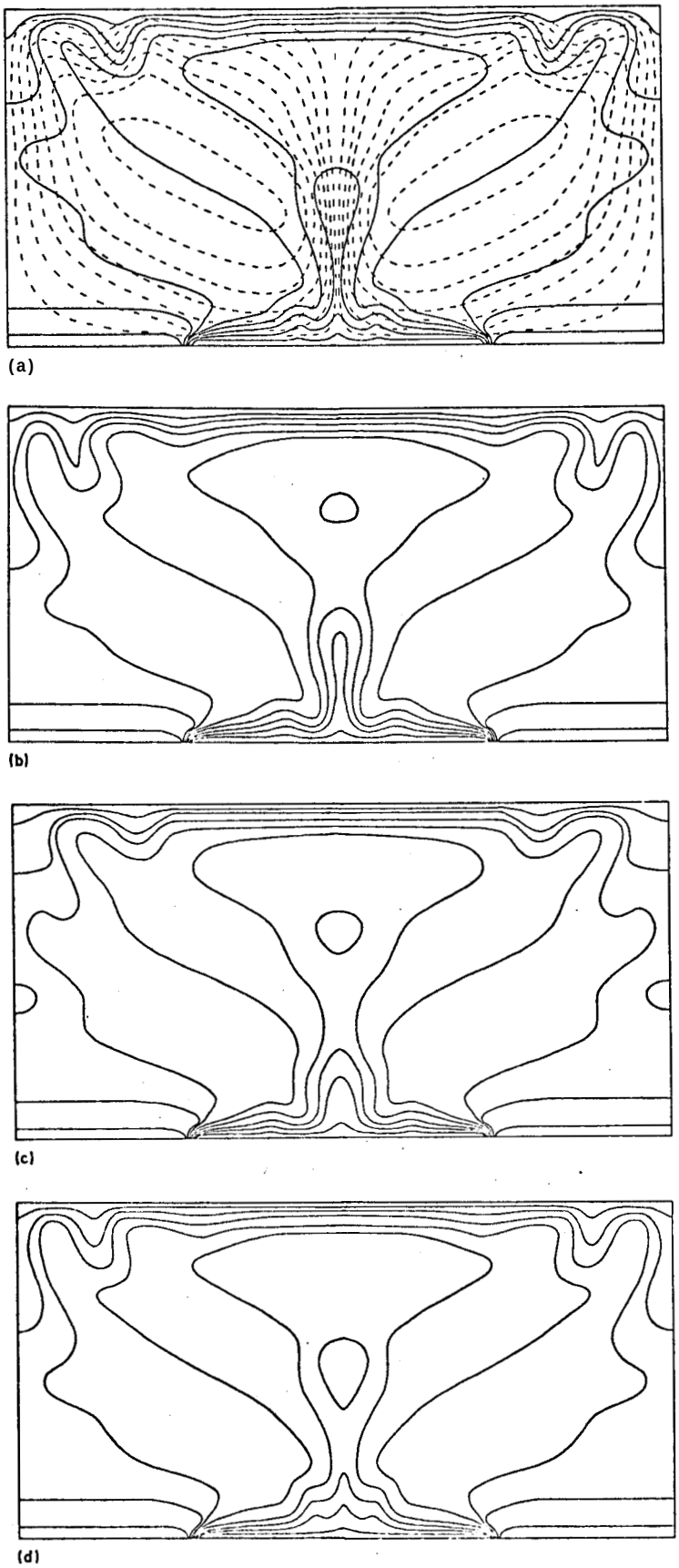

FIGURE 5.2.1 - Half heated oscillatory solution at R = **750.** A sequence of isotherms (full **lines)** equally spaced In time. Broken lines in (a) are streamlines.

the passage of the second. The progress of a solution through a pair of ascending oscillations of such a flow is illustrated in figure 5.2.1, in this case the flow is at a Rayleigh number of 750 and the solution generated on a 33x33 mesh.
The sequence is a set **of** isotherm plots and the diagrams, for greater clarity, are constructed of the solution and its mirror image, joined at the centre. **A** summary plot of the same oscillation is given in figure 5.2.2, which illustrates the variation **of** the Nusselt number and of typical temperatures in the ascending and descending portions of the flow.

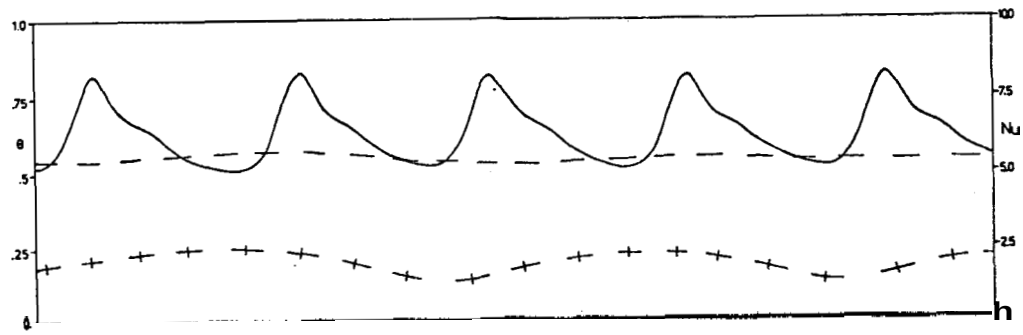

FIGURE **5.2.2** - Variation in time of the half heated oscillatory solution at R = 750. Nusselt number (---). Reference temperature at a point in the ascending flow (——), Reference temperature at a point in the descending flow (+++++).

These oscillatory solutions appear almost identically on both 17x17 and 33x33 meshes at a Rayleigh number of 500, which indicates that this behaviour is not merely the result of numerical disturbances, thus the existence of the regular oscillatory solution previously intimated in chapter 3 is confirmed. The results demonstrate that significant transiency is possible for non-uniform heat input distributions at Rayleigh numbers greater than approximately 480 for f=0.5 and 450 for 0.25.

The Oscillation Period

The dependence of oscillation period τ_P on the Rayleigh number R is indicated by figure 5.2.3 for f=0.5 and 0.25, and in both cases the lines

$$\tau_p \propto R^{-3/2}$$

approximately fit the points, as was the case for the fully heated solutions in the previous section (figure 5.1.3).

The two experimental values of τ_P for f=0.5 obtained in chapter 3 do not differ greatly from the values expected **for** numerical simulations at the same Rayleigh numbers, however they are not plotted since experimental inaccuracies make their quantitative validity doubtful.

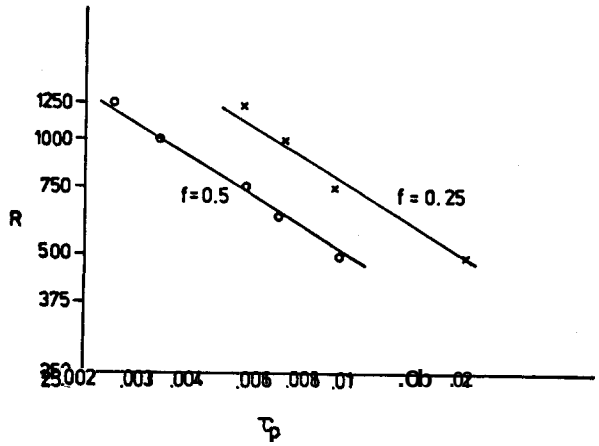

FIGURE 5.2.3 - Plot of oscillation period τ_p vs Raylelgh number R for half and quarter heated solutlons. Log-log scale.

The Three Quarters Heated Solutions

When the lower boundary is three quarters heated the flow patterns are quite different to the oscillatory solutions, being multicellular and comparatively steady. The solution at a Rayleigh number of 250 is illustrated in figure 5.2.4.

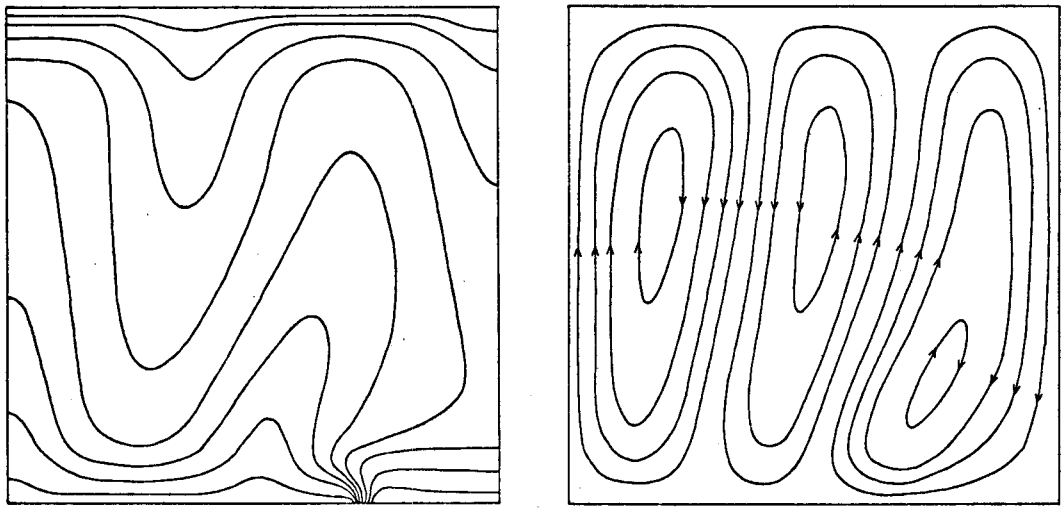

FIGURE 5.2.4 - Three quarters heated steady solution at R = 250. Left: Isotherms, Right : Streaml1nes.

The steadiness of the flows in this set of results is particular significant since it ratifies the assertion made earlier that the system achieves or attempts to achieve a preferential and minimally unsteady state whenever possible. An unheated portion of the boundary that is similar to the cell width for the preferred steady flow at a particular Rayleigh number forces a more favourable and steadier pattern to occur. The shorter heater lengths reinforce the formation of a single celled mode and discipline the flow into regular oscillations.

Rectangular Regions

If the region is elongated from the square shape it has been given so far, the temperature gradients are reduced and unsteady effects less easily established. Maintaining the heater length to he half as long as the unchanging vertical dimension and extending the region to X = 1.3 at a Rayleigh number of 750 results in the reduction of the descending effects while the ascending thermals continue to form in pairs with a period of 0.0049. The mean Nusselt number is then 5.53 (maximum 5.68) and the isotherm and streamline plots are illustrated in figure 5.2.5.

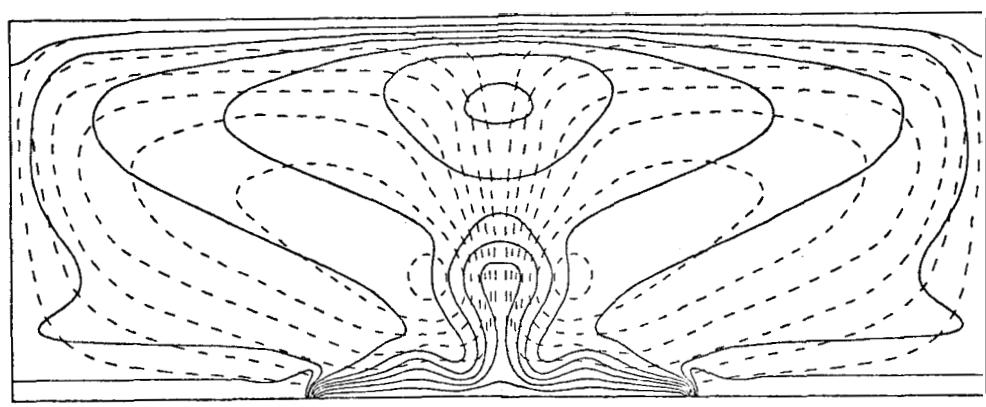

FIGURE 5.2.5 - Unsteady solution in rectangular region X = 1.3 at R = 750. Isotherm (——) and streamlines (- - -).

The extension of the region still further to X = 2.0 causes the disturbances to cease completely and the flow becomes entirely steady with a Nusselt number of 5.53 (see figure 5.2.6).

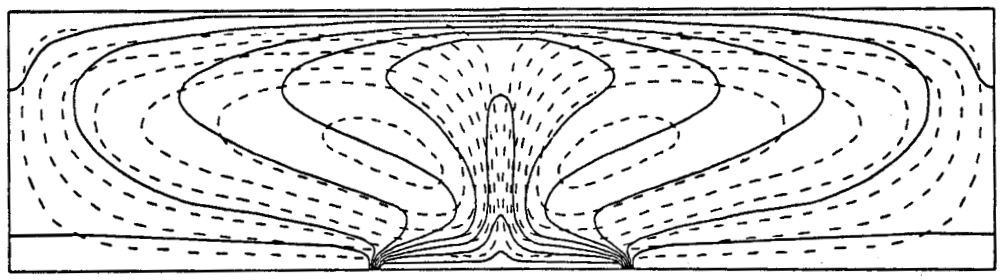

FIGURE 5.2.6 - Steady solution in rectangular region X = 2.0 at R = 750.

Insulated Lower Boundary

Replacing the low temperature condition on the unheated portion of the lower boundary by a restriction of zero heat withdrawal does not significantly affect the generation of thermals over the heater (see figure 5.2.7) except that the value of the Rayleigh number above which oscillatory flows occur is increased to around 900.

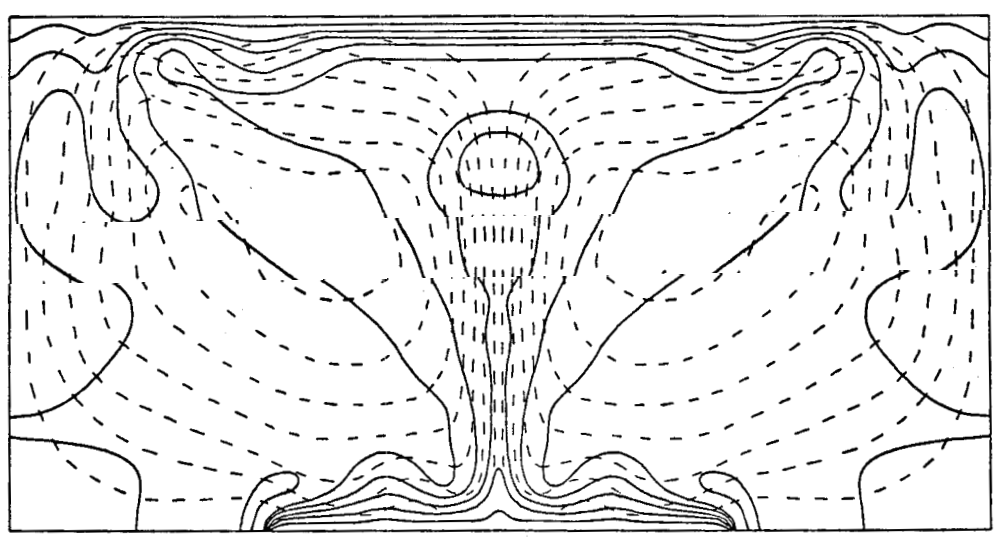

FIGURE 5.2.7 - Unsteady solution in half heated region with insulated lower boundary at R = 1000.

An insulated unheated portion of the lower boundary is more realistic physically because it does not produce the singular temperature gradients between the heated and unheated sections of the boundary that are a feature of the non-uniformly heated models considered so far. The isothermal condition was used initially to obtain a

representation of the conditions in the Hele-Shaw cell, however as it turned out, such a configuration is better for observing unsteady effects which occur at lower Rayleigh numbers than in the more realistic insulated model.

5.3 REVIEW OF CONSTANT VISCOSITY SOLUTIONS

Before continuing with the discussion of simulations using the more refined models it is possible to present a unified synopsis of the results already recorded which by themselves improve the current understanding of natural convection in porous media.

The Thermal Boundary Layer

(a) Steady Solutions

As has been mentioned already, Combarnous (1970) and O'Sullivan (1973) have observed that for an assumed quasi-steady convective state in a porous layer, the preferred cell width decreases with increasing Rayleigh number. Although quasi-steady flows may not occur, this decrease in cell width does at least indicate a tendency of the solutions.

Now, in the fully heated problem considered in section 5.1, when the lower boundary is suddenly heated a thermal boundary layer forms by conduction close to the heater. Across this thin layer the temperature varies from its maximum $\theta=1$, to a value close to its minimum $\theta=0$. Thus in this region the *effective* Rayleigh number increases with the thickness of the layer. The layer extends by conduction until it reaches a certain thickness at which the effective Rayleigh number attains its critical value. It may then be expected that a large number of small square cells will gestate inside the layer. Following this, two processes occur. Firstly the thermal layer continues to extend by conduction and convection, increasing the effective Rayleigh number and elongating the convection cells. Although the aspect ratio of the cells would normally tend to increase with Rayleigh number it does so at a lesser rate than that caused by the cell lengthening and thus the cells become too tall and thin for their thermal environment. Secondly, because these cells are now too numerous there is insufficient energy input at the lower boundary to maintain them all, and those which happen to be smaller are swept away and dissipated by larger ones. In this way the system adjusts so that by the time heat is transferred right across the region the number of cells has reduced to approximately the preferred figure. This process is the development and collapse of tho "proto-sublayer" observed by Elder (1968).

(b) Unsteady Solutions

If, on the other hand, the lower boundary is heated slowly enough, the temperature difference across the boundary layer is such that the effective Rayleigh number does not reach its critical value until the layer has extended well across the region in which case only a single cell forms. The same net result occurs if a unicellular perturbation is applied to a uniformly stratified conduction solution. Once this lower order flow regime has become dominant then higher order and more favourable flow patterns are suppressed. The smaller number of cells does not remove heat from the lower boundary as fast as the preferred pattern would, and therefore a thermal boundary layer forms by conduction in regions of stagnant flow above the heater. A small square cell then begins to form within this layer, but as in the steady case this cell has only a brief life and never reaches sufficient magnitude to enter the overall flow pattern. In this case it is ensnared into the dominant circulation and dissipated, leaving behind it a depleted thermal boundary layer.

(c) Experimental Solutions

The flows observed in the experiments of chapter 3 show features of both the unsteady and steady alternative flows, namely the initial "proto sublayer" with a decreasing number of cells and the later generation and dissipation of new cells between dominant pairs. In figure 3.2 there are initially eight cells across the base of the apparatus (in the photographs at 5 and 10 minutes after commencement of heating), but after 65 minutes the cell number has reduced to four. By 90 minutes the cell number increases to eight again but 40 minutes later (at 120) there are only four. Thus in these flows the thermal boundary layer does not form slowly enough to produce just a single cell, however it is not so rapid that there are sufficient cells in the system to reach the preferred number and therefore the flow remains unsteady.

Adjustment of Cell Number

This discussion of the behaviour of the thermal boundary layer has introduced a fundamental and major point concerning the transience of convective flow in porous media. The multicellular flow becomes steady after an initial period of development only because it is able to *reduce* the number of cells in the flow to attain a preferential pattern which results in maximum energy transfer. However the unicellular flow *remains* transient because it cannot *increase* the number of cells in the pattern, as new cells are destroyed by the existing larger one before they can absorb sufficient energy. The system continually attempts to increase the rate of heat transfer from the lower boundary by improving the favourability of the number of cells.

The Reformation Interval

After the flight of a nascent cell the depleted boundary layer requires a certain time interval, dependent on the Rayleigh number, to reform to such an extent that yet another prospective cell can evolve. These stages of gestation and flight

are also apparent in the fluid layer problem considered by Denton and Wood (1974) who observed rising thermal disturbances similar to those first described by Howard **(1964)**. Sparrow, Husar and Goldstein (1970) found that the rate of generation (in the same fluid layer problem) was proportional to $R^{2/3}$ **,** a result which has also been separately obtained by Krishnamurti (1970b) and by Willis and Deardorff (1970). An example of the approach of Sparrow, Husar and Goldstein **(1970)** applied to the present problem is given in appendix F. Their approach neglects the flow of fluid over the heater and considers only conductive heat transfer, which is a not unreasonable approximation in the case of a fluid layer problem in which there is a fluid boundary layer. However there is no fluid boundary layer in the porous medium problem and the neglection of hydrodynamic conditions in appendix F leads to the prediction of shorter reformation intervals $\tau \propto R^{-2}$ than are observed here.

Fluctuation Regularity

The fluctuations observed in the unsteady fully heated flows are less regular than the oscillations in the half-heated flows. This is due to the lack of constraint on the location at which the thermal boundary layer can fcrm in the uniformly heated configuration. When $f=0.5$ it is inevitable that for a unicellular flow the fluid must rise over the heater and fall on the opposite side of the region. Thus the thermal boundary layer is restricted to form within a certain small area **of** the heater, and the flight of thermals occurs at regular intervals from the same location. On the other hand a disturbance can evolve anywhere on a uniformly heated boundary and when $f = 1$ the disturbances are released at irregular intervals from indefinite locations. The descending "antithermals" in the half-heated case occur more randomly than the corresponding ascending disturbances because they form on a uniformly isothermal boundary. However these effects experience a certain induced regularity due to the periodic impingement on the upper boundary of oscillations in the rising plume, and therefore are not as random as those in the fully heated case.

Other Boundary Conditions

The solutions for rectangular regions confirm that the thermal boundary layer provides the mechanism for the production of transient effects, and also indicates the effect of the confining vertical boundaries. With very long, cool portions of the region, the flow is slower and the isotherms spread further than in a similarly heated square region. Thus the rising plume is wider which results in a weaker thermal boundary layer. It should be explained here that a thermal boundary layer is indicated by an area of maximum of thermal gradient which generally implies a conductive region (in a convective flow the advective regions of the **flow** transport heat more effectively than conductive regions and do not permit accumulations of thermal energy). Comparing the isothermal plots of figures 5.2.5 and 5.2.6 it is seen that the conductive region (in which isotherms and streamlines are approximately parallel) in the wider cell is approximately as thick (remembering the difference in vertical length scales) but has a much reduced temperature differential across it. Thus the effective Rayleigh number never reaches its critical value and the solution remains steady.

A similar effect occurs in the flows in a region with an insulated lower boundary. The fluid transported over the downstream end of the heater is warmer than in the isothermal lower boundary case and consequently the temperature differential and thus the effective Rayleigh number in the thermal boundary layer are both reduced.

Thus it has been demonstrated that, for the simple enclosed porous region, the natural convective flow regime is influenced both by the presence of vertical boundaries (since the steadiness of the pattern depends on the ability of the preferred number of cells to form within the problem boundaries) and by the method and extent of heat input employed.

5.4 THE RECHARGE-DISCHARGE SOLUTIONS

"Natural" Conditions

Solutions for the half-heated, constant viscosity, surface recharge prcblem (in the absence of any point fluid sinks or sources, corresponding to the natural state of a geothermal field) were generated on **33x33** meshes for selected values of the Rayleigh number in the range **250** to 1000. The finer mesh is imperative at lower values **of** R than those previously requiring this grid because the outflow of fluid through the surface draws the rising plume right to the upper boundary, resulting in severe thermal gradients in this area. In fact at higher values $R \geq 750$ a slight numerical instability becomes apparent at the top of the rising column, however the effects of this are advected out **of** the region with the surface discharge.

When the Rayleigh number exceeds a value in the vicinity of **350** the flow is regular oscillatory, periodically generating thermals **or** pairs of thermals in the ascending portion of the flow only. This behaviour may be seen in the summary plot **of** figure **5.4.1** and a thermal is illustrated in mid-flight in figure **5.4.2.**

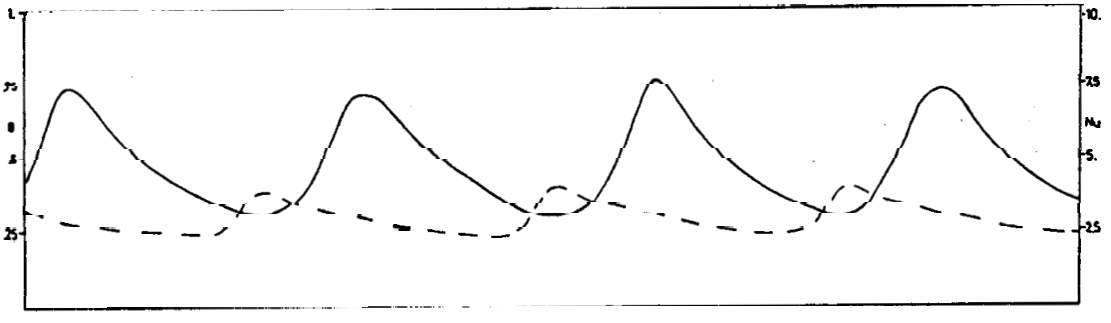

FIGURE 5.4.1 - Variation In time of the oscillatory recharge solution at R = 500. Nusselt number (– – –) and Reference temperature at a point within the rising plume (——).

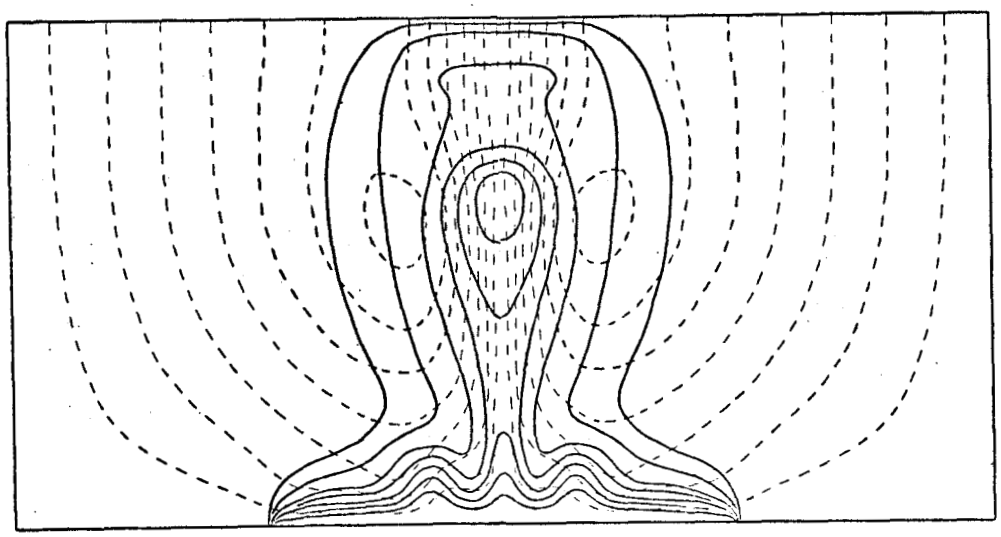

FIGURE 5.4.2 - Oscillatory solution for recharge problem at R = 500. Isotherms (——) and streamlines (- - -).

The value of the Rayleigh number at which the solution becomes unsteady (350) is lower than the value 480 observed for the half-heated, closed boundary model of section 5.2. The recharge from the surface transports cold fluid down to the heater, contracting the rising plume and reinforcing the thermal boundary layer. The large temperature differential across the layer means that the effective Rayleigh number is high, and temperature disturbances form more rapidly. The flow of fluid into the surface also prohibits the formation of a thermal gradient at the upper boundary above the descending portion of the flow, and therefore prevents the generation of descending temperature disturbances. The ascending pulses are generated by the same mechanism as their enclosed system counterparts, but with higher frequency.

Comparison of the temperature profiles on the left vertical boundary in figure 5.4.3 (which is a pair of plots of a superposition of the profiles at several successive time intervals) reveals that the recharge disturbances have a larger amplitude and move both faster and further. A summary of these natural recharge solutions is presented in table IV.

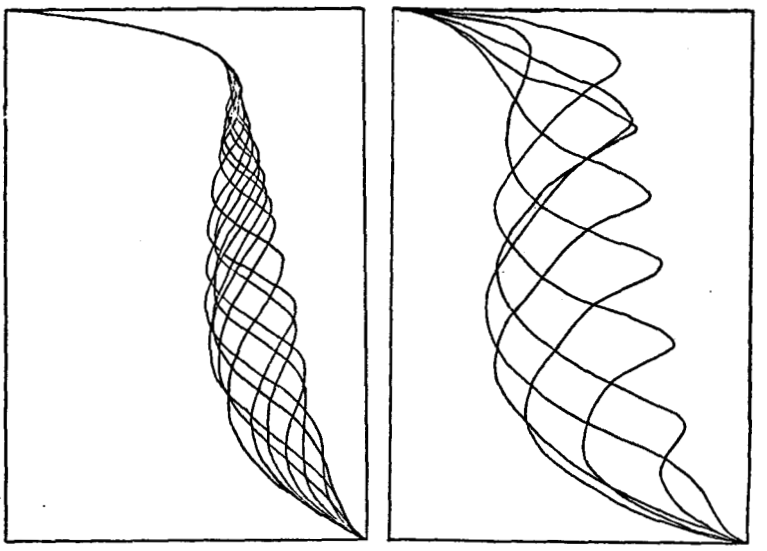

FIGURE 5.4.3 - Plots of temperature profiles along left hand vertical boundary at various times for R = **750.** Left: Closed system of Figure **5.2.1.** Right: Recharge system.

Table **IV** Recharge - Discharge Solutions

R	Nu_{min}	Nu_{max}	ψ_{max}	τ_P
250	**2.68**	**2.68**	**0.057**	-
312	**2.68**	**2.68**	**0.053**	-
375	**2.42**	**3.18**	0.051	**0.0068**
500/lst pulse	**2.29**	**3.58**	**0.051**	**0.0037**
500/2nd pulse	**2.19**	**3.88**	**0.052**	**0.0042**
750/lst pulse	**2.84**	**4.78**	**0.053**	**0.0021**
750/2nd pulse	**2.34**	**4.56**	**0.054**	**0.0024**
1000	**2.72**	**4.82**	**0.058**	0.0017

Biperiodic effects

At intermediate values of the Rayleigh number, namely **500** and **750,** successive thermals have different magnitudes and evolve unevenly spaced in pairs. **For** instance at R=500 a large pulse precedes a smaller one by an interval of **0.0037,** and the subsequent large pulse, identical to the first, follows **0.0042** after that. This biperiodicity is apparent in figure **5.4.1** above. **As** one thermal rises through the porous matrix it creates a velocity perturbation that interrupts the gestation of the thermal which has formed **on** the heater behind it. This correspondingly smaller thermal is drawn off earlier than its predecessor and makes a premature flight.

When the Rayleigh number is larger, successive disturbances appear so rapidly that the interaction between them extends beyond adjacent disturbances, and when R = 1000 the oscillations are regular, On the other hand at a lower Rayleigh number the thermals are widely spaced in both time and position and do not interact significantly at all, so when R = 375 the oscillations are again regular.

There appears to be a similar biperiodic effect in the experimental results of Sparrow, Husar and Goldstein (1970, figure 2a, p.797) for a Newtonian fluid layer heated from below. Also Krishnamurti (1970b) and Willis and Deardorff (1970) have mentioned paired effects with reference to this problem. In the half-heated closed boundary model of section 5.2 the thermals are weaker than here and do not interact noticeably in this way, however there is another biperiodicity due to the descending disturbances having approximately half the frequency. This second type of biperiodicity, due to the interaction of two different fluctuating sections of the flow, may be observed in the results of Denton and Wood (1974) for a stratified fluid layer problem except that there the different disturbances are separated physically by a fluid interface.

These effects emphasise the importance of the coupling between the velocity and the temperature fields and stress the necessity of maintaining accuracy when representing the advection terms.

The Addition of Fluid Sinks

With the existence of oscillatory effects established in a model more realistic than the enclosed model in which they were discovered, the effect of including fixed "unnatural" fluid withdrawals may be evaluated. Taking the solution at R = 500 as a typical case, sinks of strengths between 0.012 and 0.10 are installed on the left vertical boundary (corresponding to a borehole above a heat island if this boundary is envisaged as a line of symmetry). The strengths of these sinks range from ¼ to twice the natural discharge ($\psi_{max} \doteq 0.05$) observed in the preceding results, In its present state, the drawoff from the Wairakei field is approximately four or five times the natural discharge of 440 kg/sec although this fluid is withdrawn through many wells. On the scale of the model used here, several of these wells may be considered to act together as a single point sink which corresponds to the configuration modelled. The remainder of the bores are neglected for the meantime since it is the effect of the sink that is of interest rather than the faithful representation of the Wairakei system alone. The results of the flows for this "centreline sink" configuration are tabulated in table V.

Table V Sink - Recharge Solutions R = 500

Sink Strength	Nu_{min}	Nu_{max}	ψ_{max}	T_p
0/lst pulse	2.29	3.58	0,051	0.0037
0/2nd pulse	2.19	3.88	0.052	0.0042
0.012/lst pulse	3.62	4.56	0.041	0.0037
0.012/2nd pulse	3.58	4.72	0.042	0.0042
0.025/lst pulse	5.86	1.39	0.054	0.0037
0.025/2nd pulse	5.41	7.50	0.055	0.0042
0.05	3.91	8.42	0.056	0.0042
0.10/lst pulse	5.13	12.71	0.100	0.0040
0.10/2nd pulse	4.99	13.79	0.100	0.0043

It was found during introductory tests on the model that the instant at which the sink was "turned on" was not an important factor and the solution eventually reached the same state regardless *of* when the sink had been introduced. Therefore in each case the flow was permitted to develop from time zero with the sink in force. Typical flows at sink strengths of 0.025 and 0.1 are illustrated in figures 5.4.4 and 5.4.5, which should be compared to the zero withdrawal solution presented previously in figure 5.4.2.

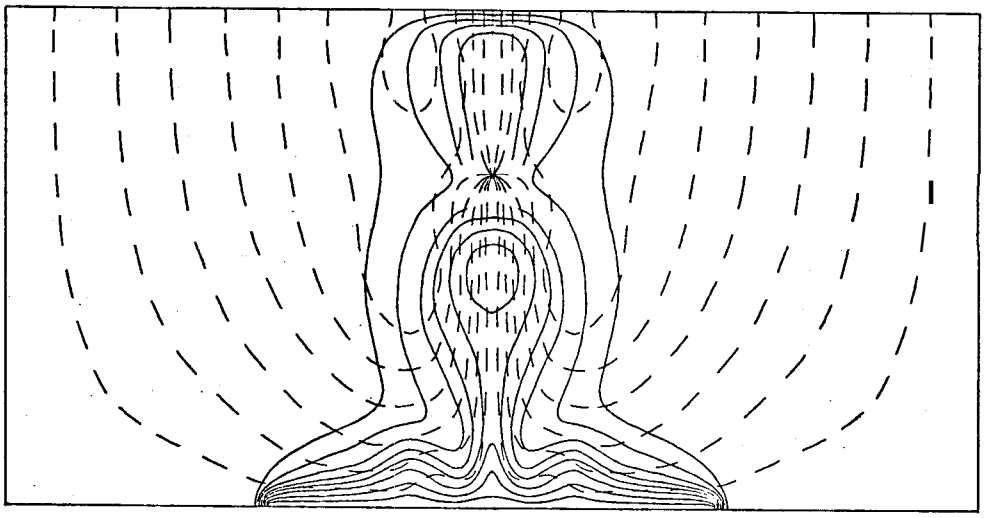

FIGURE 5.4.4 - Oscillatory solution for recharge problem at R = 500 with sink of strength 0.025 on left vertical boundary (centreline in this diagram).

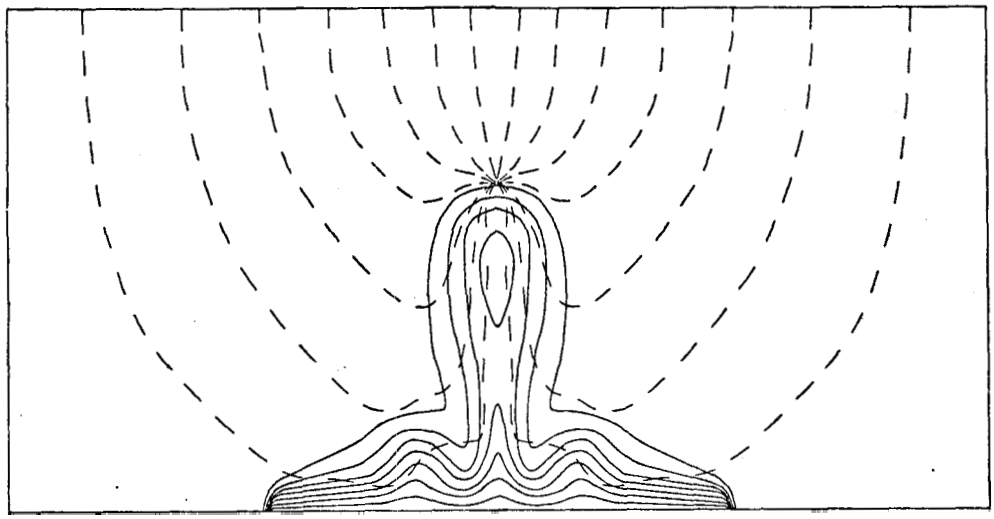

FIGURE 5.4.5 - Oscillatory solution for recharge problem at R = *500* with sink of strength 0.1 on left vertical boundary.

The Effect *of* Sink Strength

Although the rising plume contracts under the influence of the sink and the Nusselt number is considerably increased, the generation of the thermals is only slightly affected. When the sink strength is 0.1 the motion is dominated by the sink flow (indicated by the value of ψ_{max}) but the time period lengthened only slightly as the thermal boundary layer evolves less easily. The solution is unusual when the sink strength is close to that of the natural discharge **(~ 0.05)** as the maximum stream function is uncharacteristically large and the flow completely regular. The forced flow overrides the weaker coupling between the velocity and temperature fields and disrupts the interaction between thermal pairs.

Sink Location

A similar regularisation occurs if the sink is placed over the interior end of the heater, although in this case the amplitude of the oscillation is reduced to approximately 20% (see figure 5.4.6) and the period becomes 0.0041.

This repositioning of the sink also results in a reduction of the heat transported through the system as the Nusselt number varies only between **2.60** and 3.56. The increased flow through the region is choked by the flow between the surface and the sink and consequently the volume of fluid passing the heater is reduced. This is indicated by the shorter gestation period of the thermal boundary layer. The sink is also drawing fluid of much lower temperature when in this position and its usefulness is reduced to such an extent that the system produces less

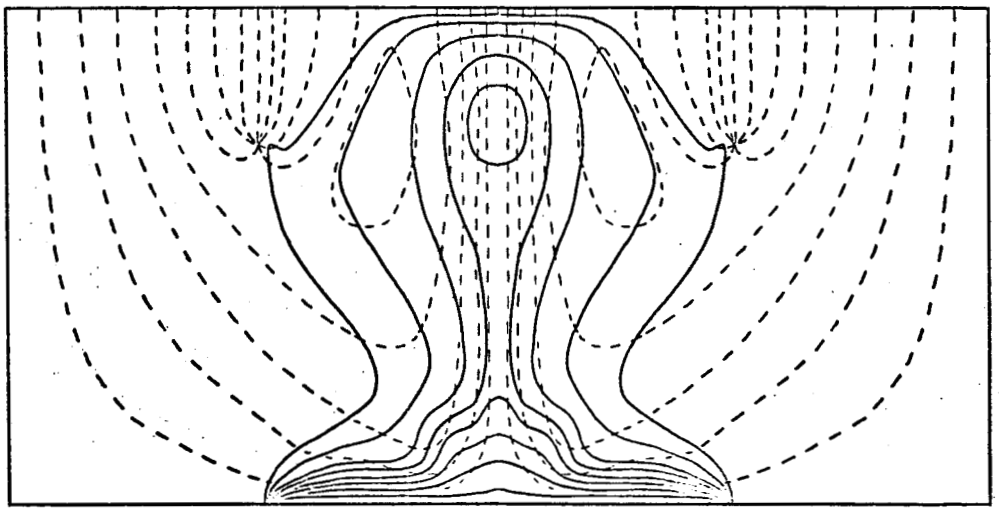

FIGURE **5.4.6** - Oscillatory solution for recharge problem at R = 500 with sink *of* strength 0.05 over interior end of heater (mid-region).

heat than in its "natural" state. Moving the sink further over the heater as in figure 5.4.7 increases the Nusselt number to vary between **3.79** and 4.62 and in this case the solution is biperiodic again.

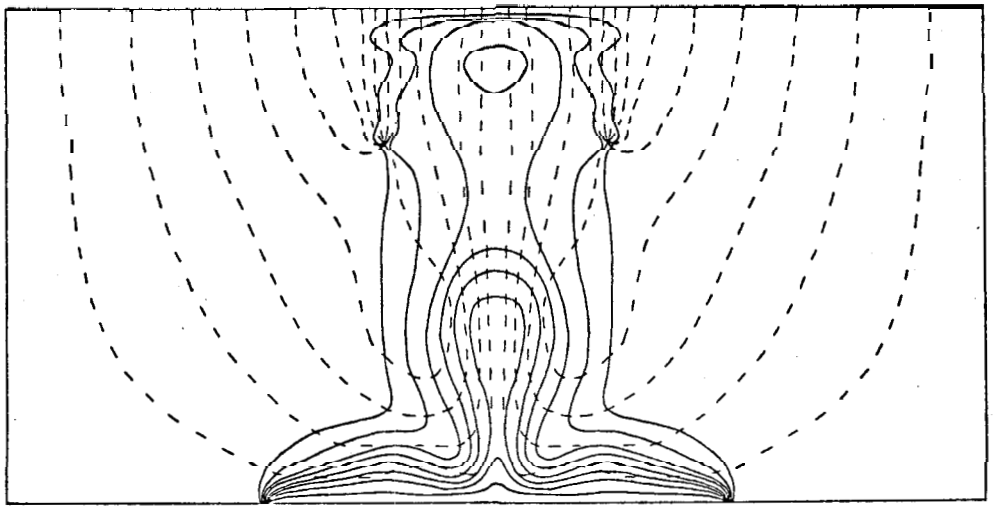

FIGURE **5.4.7** - Oscillatory solution for recharge problem at R = 500 with sink of strength 0.05 over centre of heater.

The Upper Reservoir

Now that a method has bean developed to represent surface recharge and fluid withdrawal, it is possible to construct a model of the "upper reservoir" which was described in chapter 1. The upper reservoir may be considered as a convective system in itself, fed with hot water from below, as suggested by Donaldson (1974). To represent this situation the boundary conditions remain similar to those used in the deep, natural recharge model except that now fluid is introduced through a source in the lower boundary, as in figure 5.4.8.

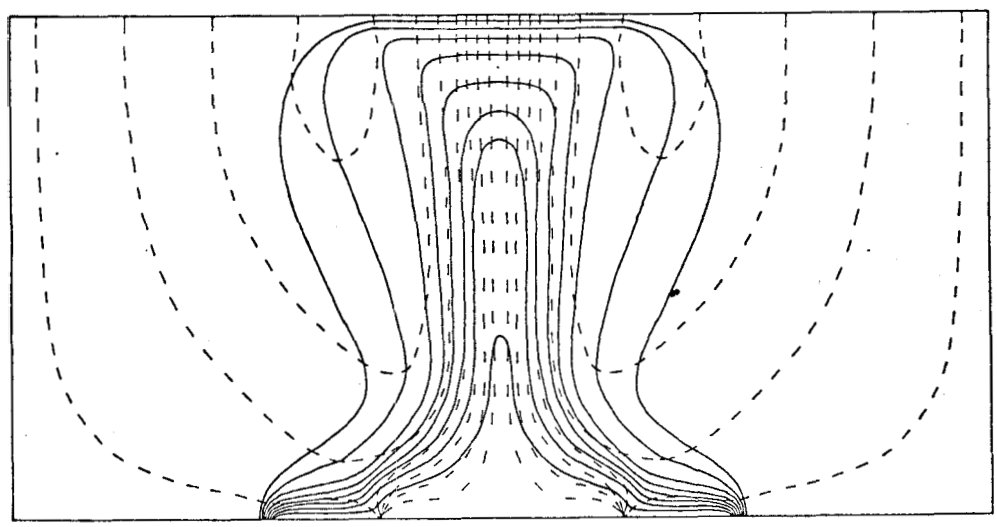

FIGURE 5.4.8 - Steady solution for recharge problem at R = 500 with point source of strength 0.05 at centre of heater.

In this case the point source is of strength 0.05 and is positioned at the centre of the heater. This corresponds to the introduction of hot water at the base of the system through a major fissure. The flow from the source expels the thermal boundary layer from the lower boundary and prevents transient behaviour. The flow patterns are similarly steady if the influx of fluid is distributed over the entire heater, as in figure 5.4.9. The results of simulations using these forced inflow models are tabulated in table VI.

Table VI Source - Discharge Solutions R = 500

Source Strength	Nu	ψ_{max}	ψ_{min}	$\lvert\Delta\psi\rvert_{max}$
0.025 point	5.70	0.025	-0.048	0.073
0.050 point	7.67	0.050	-0.049	0.099
0.050 distributed	7.17	0.050	-0.046	0.096

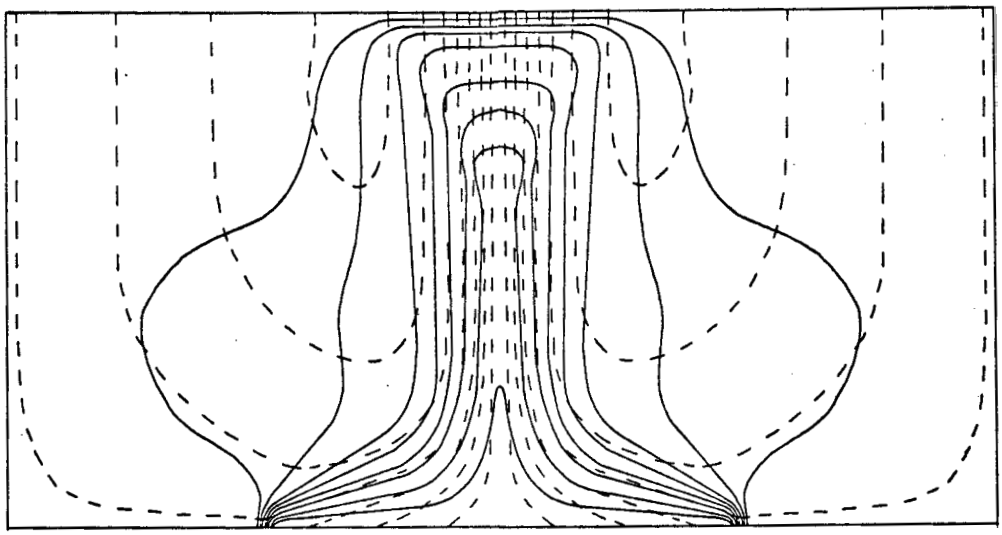

FIGURE 5.4.9 - Steady solution for recharge problem at **R** = **500** with distributed source **of** strength **0.05** over heater.

The addition of a fluid sink of strength **0.05** corresponding to exploitation of the upper reservoir, is shown in figure **5.4.10.** **In** this case the Nusselt number is increased by **a** factor of three, to approximately **21.**

These results demonstrate that unsteady effects cannot develop at higher levels of a geothermal region if the rising plume **of** hot fluid is already steady. However, when disturbances originate at depth as has been observed in the more complete models used earlier in this work, clearly these thermal anomalies will rise through the upper reservoir. Thus restricting the long term modelling of geothermal regions to just shallower sub-systems may give limited understanding of the problem.

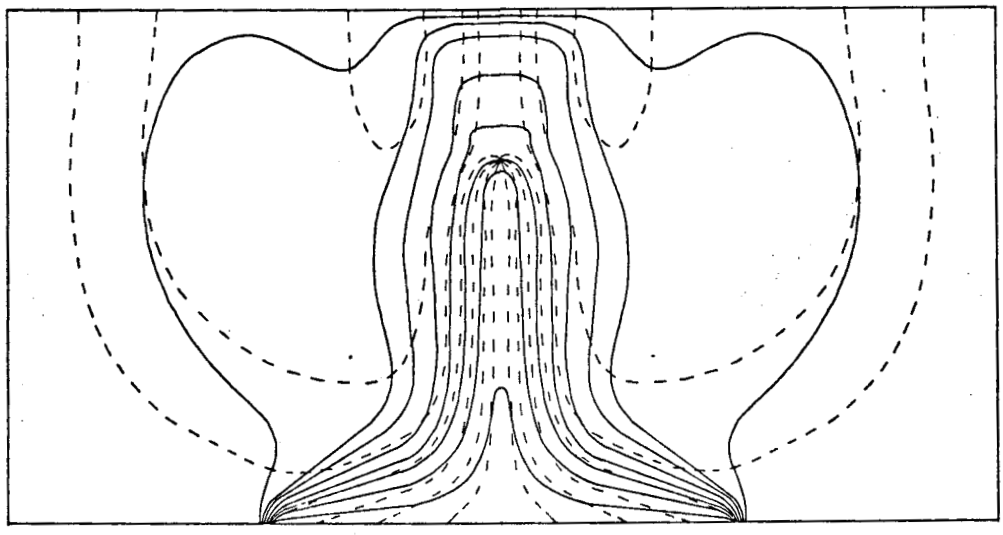

FIGURE 5.4.10 - Steady solution for recharge problem at R = **500** with source of strength **0.05** over heater and sink of strength **0.05** on left vertical boundary (centreline).

Fluid Reinjection

Recently it has been suggested that the useful output from geothermal areas may be improved by the reinjection of water to replace that removed through boreholes. This is done at the Geysers field in the U.S.A., largely as a means of disposing of excess warm water from the power station. In order to achieve the best possible results from reinjection it is necessary to inject the recharge fluid into the descending region of the flow, as in figure 5.4.11.

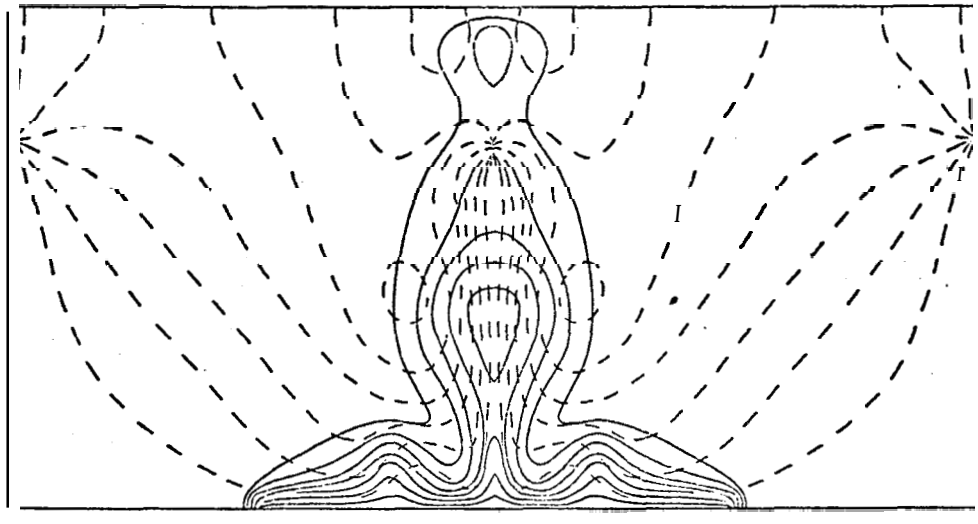

FIGURE 5.4.11 - Oscillatory solution for recharge problem at R=500 with source of strength 0.05 on right vertical boundary and sink of strength 0.05 on left vertical boundary (centreline).

The injected fluid then makes its way down to the heat source with the "natural" recharge from the surface. It should be noted that it is only necessary to reinject at a depth at which the surroundings have the same temperature as the injected fluid. In this way no heat is lost from the fluid to the surroundings, provided the source is not so strong that injected fluid tends to rise towards the surface again. A source of strength similar to the maximum stream function of the natural flow at the time the source is introduced should satisfy this requirement. There is little to be gained by introducing the fluid at greater depth, which would necessitate deeper wells and the installation of higher pressure pumps. The reinjection system illustrated in figure 5.4.11 uses a source of strength 0.05 at the same depth as a sink of strength -0.05 in theascendingplume. This results in a maximum Nusselt number of 8.60 compared to the value 8.42 for the same system without the reinjection. It should be noted that the behaviour of the system is still oscillatory.

Forced Convection

Finally, it should be noted that the models used in this section have deviated from the free convective problem for which the governing equations were derived in section 2.1. However the Reynolds number of these solutions in increased at most by a factor of two, and not by the order of magnitude that would invalidate the use of the approximations that Darcy's Law is valid, that energy dissipation is negligible, that inertia effects may be ignored and that the Boussinesq approximation is appropriate.

5.5 THE VARIABLE VISCOSITY MODEL

Physical Parameters

From empirical tables given by Engineering Sciences Data (1968) a least squares fit is obtained to determine the coefficients for the variation of the viscosity and density of water with temperature. These values are:

$$a = 0.9229 \quad \Delta T \quad ,$$
$$\beta_1 = 2.606 \quad \Delta T \quad ,$$
$$\beta_2 = 1.335 \ (\Delta T)^2 \quad ,$$
and $$\beta_3 = -0.4762(\Delta T)^3 \quad ,$$

where ΔT is expressed in units of 100°C, resulting in an approximation to the viscosity dependence illustrated in figure 5.5.1.

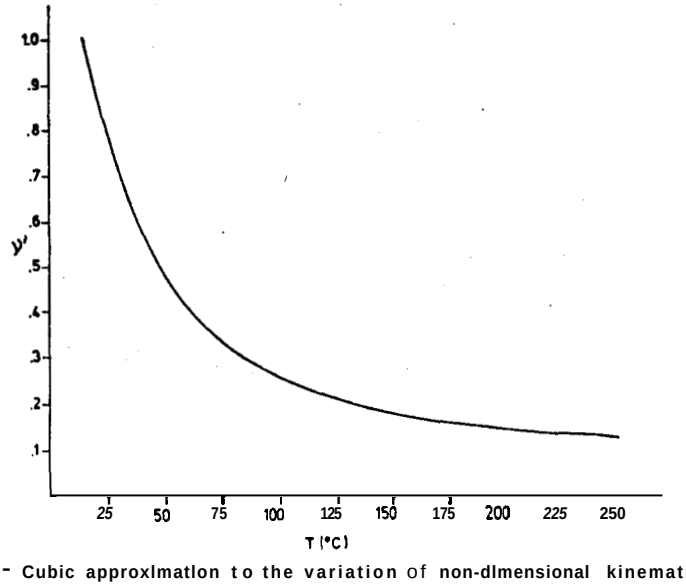

FIGURE 5.5, 1 - Cubic approximation to the variation of non-dimensional kinematic viscosity ν' with temperature T in pure water.

As has been mentioned previously, when using the variable viscosity equations, convection that is at least as vigorous as that in the constant viscosity model may occur at considerably lower *apparent* Rayleigh numbers (which are based on ν_o). Consequently for a temperature differential ΔT of 150°C a range of R between 50 and 160 is considered which corresponds to a range of "cold water" Rayleigh numbers between 400 and 1250.

The results are collated in table VII for the closed boundary conditions as in section 5.2 and the recharge conditions as in section 5.4. A 33x33 finite difference grid is necessary in all cases.

Table VII Variable Viscosity Solutions, f = 0.5, AT = 1.5

Boundaries	R	Nu_{min}	Nu_{max}	ψ_{max}	τ_p	Flow regime
Closed	50	3.60	5.10	0.259	0.0248	Regular oscillatory
	80	5.59	5.71	0.281	0.0024	Regular oscillatory
	160	8.13	8.23	0.312	0.0013	Regular oscillatory
Recharge	50	3.29	3.29	0.342	-	Steady
	80	2.80	3.55	0.265	0.0031	Approximately regular oscillatory
	160	2.75	3.80	0.295	-0.00025	Irregular fluctuation

The Flow Patterns

These solutions show greatest similarity to the constant viscosity models at the intermediate value 80 in the range of Rayleigh numbers; figures 5.5.2 and 5.5.3 are illustrations of the two configurations at this value.

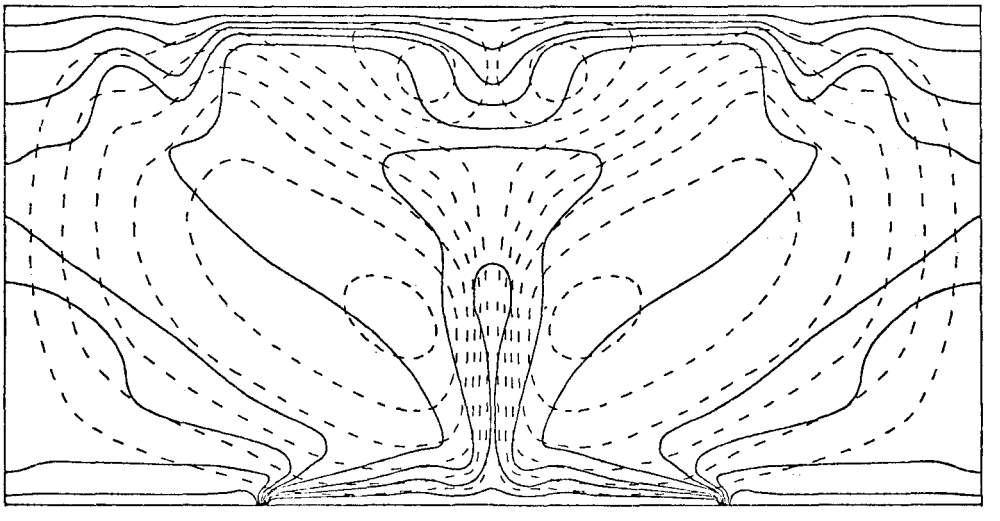

FIGURE 5.5.2 - Unsteady solution for variable viscosity, closed, half heated problem at R = 80.

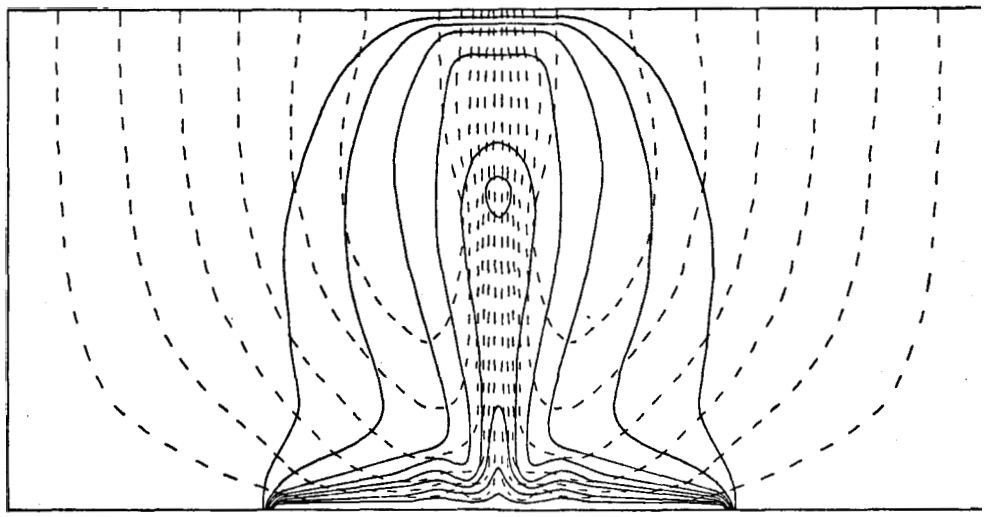

FIGURE 5.5.3 - Unsteady solution for variable viscosity, recharge problem at R = 80.

At the high value of **160** the recharge solution exhibits an almost triperiodic behaviour, generating three evenly spaced thermals at irregular intervals. The time interval reported in table VII is the spacing between these disturbances, but the sets of three occur at intervals up to six times this value. As a result **of** the sharp decrease in viscosity as a thermal boundary layer forms, the local effective Rayleigh number close to the heater increases more than it would have done had the viscosity been constant. The thermal boundary may then be thought of as a reservoir of less viscous fluid as well as of thermal energy. Thermals then form in a series that is typical of the effective Rayleigh number, stripping away the boundary layer. After **a** certain quantity of heat has been removed from the layer, usually after the flight of just three thermals, the reservoir of less viscous fluid is expended and the disturbances lapse until a new thermal boundary layer has gestated. Although this process is not identical to those in the constant viscosity model, the mechanism is basically similar.

At the lower values R = **50** and **80** the closed solution is distinctive since the comparatively small Rayleigh number and large temperature difference emphasise the viscosity effects. In this case the rising plume follows **a** less viscous "channel" that was formed early in the development of the flow when the pattern was bicellular. In all previous half-heated solutions the leftmost of the two cells was dissipated, shifting the plume towards the adjacent vertical wall as that boundary heated up. Here however the smaller reverse cell is maintained (see figure **5.5.4**), varying in size as the plume wavers during the formation of the descending disturbances in the thermal boundary layer at the surface.

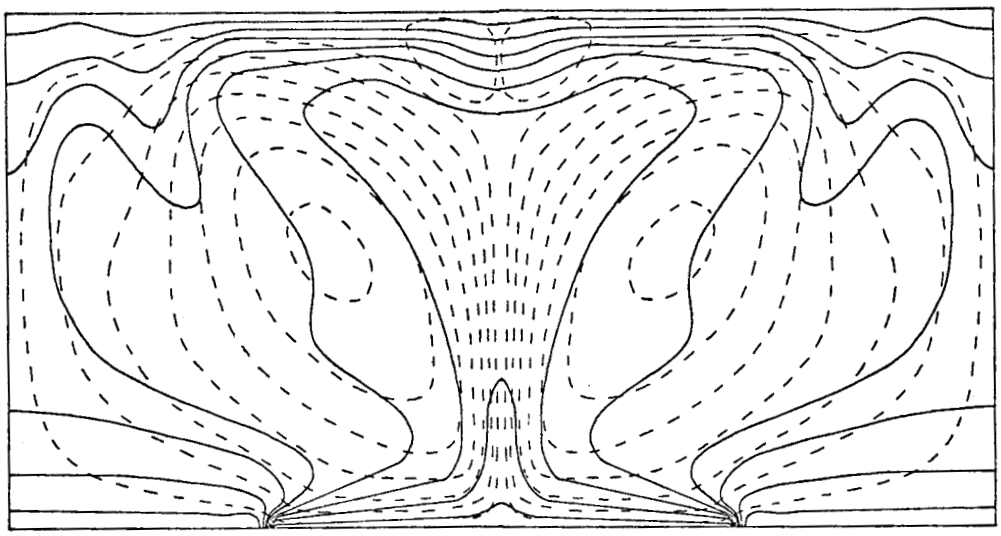

FIGURE **5.5.4** - Unsteady solution for variable viscosity, closed problem at R = 50.

Fluid Speeds

The descending disturbances are much more gradual than the ascending ones due to the acceleration **of** the fluid in higher temperature regions. Comparing the streamlines to those in a constant viscosity model, as in figure 5.5.5, the fluid is less viscous close to the heater and flows more rapidly than it does along the surface where the streamlines are more widely spaced.

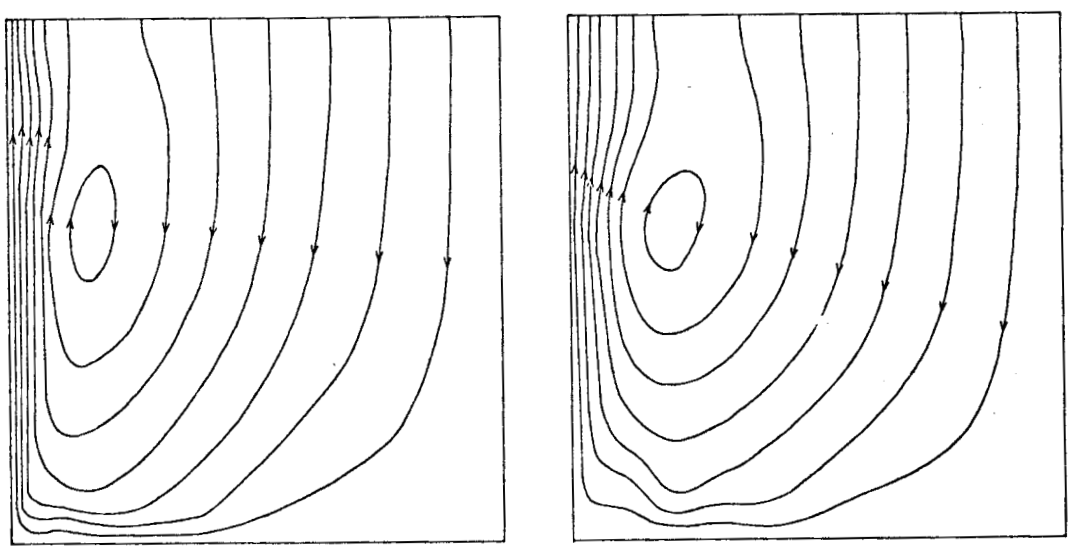

FIGURE **5.5.5** - Comparison of streamlines in vat-table and constant viscosity models. Left: Variable viscosity recharge solution at R = **80.** Right: Constant viscosity recharge solution at R = **500.**

As a further comparison, a fully heated solution is generated at a Rayleigh number of 50, and displays the now familiar three-celled pattern. The flow is unsteady with fluctuations appearing at intervals of the order 0.0045 and a Nusselt number varying approximately within the range 6-10. As before, the solution shows an acceleration of the flow close to the heater, as in figure 5.5.6.

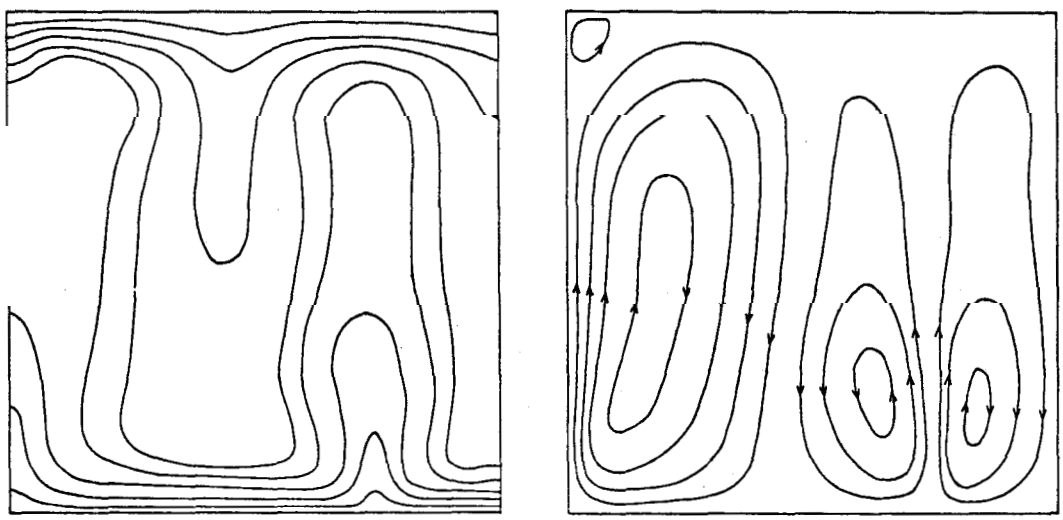

FIGURE 5.5.6 - Unsteady solution for variable viscosity, closed, uniformly heated problem at R = 50. Left: Isotherms, Right: Streamlines.

Applicability of Constant Viscosity Models

Although the simulations performed using the variable viscosity model are by no means exhaustive, they reveal that the commonly used constant viscosity models are inexact but not entirely without use. Generally the flows are similar in character for the two models, however extensive numerical experimentation is more expensive with the variable viscosity model which takes approximately twice as long to compute.

It must be remembered when using the elementary model that the effective Rayleigh number may be ten times larger than its apparent "low temperature" value. Consequently the stream function, which is scaled by the Rayleigh number, seems unrealistically large, however the actual fluid velocities are similar in both models (except for the differences noted already).

Chapter 6 - THREE-DIMENSIONAL TRANSIENT FLOW

6.1 INTRODUCTION

As the solution of the equations governing convective flow through porous media is so time consuming in two dimensions, it is not surprising that the three-dimensional situation is considered less frequently. Most of the research reported has been experimental, for example Bories and Thirriot (1969), Combarnous and Le Fur (19691, Caltagirone et al. (1971) and Combarnous and Bia (1971). However Holst and Aziz (1972b) have performed a short transient numerical solution, and Beck (19721, Busse and Joseph (1972), Gupta and Joseph (1973) and Straus (1974) have viewed the problem analytically. Mercer (1973) has a different approach to hydrothermal modelling, sectioning the region horizontally instead of vertically and using a finite element approach, but this does not take proper account of vertical fluid motion and therefore is not a three-dimensional analysis. As was explained earlier, the numerical methods of Holst and Aziz (1972b) using central differencing and iterative successive over-relaxation techniques are restrictive in that only low Rayleigh numbers can be considered, and even then with dubious accuracy. Since the numerical analysis used here has proved successful so far, it seems expedient to apply it to this new case also. The behaviour of a three-dimensional system with a non-uniform heat input is more relevant to actual geophysical systems than the simple flows modelled in previous sections since the flow patterns are unlikely to be two-dimensional in a real situation.

6.2 THE RANGE OF SOLUTIONS

The Alternative Formulations

The pressure formulation is the less attractive of the two alternatives since it has non-linear terms in a non-Jacobian form which would require the use of unsatisfactory central differencing or very time consuming Kreiss techniques, Furthermore the Neumann type of pressure boundary conditions (2.4.8) produce a singular solution sub-matrix in the Buneman algorithm which requires special treatment unless the upper surface boundary is a recharge boundary (see appendix D).

The advantages of the vector potential formulation are twofold. Firstly the non-linear terms are in Jacobian form and are therefore amenable to Arakawa differencing and secondly the boundary conditions are of Neumann type on only two of the six boundaries, a configuration which can be handled by a much more economical form of the Buneman algorithm. In fact it is possible to solve both vector potential equations (2.4.11) and (2.4.12) faster than the single pressure equation (2.4.4), although memory requirements are slightly larger. On the Burroughs B6700 calculation of a single time step of the complete pressure solution on a 17x17x17 mesh (using central differencing), requires 28 secs of processor time compared to 21 secs for the vector potential solution (using Arakawa differencing), although the latter requires 24K words of data storage against 19K for the pressure solution program.

Boundary Configurations

With such large machine requirements even the faster, more accurate vector potential formulation does not permit extensive numerical experimentation and specific solutions must be sought. For the purposes of this work it is desirable to investigate further the recent work by Straus (1974) who shows that for Rayleigh numbers larger than about 380 no two-dimensional solutions are stable in an infinitely wide region, and explains the transition below this value observed by Combarnous and Le Fur (1969) as being from two-dimensional to three-dimensional modes of flow. Now although this transition had *already* been observed by Caltagirone et al. (1971) in a layer of finite width to be a passage into a fluctuating two-dimensional state, it is not possible to confirm this with certainty from the results of chapter 5 in which the analysis is two-dimensional. Even though Straus' approach specifically precludes the existence of oscillatory solutions, his conclusions raise the question as to whether or not any pseudo-two-dimensional unsteady solution is a correct representation of a three-dimensional flow.

Having already determined in chapter 5 that in some instances there are alternative solutions in this type of flow depending on the initial conditions, it is believed that the proposed three-dimensional flows of Straus (1974) may represent an alternative to the two-dimensional flows of Caltagirone et al. (1969). This possibility is not precluded by the analysis of Straus (1974) who in stability considerations calculated only the eigenvalue with the lowest absolute value.

To resolve the apparent contradiction, flows were simulated at a Rayleigh number of 500 in two closed cubic boxes, one heated uniformly and the other heated over only half the bottom surface.

6.3 THE NUMERICAL RESULTS

Despite attempts to perturb the solutions into three-dimensional modes of flow by raising in temperature one point adjacent to the heater not on a line of symmetry, both configurations maintain two-dimensional flows. The uniformly heated case is strictly two-dimensional and generates smaller unsteady cells exactly as

observed in the experiments of Caltagirone et al. **(1971)** (see figure **6.3.1),** while the half-heated case is almost steady except **for** a **small,** non-increasing three-dimensional secondary flow just above the heater that is a residual **of** the introduced perturbation (figure **6.3.2).** The left and centre illustrations in figure **6.3.1** and **6.3.2** represent the streamlines (see appendix ***G)*** and isotherms on a vertical section passing through **a** diagonal ***of*** the horizontal surfaces and the right hand diagram is and isothermal plot on a section at the horizontal mid-plane.

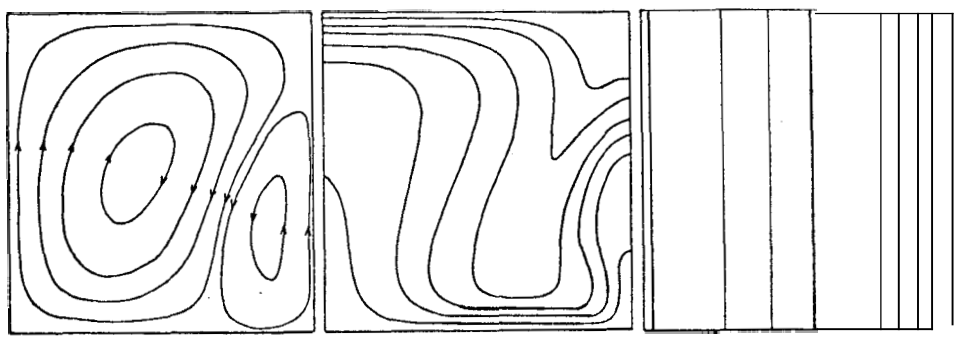

FIGURE **6.3.1** - Unsteady solution for three-dimensional uniformly heated region at R = **500.** Left: Streamlines (vertical diagonal section). Centre: isotherms (vertical diagonal section). Right: Isotherms (horizontal mid-plane).

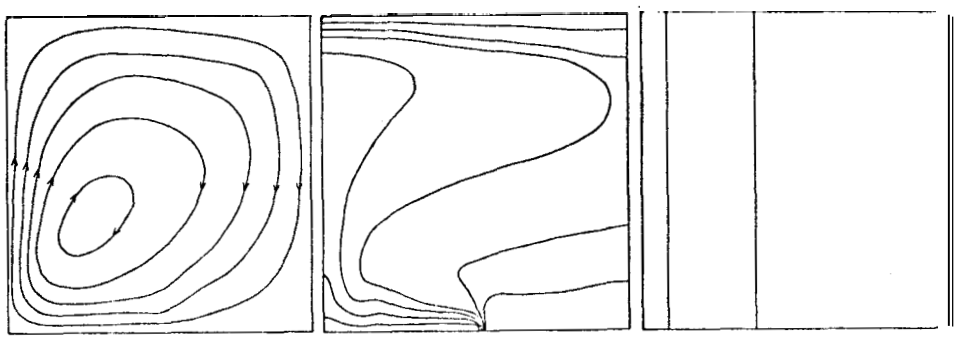

FIGURE 6.3.2 - Steady solution for three-dimensional half heated region at R = **500.**

Uniformly Heated Boundary

Thus it appears that fluctuating two-dimensional rolls *are* the most likely mode of flow in the uniformly heated problem and although the three-dimensional solution of Straus (1974) may be the preferred *steady* flow at this Rayleigh number, **it** does not necessarily occur. This behaviour corresponds to the alternative steady/unsteady solutions in section **5.1** where the supposedly preferred steady solution, which is determined originally by considering an infinitely wide layer (as is the solution of Straus 1974), is commonly rejected in favour of the unsteady solution. Once again the solution is altered by the presence of confining boundaries.

Half-Heated Boundary

Although at a Rayleigh number of **500** the solution to the half-heated problem should just be oscillatory (the cutoff value is **~480)** this behaviour is not apparent for two possible reasons. Either the 17x17x17 mesh used may be too coarse (a finer mesh is not practical for three-dimensional problems) **or** more probably the duration of simulation is too short to reach the oscillatory stage, which takes some time for marginally unsteady solutions.

Three- Dimensional Non-Uniformity

The flow is truly three-dimensional but still unsteady if only one quadrant **of** the lower boundary is heated and in this case regular oscillations occur at intervals of **0.0073** (see figures **6.3.3** and **6.3.4).**

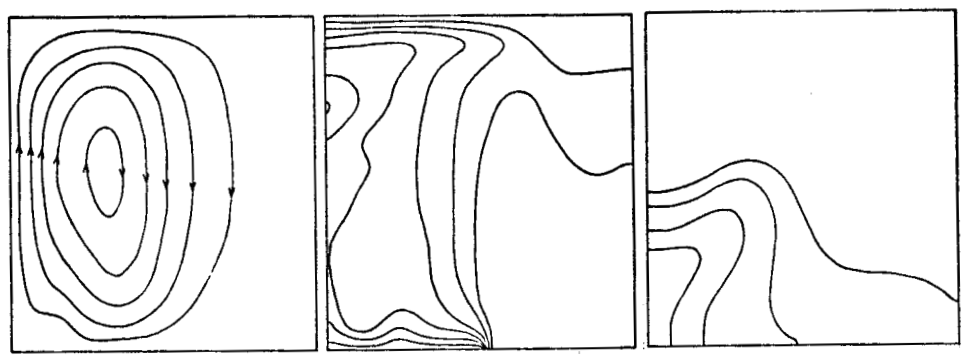

FIGURE 6.3.3 - Oscillatory solution for three-dimensional quarter heated region at R = 500.

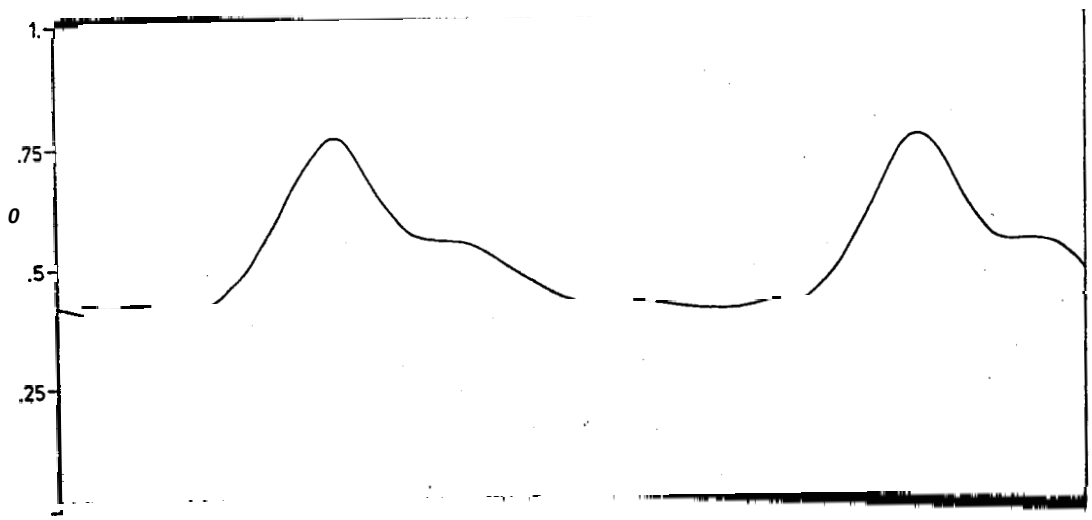

FIGURE **6.3.4 - Variation in time of reference temperature at the mid-point of the vertical edge boundary adjacent to the heater in the quarter heated three-dimensional region.**

These solutions were all generated on a 17x17x17 mesh and took of the order of 350 minutes each. This represents a considerable expenditure on computing resources, and it is expected that this type of three-dimensional modelling will have limited use in geothermal applications except for specific representations. A more suitable technique would be to use an axisymmetric analysis - this would be more useful for modelling geothermal problems but could not be used to investigate the physics of the flow as has been done here.

Chapter 7 - THERMOHALINE CONVECTION IN POROUS MEDIA

7.1 INTRODUCTION

To this point the working fluid considered has been a single component liquid, which corresponds to a pure water geothermal system, but this need not always be the case. Although Wairakei is believed to be a water dominated system (about 12000 ppm dissolved solids), there are hydrothermal areas (for example Reykjaves in Iceland and Niland, U.S.A.) where the saturating fluid is an aqueous solution, containing a significant proportion (Reykjaves 40,000 ppm, Niland 200,000 ppm) of dissolved mineral salts, which has a concentration dependent density. Although the unsteady effects observed so far have been in the thermal problem it is also known that opposing stabilising and destabilising influences in thermohaline convection can cause oscillatory instability. Thermohaline or double diffusive convection in a fluid layer has been studied numerically by Elder (1969), experimentally by Foster (1968 and 1969), Shirtcliffe and Turner (1970), Lambert and Demenkow (1971), Hurle and Jakeman (1971), Platten and Chavepayer (1973) and Shirtcliffe (1973), and analytically by Nield (1967), Baines and Gill (1969), Joseph (1970), Legros, Platten and Poty (1972) and Hart (1973). In several cases "overstable" solutions were predicted and a good summary plot of the stability of this problem is given by Baines and Gill (1969) in the Rayleigh number/solutal Rayleigh number plane. These analyses have all been performed for the fluid layer problem and represent only a small proportion of research in this field. The thermohaline problem in a porous medium which is of interest here has been less extensively investigated. Taunton, Lightfoot ana Green (1972) have performed a similar linear stability analysis to Baines and Gill (1969) in the porous medium case, and extended the earlier study by Nield (1968). Both investigations noted the possibility of overstable oscillatory solutions and determined the conditions under which they can occur, but neither revealed what form these oscillations might take or what processes cause them. An energy stability analysis was considered by Wankat and Schowalter (1970) but without specific reference to oscillatory solutions.

It seems desirable then to adapt the numerical approach used in chapters 5 and 6 to the two-dimensional thermohaline problem in a porous medium in order to explore another instability mechanism which may be present in geothermal systems.

7.2 THE EQUATIONS OF MOTION

The derivation of the governing equations closely follows that of section 2.1, except that the fluid density variation is now a function of both the change in dissolved salt concentration and the excess temperature, Thus (2.1.5) is replaced by

$$\rho = \rho_o \left[1 - \alpha(T - T_o) - \alpha' (C - C_o) \right] \quad , \tag{7.2.1}$$

where C is the saltconcentration and the prime denotes quantities associated with it (this makes α' the coefficient of solutal expansion of the fluid). Combining with (2.1.1) and (2.1.2) and invoking the Boussinesq approximation, the equations become

$$\frac{\partial q_i}{\partial x_i} = 0 \quad , \tag{7.2.2}$$

$$\frac{Dq_i}{Dt} = g_i\alpha(T-T_o) + g_i\alpha'(C-C_o) - \frac{1}{\rho}\frac{\partial p}{\partial x_i} - \frac{\nu}{k} q_i \quad , \tag{7.2.3}$$

and $$\frac{\partial T}{\partial t} = \kappa\nabla^2 T - \lambda q_i \frac{\partial T}{\partial x_i} \tag{7.2.4}$$

It is also necessary to incorporate an equation to describe the transport of dissolved salt, and this is the well known diffusion equation (Holman 1968 p.336)

$$\frac{\partial C}{\partial t} + q_j \frac{\partial C}{\partial x_j} = \kappa' \nabla^2 C \quad , \tag{7.2.5}$$

where κ' is the solutal diffusivity. As before the inertia terms may be neglected and the equations rewritten in non-dimensional form. Defining the additional variable

$$C^* = \frac{C - C_o}{C_1 - C_o}$$

and introducing ψ as in (2.3.6), the equations (7.2.3) become (dropping the * immediately for convenience),

$$\frac{\partial P}{\partial X} = - \frac{\partial \psi}{\partial Y} \quad ,$$

and $$\frac{\partial P}{\partial Y} = \theta + \gamma C + \frac{\partial \psi}{\partial X} \quad .$$

which may be simplified by cross-differentiation and subtraction, to

$$\nabla^2 \psi = - \frac{\partial \theta}{\partial X} - \gamma \frac{\partial C}{\partial X} \quad , \tag{7.2.6}$$

where γ is the buoyancy ratio $\dfrac{\alpha'(C_1 - C_o)}{a\,(T_1 - T_o)}$

Equations (7.2.4) and (7.2.5) become respectively

$$\nabla^2 \theta = \frac{\partial \theta}{\partial \tau} - R \left[\frac{\partial \psi}{\partial Y} \frac{\partial \theta}{\partial X} - \frac{\partial \psi}{\partial X} \frac{\partial \theta}{\partial Y} \right] \quad , \tag{7.2.7}$$

and $\frac{\kappa'}{\kappa} \nabla^2 C = \frac{\partial C}{\partial \tau} - R/\lambda \left[\frac{\partial \psi}{\partial Y} \frac{\partial C}{\partial X} - \frac{\partial \psi}{\partial X} \frac{\partial C}{\partial Y} \right]$. (7.2.8)

These last three equations constitute the set governing the flow,

Boundary Conditions

The problem boundaries are the same as those considered in the original enclosed model (section 2.2), but since it is expected that the appearance of a regular oscillatory solution is now dependent on the presence of the salinity gradient it is advantageous to consider a uniform high temperature source (f = 1) which would not normally produce a regularly fluctuating flow. The dissolved salt concentration varies from a minimum value C_o at the surface to a maximum of C_1 at the base, or 0 and 1 respectively in terms of the non-dimensional concentration. This corresponds to a configuration in which hotter fluid holds more solute than colder fluid closer to the surface. A uniform stratification between these two limits is initially stable if the salt solution is denser than the solvent (as is usually so), in which case a' and the buoyancy ratio γ are both negative.

Physical Parameters

The flow is destabilised by the thermal gradient and stabilised by the salinity effects, the interaction between these opposing influences being dependent on the values of the diffusivity ratio $\frac{\kappa'}{\kappa}$, the buoyancy ratio γ and the Rayleigh number R. The flow is inherently more steady than the single component case due to the stabilising solutal effects and thus for convective solutions the Rayleigh number is comparatively large (> 2000). For the purposes of this section the solid porous matrix is considered to be a poor conductor so the heat capacity ratio X is taken to be unity, and from Elder (1969) and Taunton, Lightfoot and Green (1972) the buoyancy ratio is typically of order -1. and the conductivity ratio of order 0.01. Since the solutal Rayleigh number S used by these authors is related to the thermal Rayleigh number R by the expression

$$\frac{R}{S} = \frac{(\frac{\kappa'}{\kappa})}{\gamma} \quad , \qquad (7.2.9)$$

then these values represent a situation which lies well within the completely non-convecting zone in the stability locus plot of Taunton, Lightfoot and Green (1972) with a tendency towards overstability rather than monotonic convection. The results of this section confirm that for any realistic situation that is likely to occur in an actual geothermal system, a *permanently* unstable solution is improbable with these boundary conditions. However temporarily transient flows can occur for short durations and the physical parameters may be enlarged beyond their likely physical magnitude in order to observe what form these overstable solutions may take. Steady convection patterns can also occur for very weak salinity gradients but these are less likely to occur than the overstable flows, and in any case are closely aligned to the thermal convective solutions which have already been obtained in section 5.1. It would be possible to study the effect of a destabilising salinity gradient (as might be the situation in the case of heavily mineralled waters flashing to steam at higher levels and depositing their solutes) but as the equations are so similar the solutions would also be not unlike the thermal solutions of the previous chapters.

7.3 THE NUMERICAL RESULTS

The numerical representation of **(7.2.6), (7.2.7)** and **(7.2.8)** may be achieved in a manner similar to that of chapter 4, using fourth order Arakawa differencing for the advection terms and Bunemen odd-even reduction for the Poisson equation. The system is initially presented with a conduction solution and a small unicellular perturbation. The solutions **so** generated are summarised in table **VIII** and fall into three main groups - a set at realistic values of the diffusivity and buoyancy ratios over a range **of** Rayleigh numbers, a set at similar Rayleigh numbers with a more positively stabilising salinity gradient, and a third set with an unrealistically strong salinity gradient. In all solutions the final result is a motionless flow with uniformly stratified temperature and salinity fields, but in some cases a decaying oscillation with period τ_P occurs beforehand.

Table **VIII** Thermohaline Solutions

	κ'/κ	v	τ_P	Process Observed
	0.01	**-1.0**	-	Conduction
	0.01	**-1.0**	-	Conduction
	0.01	**-1.0**	-	Conduction
	0.01	**-1.0**	**0.0465**	Decaying Oscillation
	0.01	**-1.0**	**0.0250**	Decaying Oscillation
3500	**0.01**	**-1.0**	**0.0170**	Decaying Oscillation
1000	**0.05**	**-1.0**	-	Conduction
1000	**0.05**	**-0.5**	-	Conduction
1000	**0.05**	**-0.75**	0.024	Decaying Oscillation
500	**0.10**	**-1.0**	-	Conduction
1000	**0.10**	**-1.0**	-	Conduction
1500	0.10	-1.0	**0.055**	Decaying Oscillation
2000	**0.10**	**-1.0**	**0.025**	Decaying Oscillation
2500	0.10	**-1.0**	**0.013**	Decaying Oscillation
500	**0.5**	-1.0	-	Conduction
500	**1.0**	**-1.0**	-	Conduction
1000	**1.0**	**-1.0**	-	Conduction
2000	1.0	-1.0	-	Conduction
3000	**1.0**	**-1.0**	-	Conduction

This oscillation takes the **form** of a pair **of** cells that periodically change their direction of rotation *so* that the central plume between them alternatively rises and falls (see figure **7.3.1**).

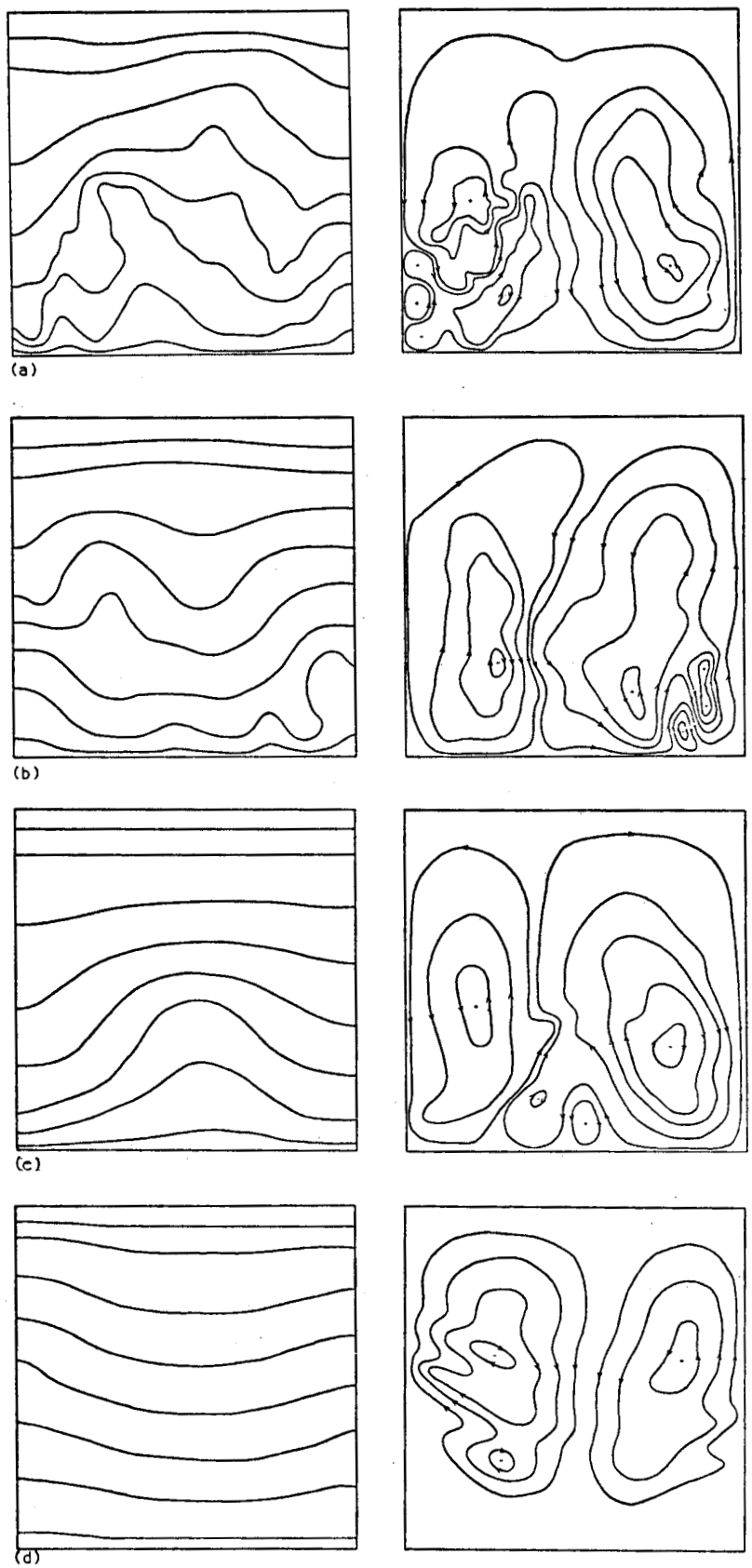

FIGURE **7.3.1** - Oscillatory soluti'on for thermohaline problem at R = 3500, γ = -1, dIffusivity ratlo = 0.01. Evenly spaced sequence of isotherms (left) and streamlines (right).

This results in a characteristic "flag-waving" motion of the isotherms which is reflected in the salinity isoclines only rather more diffusely. Increasing the stabilising salinity gradient intensifies the effect which then takes place with greater frequency.

The Oscillation Mechanism

The mechanism of these oscillations depends on the coupling between the temperature and concentration fields. The two components of the system diffuse at different rates (the diffusivity of heat is 100 times greater) and thus a parcel of fluid which is displaced vertically loses excess heat faster than excess salinity. The parcel of fluid then has a strongly stabilising force acting upon it and it tends to descend again, producing the reversal of the plume. As it descends the opposite effect occurs as heat diffuses in faster than salinity diffuses out and the concentration effects have a decreasingly stabilising influence as the lower and denser levels of the salinity stratification are reached. The oscillation continues several more times, decaying due to thermal dissipation. At no time does the flow become significantly convective with major circulations like those in the thermal solutions in previous chapters, and the motion is due entirely to the temperature/concentration interaction (this is indicated by the fact that the oscillations do not appear when the diffusivity ratio is increased).

Interpreting these results in a physical sense, it is seen that stabilising salinity gradients could have the effect of preventing motion in a geothermal system. However, this is not the case in actual systems such as Reykjaves and Niland in which convective heat transfer is prominent, where more complex processes occur. Firstly a major characteristic of a brine geothermal system is the importance of the steam phase. Flashing of water to steam at shallow levels produces a heavy concentration of salts at the surface, which produces a local destabilising gradient. Secondly a constant heat flux source at the base cf the formation will accumulate thermal energy in a stabilised, non-convecting system until a stage is reached where locally the destabilising temperature gradient may overcome the stabi1ising salinity gradient and the system being to convect. These two phenomena lie beyond the capabilities of the present model which considers only single phase flow and an isothermal heat source. This simpler model is useful for demonstrating the mechanics of the interactions which may occur between conflicting influences on the flow, without paying too much attention to specific instances of occurrence.

Chapter 8 - THE POROUS INSULATOR PROBLEM

8.1 INTRODUCTION

The model regions considered in chapters 4 - 7 have all been heated from below, and although this is the more commonly studied case, a porous enclosure raised in temperature on one of its vertical sides as in figure 8.1.1 is of some interest also.

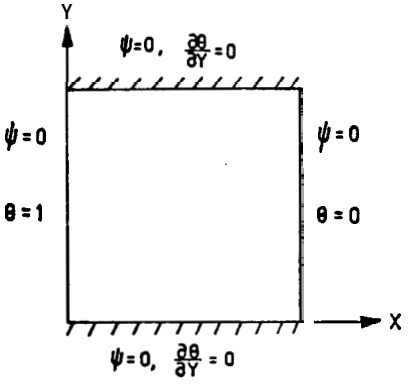

FIGURE 8.1.1 - Problem boundaries for porous insulator problem.

Such a situation arises in porous insulators; for example within nuclear reactors, fibreglass building materials, hot water pipe lagging and refrigerator walls. If convection occurs in a homogeneous layer of insulating fluid, for instance an air gap in a house wall, the heat transfer across the layer is greater than if only conduction takes place. If the gap is of finite thickness but infinite height and width it has been proven by Gill (1969) that the introduction of a porous material reduces inertial effects to such a point that convection cannot happen, and improves the effectiveness of the system as an insulator (provided of course that the permeable solid is not highly conductive). However for a sealed porous slab of finite proportions Betbeder and Jolas (1972) found experimentally and numerically that convective motion is possible, which confirmed the earlier numerical results of Chan, Ivey and Barry (1970). Jannot, Naudin and Viannay (1973) investigated a different case in which the unheated and cooler vertical boundary is open to the environment with a forced flow of fluid through it, but they too observed convective solutions.

8.2 THE NUMERICAL SOLUTIONS

The solution process for this problem is essentially similar to that for the fully-heated region in chapter 2 except that the gravity vector is rotated through ϑ with respect to the region boundaries - so that (2.3.10) becomes

$$\nabla^2\psi = -\frac{\partial\theta}{\partial X} \quad , \tag{8.2.1}$$

and the heat transport equation (2.3.9) remains unchanged. As it happens the flows obtained are always steady and unicellular which permits the use of a variable sized time step in the numerical scheme, increasing the increment as the solution approaches a steady state, thereby reducing the length and increasing the accuracy of the calculation. At each stage of the computation the prospective alterations to the temperature matrix $(\frac{\partial\theta}{\partial\tau} . \Delta\tau)$ are scanned and then scaled uniformly so that the maximum alteration is always by the same amount at every time step. This ensures both that the time differencing does not become numerically unstable due to the temperature changes becoming too large and that the solution proceeds as rapidly as possible without it becoming so. This procedure is analogous to successive over-relaxation in a quasi-steady solution method.

The results presented below in table IX are not as remarkable as the unsteady flows observed in earlier chapters, however they confirm and extend the experimental results of Betbeder and Jolas (1972) and verify once again the viability of the numerical method.

Table IX Horizontal Temperature Gradient Solutions

R	Square Cell			Rectangular Cell (2x1)		
	Mesh Size	Nu	ψ_{max}	Mesh Size	Nu	ψ_{max}
25	17x17	1.11	0.065	17x33	1.10	0.055
50	17x17	1.99	0.057	17x33	1.42	0.053
200	17x17	4.89	0.038	17x33	3.03	0,040
500	33x33	8.78	0.028	33x65	4.98	0.029
1000	33x33	12.40	0.022	33x65	7.21	0.021
1250	33x33	13.09	0.020	33x65	8.11	0.019
1500	33x33	14.42	0.018	33x65	8.65	0.018

Nusselt Number Dependence

Comparison of the results for the square and for the tall rectangular cell reveals that if the height of the cell is increased without changing its width or the value of the Rayleigh number, then the Nusselt number decreases, as in figure (8.2.1), in accordance with the assertions of Betbeder and Jolas (1972) which are also compatible with the conclusions of Gill (1969) for the infinitely tall cell. Typical solutions at Rayleigh numbers of 50 and 1000 are illustrated in figures 8.2.2, 8.2.3, 8.2.4 and 8.2.5.

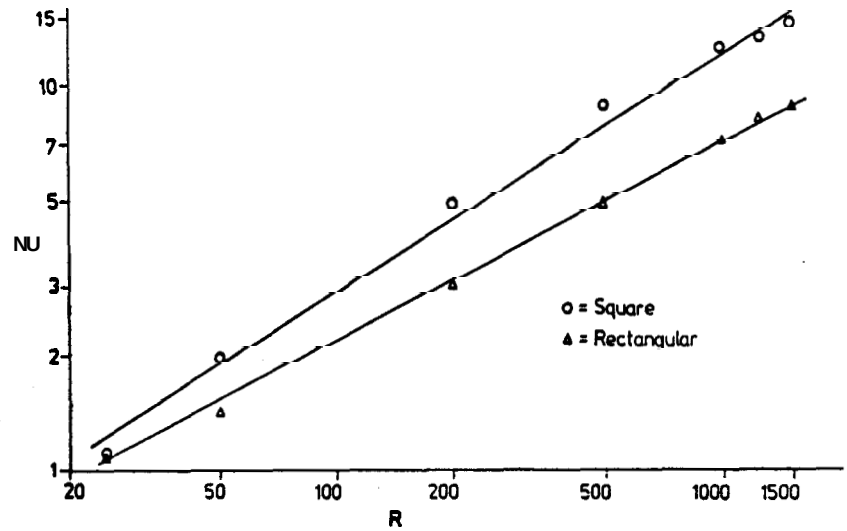

FIGURE 8.2.1 - Plot of Nusselt number Nu vs Rayleigh number R for porous insulator problem.

Horizontal Boundaries

This analysis serves to highlight the artificiality of the conditions considered by Gill (1969) - although in the infinite case there is no convective heat transfer, for all real regions the flow is convective even at very small Rayleigh numbers. The introduction of a horizontal boundary into the path of fluid rising adjacent to the vertical heater redirects the flow perpendicularly and thus results in a transverse advection of heat. Thus in this case it is the presence of the enclosing horizontal boundaries that is instrumental in producing a convective solution. Although this effect is clearly unlike the influence that the vertical boundaries have on the hypothetical steady multicellular motions of section 5.1 and three-dimensional motions of chapter 6, this is the third time that it has been demonstrated that solutions derived for an infinite region are inapplicable to real boundaries.

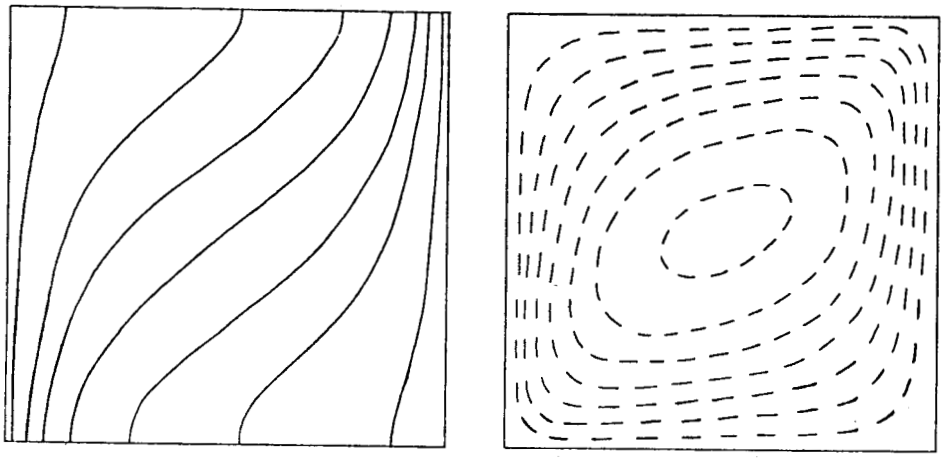

FIGURE 8.2.2 - Porous insulator solution, R = 50. square cell. Isotherms (——) and streamlines (– – –).

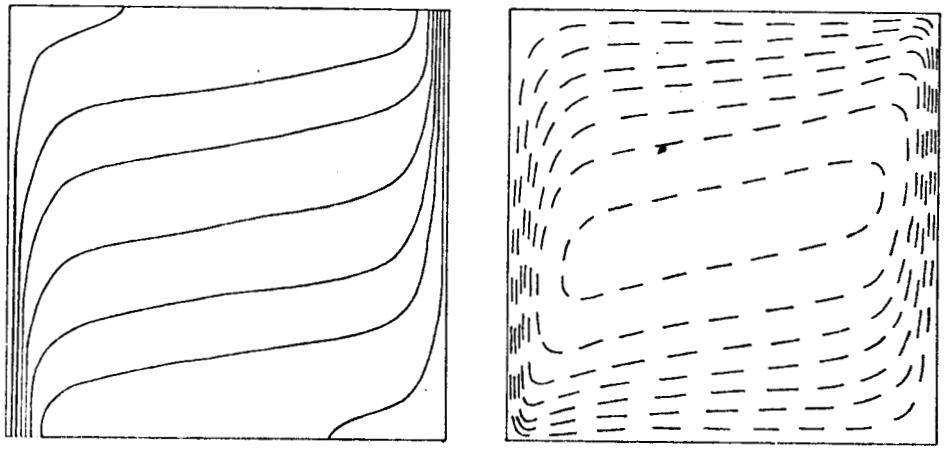

FIGURE 8.2.3 - Porous insulator problem, R = 1000, square cell

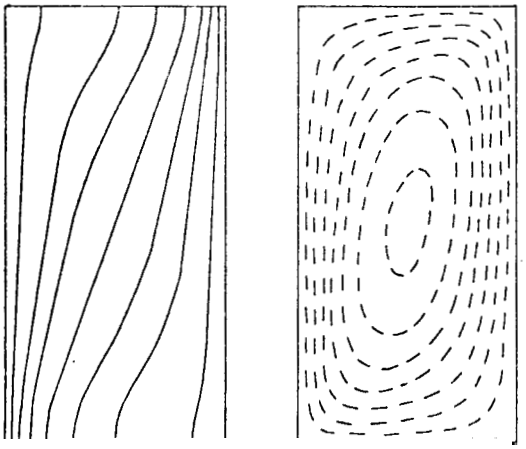

FIGURE 8.2.4 - Porous insulator problem, R = 50, rectangular cell. Isotherms (left) and streamlines (right).

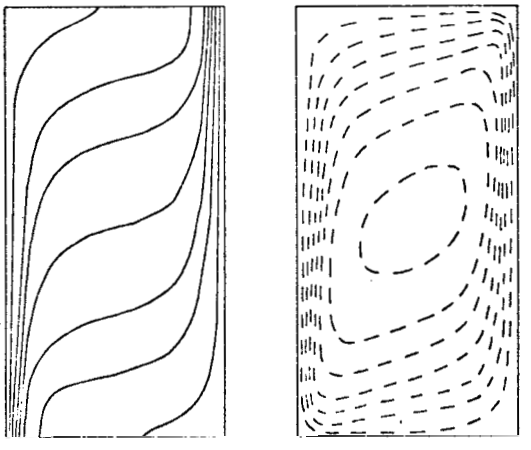

FIGURE 8.2.5 - Porous Insulator problem, R = 1000 rectangular cell.

Chapter 9 - SUMMARY AND CONCLUSIONS

9.1 EVALUATION OF THE RESULTS

The character of the flow of a fluid in a porous medium is not only governed by its equations of motion, but is also shown to be influenced by the presence of the boundaries of the region. This configuration dependency is evident in the results both for regions heated from below and those heated from the side. The dependency of the flow on inherent fluid properties is demonstrated in the thermohaline instabilities in chapter 7 and in the generation of thermals observed in chapters 5 and 6 (most clearly in the recharge solutions of section 5.4). Although the two different dependencies are contiguous and often cannot be disassociated, it is useful to review them separately.

9.2 THE THERMAL BOUNDARY LAYER

The generation of thermal disturbances is the most notable characteristic of the behaviour of fluid flowing in a porous medium. The fundamental mechanism of this process is the coupling between the temperature and velocity fields within a thermal boundary layer which is formed over the heat source. Thermal anomalies evolve in this layer by conduction and are swept away and dissipated by dominant circulating velocities.

The appearance of the thermal boundary layer depends on the flow conditions that already exist in the region. In general, a flow pattern with a larger number of convection cells removes energy from the heater more quickly than a single celled flow, and so the thermal boundary layer may not necessarily form sufficiently to produce thermal disturbances when the cell number is increased. The layer may also be expelled by the injection of fluid close to the heater or by the expansion of the rising convective plume caused by the lateral extension of a rectangular region.

9.3 THE PREFERRED SOLUTION

At any particular Rayleigh number, a region of a certain shape has a ***preferred solution*** that results in maximum heat transfer across the system. For example in a square, uniformly heated, closed boundary region at R = 400 the preferred solution is a steady two-dimensional tricellular flow. The preferred solution is Rayleigh number dependent and **so** the alteration of the effective Rayleigh number during the course of the development of a flow can have quite remarkable effects on the eventual solution (which need not necessarily be the preferred one). This is one of the most significant consequences of the results presented in this work.

If the actual Rayleigh number is ***less*** than the Rayleigh number which is characteristic of the number of cells in the flow at the time, then it is possible for the flow pattern to adjust by dissipating excess cells to form the preferred solution. However when the actual Rayleigh number ***exceeds*** the value implied by the number of cells, the flow pattern cannot adjust because potential new cells do not form properly before being absorbed by the dominant flow. The flow then becomes fluctuating or regularly oscillatory as new cells continue to form and disappear.

9.4 DISTURBANCE INTERACTIONS

The regularity of an unsteady solution depends on the interaction between the temperature disturbances. **In** the closed boundary model there is a forward interaction, as ascending disturbances may influence descending ones which are forming in front of them, however the effect is only weak. A much stronger backward interaction is seen in the recharge solutions in section **5.4** ; this is caused by the interruption of a gestating disturbance by its predecessor.

These reactions are different to those proposed by Keller **(1966)** and Welander **(1967)** for a simple loop model, in which a disturbance is envisaged as being preserved throughout a complete circuit of the convection cell (a loop in their case). The disturbance then receives a boost on rearrival over the heater and makes another circuit of the cell. This conception may be used to explain periodic effects in the loop models, and also in the fluid layer model of Moore and Weiss **(1973)**, but cannot account for periodicity in convection through porous media. The presence *of* the porous matrix dissipates the thermal disturbances before they can complete a circuit *of* the cell. Furthermore the periodicity persists even in the recharge solutions in which fluid enters and leaves the system through the upper surface and only passes the heater ***once*** in its path. In the porous medium problem the regularity is inherent in the ***generation*** of thermal anomalies rather than their behaviour after formation as in the fluid loop. The intervals between the disturbances is Rayleigh number dependent and obeys a *312* power relationship.

9.5 TEMPERATURE/SALINITY EFFECTS

In the thermohaline convection problem in a porous medium there is a coupling between the temperature and salinity concentration equations (via the momentum equation), and it is the interaction of these two influences that produces the motion. The pulsating flow which ensues is simpler to explain than the unsteady flows in the thermal problem since in this case the effects are explicitly opposing and there is no overlying convective motion. A thermal disturbance carries with it an increasingly stabilising concentration anomaly that eventually halts it and reverses the direction of travel. This behaviour is less prevalent than in the fluid layer thermohaline problem due to the less significant inertial effects.

9.6 THE PRESENCE OF BOUNDARIES

One of the most unexpected discoveries in this investigation is the significance of physical boundaries in this problem. Elder (1967a) refers to "end effects" in his solutions at low Rayleigh numbers, however it is well established here that at higher Rayleigh numbers certain major features of the flow in porous media are produced by the presence of boundaries. The flow in the uniformly heated regions of section 5.1 has alternative steady and unsteady modes depending on how much of the preferred solution has been introduced into the closed region. In an infinite region the comment made earlier, that the number of convection cells cannot increase, does not apply. Therefore the unsteady two-dimensional rolls occur only in finite regions.

A similar argument may be used when considering the three-dimensional flows. Once a two-dimensional mode of flow has been set up in the region it is not possible to increase the number of cells in the (finite) third dimension. The flow remains two-dimensional even though the preferred solution in an infinite region would be three-dimensional.

The flow in the horizontal temperature gradient configurations of chapter 8 also differs significantly from the infinite region solution, since the flows are convective if horizontal boundaries are present.

9.7 THE PHYSICAL IMPLICATIONS

Assuming a depth of 5 km fluctuations such as those observed in chapter 5 would appear in a real geothermal system at intervals of the order of 500-1000 years and the simulations predict that they would require up to 50,000 years from the initial evolution of the system before they occurred. The calculated history of the

Wairakei system suggest a past life of around 10^6 years (Elder 1966a). It has been suggested by Hochstein **(1974)** that geological evidence from bore samples and gravimetric surveys of the Broadlands geothermal field indicate that mineral deposits are in excess of those expected from the system in its current form. This suggests that the region has existed as a steam **or** brine system at some time in the past, as might have been the case if a higher temperature anomaly had risen up through the system. Using a statistical survey of the world's hydrothermal systems Hochstein **(1974)** deduced that the interval for which the anomalous system might exist would be of the order of **500** years. The large variability of the parameters and the simplistic structures modelled in this work do not permit quantitative conclusions concerning the effects, however the implication of the transient behaviour observed in the numerical models is suggestive.

9.8 EXPLOITATION

Although the removal of water from a geothermal system would not prevent the appearance of low frequency transiency, the reinjection of water might do **so.** If cold water is introduced into fissures which feed fluid to the heat source the thermal boundary layer over the hot rock is interrupted and unsteady effects would not occur. The more realistic injection system which introduces fluid at shallower depths, results in an increase in the quantity of heat that may be retrieved from the system, however in this case transient behaviour is still possible. In order to achieve maximum heat transfer through the system from the energy source to the surface, it is necessary to properly locate the collection and reinjection bores. Such an optimisation has not been performed here, but the possible wastage of heat by the incorrect positioning of wells is indicated.

9.9 FUTURE MODELLING OF GEOTHERMAL FIELDS

The range of conditions considered in this work falls short of a complete representation of a real geothermal region. In the Wairakei geothernal system the additional features of two-phase flow, non-isotropic permeability and mechanical response of the porous rock still need **to** be accommodated. Two-phase considerations are necessary for the simulation **of** upper "reservoir" although they may be omitted from the deep models used here. Incorporation of permeability variation requires a more concise description of the geophysical structure of the system than is currently available. The mechanical response of the medium to alterations in the flow (changes from water to steam, closing of fissures, subsidence etc.) is a problem in solid mechanics and is as important a field for investigation as the investigation of the convective flow itself. Although three-dimensional flows in a simple model

have been simulated in this work, the full scale numerical representation of an actual geothermal system in three dimensions is likely to be enormously expensive (although not impossible). However this difficulty may be evaded by the development of an axisymmetric model - in terms of applicability to geothermal regions this would lie somewhere between the two-dimensional and three-dimensional models derived in this work.

APPENDIX A - THE ARAKAWA DIFFERENCING SCHEMES

The Arakawa finite difference representations of the advection term (equation 4.2.1) are as follows (Arakawa **1966**):

$$
\begin{aligned}
J^{(1)}_{i,j} = -\frac{1}{12(\Delta X)(\Delta Y)} \big[& (\psi_{i,j-1} + \psi_{i+1,j-1} - \psi_{i,j+1} - \psi_{i+1,j+1})(\theta_{i+1,j} - \theta_{i,j}) \\
& + (\psi_{i-1,j-1} + \psi_{i,j-1} - \psi_{i-1,j+1} - \psi_{i,j+1})(\theta_{i,j} - \theta_{i-1,j}) \\
& + (\psi_{i+1,j} + \psi_{i+1,j+1} - \psi_{i-1,j} - \psi_{i-1,j+1})(\theta_{i,j+1} - \theta_{i,j}) \\
& + (\psi_{i+1,j-1} + \psi_{i+1,j} - \psi_{i-1,j-1} - \psi_{i-1,j})(\theta_{i,j} - \theta_{i,j-1}) \\
& + (\psi_{i+1,j} - \psi_{i,j+1})(\theta_{i+1,j+1} - \theta_{i,j}) \\
& + (\psi_{i,j-1} - \psi_{i-1,j})(\theta_{i,j} - \theta_{i-1,j-1}) \\
& + (\psi_{i,j+1} - \psi_{i-1,j})(\theta_{i-1,j+1} - \theta_{i,j}) \\
& + (\psi_{i+1,j} - \psi_{i,j-1})(\theta_{i,j} - \theta_{i+1,j-1}) \big] \qquad \text{(A.1)}
\end{aligned}
$$

this being the second-order scheme, and

$$
\begin{aligned}
J^{(2)}_{i,j} = \frac{1}{24(\Delta X)(\Delta Y)} \big[& \theta_{i+1,j+1}(\psi_{i,j+2} - \psi_{i+2,j}) - \theta_{i-1,j-1}(\psi_{i-2,j} - \psi_{i,j-2}) \\
& - \theta_{i-1,j+1}(\psi_{i,j+2} - \psi_{i-2,j}) + \theta_{i+1,j-1}(\psi_{i+2,j} - \psi_{i,j-2}) \\
& + \theta_{i+2,j}(\psi_{i+1,j+1} - \psi_{i+1,j-1}) - \theta_{i-2,j}(\psi_{i-1,j+1} - \psi_{i-1,j-1}) \\
& - \theta_{i,j+2}(\psi_{i+1,j+1} - \psi_{i-1,j+1}) + \theta_{i,j-2}(\psi_{i+1,j-1} - \psi_{i-1,j-1}) \\
& + (\theta_{i+1,j+1} - \theta_{i-1,j-1})(\psi_{i-1,j+1} - \psi_{i+1,j-1}) \\
& - (\theta_{i-1,j+1} - \theta_{i+1,j-1})(\psi_{i+1,j+1} - \psi_{i-1,j-1}) \big] \qquad \text{(A.2)}
\end{aligned}
$$

forms the fourth-order correction where the fourth order scheme is given by

$$
J^{(3)}_{i,j} = 2J^{(1)}_{i,j} - J^{(2)}_{i,j} \quad . \qquad \text{(A.3)}
$$

Equation (A.2) differs from that in the original paper in which there is a typographical error. Also the $\theta_{i,j}$ terms in (A.1) are redundant and may be cancelled out, resulting in a slightly faster calculation.

APPENDIX B - AN EXTENSION OF THE BUNEMAN ALGORITHM TO FOURTH-ORDER ACCURACY

The algorithm of Busbee, Golub and Nielson (1970) for the solution of Poisson's equation

$$\nabla^2 X = Y \quad , \tag{B.1}$$

with Dirichlet boundary conditions, uses the usual second-order accurate representation of the Laplacian

$$\nabla^2 X = (X_{i+1,j} + X_{i,j-1} + X_{i-1,j} + X_{i,j+1} - 4X_{i,j}) \frac{1}{h^2} \quad , \tag{B.2}$$

where h is the spatial increment in a square MxN mesh (M = N), and constructs a solution matrix equation in the form

$$\underset{(N-2)\times(N-2)}{\begin{bmatrix} A & T & & & & \\ T & A & T & & & \\ & T & A & T & \cdots & \\ & & & \vdots & & \\ & & & T & A & \end{bmatrix}} \underset{(N-2)\times 1}{\begin{bmatrix} \underset{\sim}{x}_2 \\ \underset{\sim}{x}_3 \\ \underset{\sim}{x}_4 \\ \vdots \\ \underset{\sim}{x}_{N-1} \end{bmatrix}} = \underset{(N-2)\times 1}{\begin{bmatrix} \underset{\sim}{y}_2 \\ \underset{\sim}{y}_3 \\ \underset{\sim}{y}_4 \\ \vdots \\ \underset{\sim}{y}_{N-1} \end{bmatrix}} \quad , \tag{B.3}$$

where $\underset{\sim}{x}_j = X_{i,j}$ $\quad i = 2,3,4 \ldots M-1$

and $\underset{\sim}{y}_j = Y_{i,j}$ $\quad i = 2,3,4 \ldots M-1$,

and A is a tridiagonal matrix of the form

$$A = \underset{(M-2)\times(M-2)}{\begin{bmatrix} -4 & 1 & & & & \\ 1 & -4 & 1 & & & \\ & 1 & -4 & 1 & \cdots & \\ & & & \vdots & & \\ & & & 1 & -4 & \end{bmatrix}} \quad , \tag{B.4}$$

and T is an (M-2)x(M-2) identity matrix. Now the substitution I for T allows the derivation of a simple and particularly useful computational procedure, however if the fourth-order representation

$$\nabla^2 X = \frac{1}{h^2}\left[\frac{2}{3}(X_{i,j+1} + X_{i,j-1} + X_{i+1,j} + X_{i-1,j}) - \frac{10}{3} X_{i,j} + \frac{1}{6}(X_{i+1,j+1} + X_{i+1,j-1} + X_{i-1,j+1} + X_{i-1,j-1})\right] \tag{B.5}$$

is used as suggested by Orszag and Israeli (1974) then A is of the form

$$A = \begin{bmatrix} -\frac{10}{3} & \frac{2}{5} & & & \\ \frac{2}{3} & -\frac{10}{3} & \frac{2}{3} & & \\ & \frac{2}{5} & -\frac{10}{3} & \frac{2}{3} \cdots & \\ & & & \vdots & \\ & & & \frac{2}{3} & -\frac{10}{3} \end{bmatrix} \qquad \text{(B.6)}$$

$(M-2) \times (M-2)$

and T is of the form

$$T = \begin{bmatrix} \frac{2}{3} & \frac{1}{6} & & & \\ \frac{1}{6} & \frac{2}{3} & \frac{1}{6} & & \\ & \frac{1}{6} & \frac{2}{3} & \frac{1}{6} \cdots & \\ & & & \vdots & \\ & & & \frac{1}{6} & \frac{2}{3} \end{bmatrix} \qquad \text{(B.7)}$$

$(M-2) \times (M-2)$

In this case the simplified derivation of Busbee, Golub and Nielson **(1970)** does not follow, and must be generalised to accommodate the case $T \neq \mathbf{I}$.

Considering the rows $(j-1)$, j and $(j+1)$ of the original (and perfectly general) equations (B.3), dropping the vector signs for simplicity -

$$\begin{aligned} T x_{j-2} + A x_{j-1} + T x_j &= y_{j-1} \\ T x_{j-1} + A x_j + T x_{j+1} &= y_j \\ T x_j + A x_{j+1} + T x_{j+2} &= y_{j+1} \end{aligned} \quad .$$

The first reduction is achieved by multiplying the first and third equations by T and the second by A and subtracting the second from the sum of the first and third -

$$T^2 x_{j-2} + (2T^2 - A^2) x_j + T^2 x_{j+2} = T y_{j-1} + T y_{j+1} - A y_j \quad .$$

This reduction is performed on every alternate row $j = 3,5,7$ etc. and therefore halves the number of rows in the solution matrix. Following the complete reduction new contracted matrices and vectors may be defined as

$$y_j^{(1)} = T y_{j-1} + T y_{j+1} - A y_j$$

or $$y_j^{(1)} = A^{(1)} A^{-1} y_j + T y_{j-1} + T y_{j+1} - 2T^2 A^{-1} y_j \quad ,$$

where $$A^{(1)} \equiv (2T^2 - A^2)$$

and $$T^{(1)} = T^2$$

or introducing

$$p_j^{(1)} = A^{-1} y_j$$

and $$q_j^{(1)} = T(y_{j-1} + y_{j+1} - 2T\, p_j^{(1)}) \quad ,$$

then $$y_j^{(1)} = A^{(1)} p_j^{(1)} + q_j^{(1)} \quad .$$

Now after performing similar reductions r+l times

$$y_j^{(r+1)} = T^{(r)}(y^{(r)}_{j-2^r} + y^{(r)}_{j+2^r}) - A^{(r)} y_j^{(r)} \quad ,$$

and $$y_j^{(r)} = A^{(r)} p_j^{(r)} + q_j^{(r)} \quad .$$

Combining these last two equations

$$A^{(r+1)} p_j^{(r+1)} + q_j^{(r+1)} = T^{(r)}[\, A^{(r)}(p^{(r)}_{j-2^r} + p^{(r)}_{j+2^r}) + (q^{(r)}_{j-2^r} + q^{(r)}_{j+2^r})] - A^{(r)}(A^{(r)} p_j^{(r)} + q_j^{(r)}) \quad ,$$

and substituting

$$A^{(r+1)} = 2\, T^{(r)} T^{(r)} - A^{(r)} A^{(r)}$$

implies

$$q_j^{(r+1)} = T^{(r)} [\, q^{(r)}_{j-2^r} + q^{(r)}_{j+2^r} - 2T^{(r)} p_j^{(r+1)}] \quad , \qquad \text{(B.8)}$$

and $$p_j^{(r+1)} = p_j^{(r)} - (A^{(r)})^{-1} [\, T^{(r)}(p^{(r)}_{j-2^r} + p^{(r)}_{j+2^r}) - q_j^{(r)}] \quad . \qquad \text{(B.9)}$$

Now if $N = 2^{k+1} + 1$, then k reductions may be performed resulting in the single vector equation (provided the boundary conditions are homogeneous)

$$A^{(k)} x_{2^k+1} = A^{(k)} p_{2^k+1}^{(k)} + q_{2^k+1}^{(k)} \quad ,$$

which is readily solved for the vector x_{2^k+1}, since $A^{(k)}$ may be reduced to a set of 2^k tridiagonal factor matrices, after which the remaining vectors x may be solved by back solving

$$T^{(r)} x_{j-2^r} + A^{(r)} x_j + T^{(r)} x_{j+2^r} = A^{(r)} p_j^{(r)} + q_j^{(r)}$$

for $j = i.2^r + 1$, $\quad i = 1,2,\ldots,2^{k+1-r} - 1$,

or in rewritten form

$$A^{(r)}(x_j - p_j^{(r)}) = q_j^{(r)} - T^{(r)}(x_{j-2^r} + x_{j+2^r}) \quad .$$

The algorithm hinges on the calculation of the sets of vectors $p_j^{(r)}$ **and** $q_j^{(r)}$ defined by (B. 8) and (B. 9). It is seen that these equations are greatly simplified if **T** (and hence all $T^{(r)}$) are identity matrices since in this case the

solution reduces to the solving of the 2^r tridiagonal factors of $A^{(r)}$, a process which is computationally efficient. It is therefore a single matrix solution for $p_j^{(r)}$ then simple addition to obtain $q_j^{(r)}$, and it is this benevolent simplicity that makes the Buneman algorithm so computationally streamlined. However if T is not an identity matrix there are three additional matrix solutions to be performed at each reduction, with the result that the problem is greatly complicated and the procedure as a whole takes longer.

APPENDIX C - THE NUSSELT NUMBER

The Nusselt number is defined as the ratio of the total heat transfer through a system to the heat transfer by conduction alone. For example, in the simple partially heated model proposed in section 2.2 the heat lost (per unit width) through the unheated and uninsulated boundaries will be

$$Q_{tot} = -k\,(T_1-T_o)\left\{\int_o^1 \frac{\partial\theta}{\partial Y}\Big|_{Y=1} dX - \int_f^1 \frac{\partial\theta}{\partial Y}\Big|_{Y=0} dX\right\}, \qquad (C.1)$$

where k in this case is the conductivity of the fluid filled medium, and the purely conductive heat loss would be

$$Q'_{cond} = -k(T_1-T_o)\left\{\int_o^1 \frac{\partial\theta'}{\partial Y}\Big|_{Y=1} dX - \int_f^1 \frac{\partial\theta'}{\partial Y}\Big|_{Y=0} dX\right\}, \qquad (C.2)$$

where θ' is the temperature field which would exist if fluid motion was disallowed. Provided the boundary is held at temperature $\theta=0$, these equations are equally viable for closed or recharge boundaries. Thus the Nusselt number is given by the ratio

$$Nu = \frac{\int_o^1 \frac{\partial\theta}{\partial Y}\Big|_{Y=1} dX - \int_f^1 \frac{\partial\theta}{\partial Y}\Big|_{Y=0} dX}{\int_o^1 \frac{\partial\theta'}{\partial Y}\Big|_{Y=1} dX - \int_f^1 \frac{\partial\theta'}{\partial Y}\Big|_{Y=0} dX} \qquad (C.3)$$

which may be calculated approximately from the fields θ and θ' using Simpson's rule. The purely conductive terms in the denominator are termed the "conduction coefficient" and need only be calculated once for each configuration that is considered. A table of conduction coefficients is given in table X below.

Table X - Conduction Coefficients

Dimensionality	Shape	Heat input	Conduction Coefficient
Two-dimensional	Square	Uniform f=1.0	**1.0**
		Non-uniform f=0.75	1.43
		f=0.5	1.40
		f=0.25	0.94
	Rectangular nxl	Uniform	n
	Rectangular 2x1	Non-uniform f=0.5	1.13
	4x3	Non-uniform f=0.5	**1.23**
	Square-insulated lower boundary	Non-uniform f=0.5	**0.55**
Three-dimensional	Cube	Uniform	**8.0**
		Two quadrants	9.94
		One quadrant	1.37

The presence **of** a source **or** sink **also** affects the heat transfer through the system. The flow of fluid out of the system (per unit width) wil be R.q κ (taking into account the non-dimensionalisation) which results in an additional heat transfer of

$$Q_{source} = R.(\rho c_v)(q\ \kappa)\ \theta(T_1-T_o)$$

which is added to the transfer (C.1) and appears on the top line of (C. 3) as a term **R.q.8** since the factor $\frac{\rho c_v \kappa}{k}$ is unity from the definition of the thermal diffusivity.

APPENDIX D - AN EXTENSION OF THE BUNEMAN ALGORITHM TO NEUMANN-TYPE BOUNDARY CONDITIONS IN TWO AND THREE DIMENSIONS

The Buneman algorithm as previously described by Busbee, Golub and Nielson (1970) and in appendix B, can be extended to the three-dimensional solution of Poisson's equation, in which case the vectors x_{-1} and y_j in (B.3) are replaced by corresponding plane matrices

$$\left.\begin{aligned} [x_k]\ 1 &= X_{i,j,k} \\ [y_k] &= Y_{i,j,k} \end{aligned}\right\} \qquad \begin{aligned} i &= 2,3 \ldots, M-1 \\ j &= 2,3 \ldots, N-1 \end{aligned}$$

and the new A sub-matrix will itself be of the same form as the entire solution matrix on the left hand side of (B.3) except with **a -6** instead of a **-4** down the leading principal diagonal. Since the second-order representation is used, T is an identity matrix. The solutions of the reduction equations of the type

$$A^{(r)}(p_j^{(r)} - p_j^{(r+1)}) = p_{j-2^r}^{(r)} + p_{j+2^r}^{(r)} - q_j^{(r)}$$

are now each achieved by using a complete two-dimensional odd-even reduction sequence that is similar to the entire solution in the previous case (the only difference being the value of the diagonal element). In the case of Dirichlet boundary conditions this is not difficult to perform, but the Neumann conditions required for the pressure solutions of section 4.2 introduce difficulties as outlined below.

When the $A^{(r)}$ matrices are factorised they take the form

$$A^{(r)} = -\prod_{j=1}^{2^r} (A + 2\cos\theta_j^{(r)}) \qquad (D.1)$$

where $\theta_j^{(r)} = \frac{(2j-1)}{2^{r+1}}\pi$,

for Dirichlet boundary conditions, and are always non-singular. However when Neumann conditions are specified the final solution matrix becomes

$$A^{(k+1)} = -\prod_{j=1}^{2^{k+1}} (A + 2\cos\theta_j^{(k+1)}) \ , \qquad (D.2)$$

where $\theta_j^{(k+1)} = \frac{j\pi}{2^{k+1}}$,

and in two dimensions one of the factors (when j = 2k) is singular. This is to be expected as the solution of Poisson's equation is not unique in this case, however this one singular factor matrix may be modified such that effectively a Dirichlet condition is specified at one end of the row. This is equivalent to setting a reference pressure at a single point in the region to be zero, thereby restraining the entire field to be relative to that point.

In three dimensions the factor matrices must themselves be factorised and in this case the A in (D.2) is of the form

$$-\prod_{j}^{2^r} (A' + 2\cos\alpha_j^{(r)})$$

where A' is the original tridiagonal matrix

$$A' = \begin{bmatrix} -6 & 2 & & & \\ 1 & -6 & 1 & & \\ & 1 & -6 & 1 & \cdots \\ & & & \ddots & \\ & & & 2 & -6 \end{bmatrix}$$

Thus the general form of the most basic factor matrix is

$$\begin{bmatrix} d & 2 & & & \\ 1 & d & 1 & & \\ & 1 & d & 1 & \cdots \\ & & & \vdots & \\ & & & 2 & d \end{bmatrix}$$

where $d = -6 + 2\cos\alpha_j + 2\cos\theta_j$.

This matrix has zero determinant and one zero eigenvalue when

$d=0$ or $d = \pm 2$

which is only possible when

$$2\cos\alpha_j + 2\cos\theta_j = 4$$

or $$\cos\theta_j = 2 - \cos\alpha_j$$

Thus the matrix is singular if but only if α_j and θ_j are both $\frac{2k+1}{2^k}\pi$. Once again this is equivalent to specifying a reference pressure in the field.

APPENDIX E - SPECTRAL REPRESENTATION OF EQUATIONS OF MOTION

Considering the equations of motion **(2.3.8)** and **(2.3.11)** with the uniform boundary conditions **(2.3.12)**, **(2.3.13)** and **(2.3.14)** and f = **1,** the transformation into Fourier space is made by defining

$$\psi = \sum_{m=1}^{M} \sum_{n=1}^{N} \psi^*_{mn} \sin m\pi X \sin n\pi Y \quad , \qquad \text{(E.1)}$$

and $$\theta = (1-Y) + \sum_{m=0}^{M} \sum_{n=1}^{N} \theta^*_{mn} \cos m\pi X \sin n\pi Y \qquad \text{(E.2)}$$

The conduction solution (1-Y) is separated making the Fourier boundary conditions homogeneous and identically satisfied by the choice of transform. To simplify the notation the stars are dropped on the Fourier coefficients θ^*_{mn} and ψ^*_{mn} - confusion may be avoided by remembering that only the transformed variables carry subscripts.

The transformed equations are determined by substitution of (E.1) and **(E.2)** into the two original equations **(2.3.8)** and **(2.3.11)**, multiplying throughout by $\sin k\pi X \sin \ell\pi Y$ and $\cos k\pi X \sin \ell\pi Y$ respectively, integrating over the range $0 \leq X \leq 1$, $0 \leq Y \leq 1$ and substituting the Euler properties of transcendental integrals. This procedure is well known and is not set out fully here.

The streamfunction equation transforms to

$$\psi_{k\ell} = - \frac{k\theta_{k\ell}}{(k^2+\ell^2)\pi} \qquad \text{(E.3)}$$

which may be substituted into the transformed temperature equation which is

$$\begin{aligned} -\tfrac{1}{4}(k^2+\ell^2)\pi^2\theta_{k\ell} = \tfrac{1}{4}\frac{\partial\theta_{k\ell}}{\partial\tau} + \frac{Rk\pi}{4}\psi_{k\ell} \\ + \frac{R\pi^2}{16} \sum_{m=1}^{M} \sum_{n=1}^{N} \psi_{mn} [\theta_{|m-k|,|\ell-n|} \{ -m|\ell-n| - n(m-k) \frac{(\ell-n)}{|\ell-n|} \} \\ + \theta_{(m+k),|\ell-n|} \{ -m|\ell-n| - n(m+k) \frac{(\ell-n)}{|\ell-n|} \} \\ + \theta_{(m+k),(\ell+n)} \{ +m(\ell+n) - n(m+k) \} \\ + \theta_{|m-k|,(\ell+n)} \{ +m(\ell+n) - n(m-k) \}] \quad , \end{aligned} \qquad \text{(E.4)}$$

provided $m + k \leq M$ and $n + \ell \leq N$ and $n \neq \ell$ in appropriate terms (which are otherwise zero). Since the Euler property **is** only valid for non-zero integers the case $k = 0$ requires special attention and is described by the equation

$$\begin{aligned} -\ell^2\pi^2\theta_{o\ell} = \frac{\partial\theta_{o\ell}}{\partial\tau} + \frac{R\pi^2}{4} \{ \sum_{m=1}^{M} \sum_{n=1}^{N} mn\, \psi_{mn} [-\theta_{m,\ell+n} \\ - \theta_{m,|\ell-n|} \frac{(\ell-n)}{|\ell-n|}] - m\, \psi_{mn} [\theta_{m,|\ell-n|}.|\ell-n| - \theta_{m,\ell+n}.(\ell+n)] \} \quad . \end{aligned} \qquad \text{(E.5)}$$

These equations may be solved simultaneously using the fourth-order Runge-Kutta method described in Carnahan, Luther and Wilkes **(1969** p.361). The solution process is much lengthier than a similar finite difference procedure since each "point" in the spectral mesh references every other "point". In a finite difference solution the temperature at each point in the grid depends only on the values at the points on the grid which are immediately adjacent to it. The spectral method may be computed far more efficiently by using further transforms (Orszag 1971a) although it is then not possible to use the simple transforms defined here in (E.1) and **(E.2).**

APPENDIX F - EVOLUTION OF THE THERMAL BOUNDARY LAYER

As an example of the analysis of Sparrow, Husar and Goldstein (1970) to determine the rate of evolution of the thermal boundary layer, the hydrodynamic conditions are ignored and only conductive heat transfer considered. For a sudden temperature rise at the boundary of a semi-infinite region, the temperature θ in the medium obeys the relationship

$$\theta = \text{erf}\left(\frac{Y}{2\sqrt{\tau}}\right) , \qquad \text{(F.1)}$$

as given by Holman (1968 p.79). In the range 0 - 0.8 the error function is approximately linear, so if the conduction layer is considered to lie between temperatures of 1.0 and 0.2 then the non-dimensional thickness δ of this layer is

$$\delta \simeq 1.6\sqrt{\tau} . \qquad \text{(F.2)}$$

Now since the effective local Rayleigh number is directly dependent on the thickness δ, then it follows that R_{local} in the boundary layer increases as $\sqrt{\tau}$ until it reaches its critical value when convection begins to occur in the layer. The interval τ_p required for the solution to reach this stage is dependent on the temperature differential across the layer, which is derived from the *true* Rayleigh number for the overall system. Thus the interval is related to R by the expression

$$\tau_p \propto R^{-2} . \qquad \text{(F.3)}$$

This relationship describes the rate of formation of the boundary layer in the absence of other cooling effects, particularly the flow of fluid across the heater. It is not surprising then that (F.3) predicts shorter gestation times than the relationship

$$\tau_p \propto R^{-3/2}$$

that is observed in the flows of chapter 5, in which there is no fluid boundary layer.

Unfortunately it is not possible to perform a similar analysis for the case of forced cooling of the boundary layer since the velocities are not constant. However the result (F.3) does indicate a tendency of the flow and correctly predicts that the boundary layer evolves more quickly than in the fluid layer (Benard) problem. For a porous medium problem without major circulating velocities, Wooding (1969) determined that the cell width is dependent on the square root of the time interval, which confirms the rate of growth of the boundary layer predicted by (F.2).

Therefore defining a pseudo-streamfunction

$$\psi^* = \frac{1}{\sqrt{2}} (\psi_3 - \psi_1) \quad ,$$

then $V_1 = -\frac{\partial \psi^*}{\partial X'}$,

and $U' = \frac{\partial \psi^*}{\partial Y'}$,

and a representation of the streamlines on the centre diagonal plane may be obtained by plotting contours of this function.

APPENDIX G - STREAMLINE REPRESENTATION IN THREE-DIMENSIONAL FLOWS

In two dimensions streamlines are easily determined as lines of equal stream function value, but in three dimensions their visualisation is not so simple. The velocity field in three dimensions is given by

$$U = \frac{\partial \psi_3}{\partial Y} \quad ,$$

$$V = \frac{\partial \psi_1}{\partial Z} - \frac{\partial \psi_3}{\partial X} \quad ,$$

and $$W = -\frac{\partial \psi_1}{\partial Y} \quad .$$

Now the horizontal axes X and Z are rotated through 45° as in figure G.1 so that the new axis X' lies along the diagonal of the region.

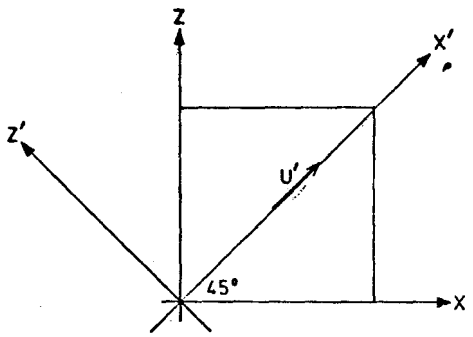

FIGURE G.1 - Rotation of Axes

Now $$\frac{\partial}{\partial X} \equiv \frac{1}{\sqrt{2}} \left(\frac{\partial}{\partial X'} - \frac{\partial}{\partial Z'} \right) \quad ,$$

and $$\frac{\partial}{\partial Z} \equiv \frac{1}{\sqrt{2}} \left(\frac{\partial}{\partial X'} + \frac{\partial}{\partial Z'} \right) \quad ,$$

so that the vertical velocity

$$V = \frac{1}{\sqrt{2}} \left(\frac{\partial \psi_1}{\partial X'} + \frac{\partial \psi_1}{\partial Z'} - \frac{\partial \psi_3}{\partial X'} + \frac{\partial \psi_3}{\partial Z'} \right) \quad ,$$

and, provided X' is an axis of symmetry,

$$V = -\frac{1}{\sqrt{2}} \frac{\partial}{\partial X'} (\$3 - \psi_1) \quad . \qquad \text{(G.1)}$$

The velocity along the X' axis is given by

$$U' = \frac{1}{\sqrt{2}} \left(\frac{\partial \psi_3}{\partial Y} - \frac{\partial \psi_1}{\partial Y} \right)$$

or $$U' = \frac{1}{\sqrt{2}} \frac{\partial}{\partial Y} (\psi_3 - \psi_1) \quad . \qquad \text{(G.2)}$$

REFERENCES

Arakawa, A., 1966, J. Comp. Phys. **1,** 119

Aravin, V.I., and Numerov, S.N., 1965, "Theory of Fluid Flow in Undeformable Porous Media". Israel Program for Scientific Translations, Jerusalem.

Aziz, K., and Hellums, J.D., 1967, Phys. **of** Fluids **10,** 314

Baines, P.G., and Gill, A.E., 1969, J. Fluid Mech. 37, 289

Batchelor, G.K., 1967, "An Introduction to Fluid Dynamics", Cambridge University Press

Beck, J.L., 1972, Phys. of Fluids 15, 1377

Betbeder, J., and Jolas, P., 1972, Int. **J.** Heat Mass Transfer 15, 721

Birikh, R.V., Gershuni, G.Z., Zhukhovitskii, E.M., and Rudakov, R.N., 1972, P.M.M. **36**, 745

Bories, S., and Combarnous, M.A., 1973, J. Fluid Mech. 57, 63

Bories, S., Combarnous, M.A., and Jaffrenou, J.Y., 1972, Comptes Rendus Acad. Sci. Paris 275A, 857

Bories, S., and Thirriot, C., 1969, La Houille Blanche 24, 237

Brown, W.S., 1973, J. Fluid Mech. 60, 539

Buretta, R., and Berman, A.S., 1974, "Convective heat transfer in a liquid-saturated porous layer" (To appear)

Busbee, B.L., Golub, C.H., and Nielson, C.W., 1970, S.I.A.M. Journ. on Num. Anal. 7, 627

Busse, F.H., and Joseph, D.D., 1972, J. Fluid Mech. 54, 521

Busse, F.H., and Whitehead, J.A., 1971, J. Fluid Mech. 47, 305
1974, J. Fluid Mech. 66, 67

Caltagirone, J.P., Cloupeau, M., and Combarnous, M.A., 1971, Comptes Rendus Acad. Sci. Paris 273B, 833

Carnahan, B., Luther, H.A., and Wilkes, J.D., 1969, "Applied Numerical Methods" John Wiley and Sons, New York

Chandrasekhar, S., 1961, "Hydrodynamic and Hydromagnetic Stability", Oxford Clarendon Press, London

Chan, B.K.C., Ivey, C.M., and Barry, J.M., 1970, J. Heat Transfer, Trans. ASME 92 Series C, 21

Combarnous, M.A., 1970, Revue Generale de Thermique **108**, 1355
1972, Comptes Rendus Acad. Sci. Paris 275A, 1375

Combarnous, M.A., and Bia, F., 1971, Soc. Petr. Eng. Journ. December, 399

Combarnous, M.A., and Bories, S., 1974, Int. J. Heat Mass Transfer 17, 505

Combarnous, M.A., and LeFur, B., 1969, Comptes Rendus Acad. Sci. Paris 269B, 1009

Cooley, J.W., Lewis, P.A.W., and Welch, P.D., 1967, I.E.E.E. Transactions AU-15, 79

Crowley, W.P., 1967, J. Comp. Phys. **1,** 471

Cullen, M.J.P., 1974, J. Inst. Maths. Applics. **13**, 233

Curry, D.M., 1974, N.A.S.A. Technical Note TN D-7606

Denton, R.A., and Wood, I.R., 1974, Proc. 5th Austr. Conf. Hydr. and Fluid Mech., 361

Donaldson, I.G., 1962, **J.** Geoph. Res. 67, 3449
1968, **N.Z.** Journ. Sci. **11, 3**
1970, Geothermics - Special Issue 2, ***649***
1974, Private communication, D.S.I.R. Wellington

Dybbs, A., and Schweitzer, S., 1973, Journ. Hydrology 20, 171

Engineering Sciences Data, (1968), Items no. 68009, **68010**.

Elder, J.W., 1966a, N.Z. D.S.I.R. Bulletin 169
1966b, J. Fluid Mech. 24, 823
1967a, **J.** Fluid Mech. 27, 29

Elder, J.W., 1967b, J. Fluid Mech. 27, 609
1968, J. Fluid Mech. 32, 69
1969, Phys. of Fluids Suppl. II 12, 194
Fisher, R.G., 1964, N.Z. Jour. Geol. Geophys. 7, 172
Foster, T.D., 1968, J. Geoph. Res. 73, 1933
1969, J. Geoph. Res. 74, 6967
From, J.E., 1965, Phys. of Fluids 8, 1757
1969a, Phys. of Fluids Suppl. II 12, 3
1969b, J. Comp. Phys. 3, 176
Gebhart, B., 1973, Ann. Rev. Fluid Mech. 5, 213
Gill, A.E., 1969, J. Fluid Mech. 35, 545
Gill, A.E., and Davey, A., 1969, J. Fluid Mech. 35
Gill, A.E., and Kirkham, C.C., 1970, J. Fluid Mech. 42, 125
Gupta, V.P., and Joseph, D.D., 1973, J. Fluid Mech. 57, 491
Hart, J.E., 1973, J. Fluid Mech. 59, 47
Healy, J., and Hochstein, M.P., 1973, Journ. Hydrology (N.Z.) 12, 71
Hochstein, M.P., 1974, Private communication, University of Auckland
Holman, J.P., 1968, "Heat Transfer", McGraw-Hill
Holst, P.H., and Aziz, K., 1972a, Canadian J. Chem, Eng. 50, 232
1972b, Int. J. Heat Mass Transfer 15, 73
Homsy, G.M., 1973, J. Fluid Mech. 60, 129
1974, J. Fluid Mech. 62, 387
Horne, R.N., and O'Sullivan, M.J., 1974a, J. Fluid Mech. 66, 339
1974b, Proc. 5th Austr. Conf. Hydr. and Fluid Mech., 231
Horton, C.W., and Rogers, F.T.Jr., 1945, J. Appl. Phys. 16, 367
Howard, L.N., 1964, Proc. 11th Int. Congr. Appl. Mech, Munich, ed. H. Gortler, Berlin : Springer-Verlag.
Hurle, D.T.J., and Jakeman, E., 1971, J. Fluid Mech. 47, 667
Jannot, M., Naudin, P., and Viannay, S., 1973, Int. J. Heat Mass Transfer 16, 395
Joseph, D.D., 1971, J. Fluid Mech. 47, 257
Kaneko, T., Mohtadi, M.F., and Aziz, K., 1974, Int. J. Heat Mass Transfer 17, 485
Kantorovich, L.V., and Krylov, V.I., 1964, "Approximate Methods of Higher Analysis", Groningen : P. Noordhof Ltd.
Katto, Y., and Masuoka, T., 1967, Int. J. Heat Mass Transfer 10, 297
Keller, J.B., 1966, J. Fluid Mech. 26, 599
Kreiss, H., and Oliger, J., 1973, "Methods for the Approximate Solution of Time Dependent Problems", G.A.R.P. Publ. Ser. 10, World Meteor. Org.
Krishnamurti, R., 1970a, J. Fluid Mech. 42, 295
1970b, J. Fluid Mech. 42, 309
Kruger, P. (ed.), 1973, "Geothermal Energy Resources, Production and Stimulation", Stanford University Press.
Lambert, R.B., and Demenkow, J.W., 1971, J. Fluid Mech. 54, 627
Lapwood, E.R., 1948, Proc. Camb. Phil. Soc. 44, 508
Legros, J.C., Platten, J.K., and Poty, P.G., 1972, Phys. of Fluids 15, 1383
Lilly, D.K., 1965, Mon. Weath. Rev. 93, 11
McNabb, A., 1965, Proc. 2nd Austr. Conf. Hydr. and Fluid Mech., C 161
Maksimov, E.A., and Stradomskii, M.V., 1971, Inzhenerno-Fizicheskii Zhurnal 20, 588
Mercer, J.W., 1973, "Finite Element Approach to the Modelling of Hydrothermal Systems", Ph.D. Thesis, Univ. of Illinois
1974, Private communication
Mikhlin, S.G., and Smolitsky, K.L., 1967, "Approximate Methods for the Solution of Differential and Integral Equations", Elsevier, N.Y.

Mitchell, A.R., 1969, "Computational Methods in Partial Differential Equations", John Wiley
Moore, D.R., and Weiss, N.O., 1973, J. Fluid Mech. 58, 289
Nield, D.A., 1967, J. Fluid Mech. 29, 545
1968, Water Resources Research 4, 553
Orszag, S.A., 1971a, M.I.T. Stud. Appl. Math. 50, 293
1971b, J. Fluid Mech. 49, 75
1971c, J. Fluid Mech. 50, 689
Orszag, S.A., and Israeli, M., 1974, Ann. Rev. Fluid Mech. 6, 281
O'Sullivan, M.J., 1973, "Steady Convection in a Porous Medium", Private communication
Palm, E., Weber, J.E., and Kvernvold, O., 1972, J. Fluid Mech. 54, 153
Platten, J.K., and Chavepayer, G., 1973, J. Fluid Mech. 60, 305
Platzman, G.W., 1965, J. Fluid Mech. 23, 481
Plows, W.H., 1968, Phys. of Fluids 11, 1593
Prats, M., 1966, J. Geoph. Res. 71, 4835
Rubin, H., 1974, Journ. Hydrology 21, 173
Runchal, A.K., Spalding, P.B., and Wolfshtein, M., 1959, Phys. of Fluids Suppl. 11, 12, 21
Schecter, R.S., 1967, "The Variational Method in Engineering", McGraw-Hill
Shirtcliffe, T.G.L., 1973, J. Fluid Mech. 57, 27
Shirtcliffe, T.G.L., and Turner, J.S., 1970, J. Fluid Mech. 41, 707
Sparrow, E.M., Husar, R.B., and Goldstein, R.J., 1970, J. Fluid Mech. 41, 793
Straus, J.M., 1974, J. Fluid Mech. 64, 51
Taunton, J.W., and Lightfoot, E.N., 1970, Chem. Eng. Sei. 25, 1939
Taunton, J.W., Lightfoot, E.N., and Green, T., 1972, Phys. of Fluids 15, 748
Torrance, K.E., 1968, J. Res. N.B.S. 72B, 281
Torrance, K.E. and Turcotte, D.L., 1971, J. Fluid Mech. 47, 113
Veronis, G., 1966, J. Fluid Mech. 26, 49
Wankat, P.C., and Schowalter, W.R., 1970, Phys. of Fluids 13, 2418
Weber, J.E., 1973, Int. J. Heat Mass Transfer 16, 961
Welander, P., 1967, J. Fluid Mech. 29, 17
1971, J. Fluid Mech. 47, 51
Westbrook, D.R., 1969, Phys. of Fluids 12, 1547
Wilkes, J.O., and Churchill, S.W., 1966, Am. Inst. Chem. Eng. J. 12, 161
Willis, G.E., and Deardorff, J.W., 1967, Phys. of Fluids 10, 931
1970, J. Fluid Mech. 44, 661
Wirtz, R.A., Briggs, D.G., and Chen, C.F., 1972, Geoph. Fluid Dyn. 3, 265
Wooding R.A., 1957, J. Fluid Mech. 2, 273
1960, J. Fluid Mech. 7, 501
1969, J. Fluid Mech. 39, 477
Yen, Y.C., 1974, Int. J. Heat Mass Transfer 17, 1349
Yih, C.S., 1969, "Fluid Mechanics", McGraw-Hill
Young, R.E., 1974, J. Fluid Mech. 63, 695